Breakup phenomena in nuclear collision processes with He projectiles

R. J. de Meijer

Kernfysisch Versneller Instituut, Rijksuniversiteit Groningen, 9747 AA Groningen, The Netherlands

R. Kamermans

Robert J. Van de Graaff Laboratorium, Rijksuniversiteit Utrecht, 3508 TA Utrecht, The Netherlands

This paper reviews the experimental and theoretical studies of breakup processes induced by He projectiles. For this type of reaction knowledge of three-body kinematics is imperative; hence important aspects are summarized. Although some nuclear structure information has been studied with this type of reaction, the emphasis of this review is mainly on the reaction mechanism. The phenomena described here are quite general, so the consequences for other projectiles (i.e., heavy ions) are also discussed.

CONTENTS

I. INTRODUCTION

Energy spectra of particles emitted in nuclear reactions show a characteristic pattern. An example, for reactions at beam energies of 10—40 MeV per nucleon, is schematically presented in Fig. 1. Three different regions can be distinguished: at high ejectile energies one observes the transitions to the well-isolated states in the residual nucleus whereas at the low-energy side of the spectrum contributions from (pre-)equilibrium emission are present. A large part of the cross section, however, goes into the so-called continuum region. This third region may originate from different reaction processes. Binary reactions can contribute via transitions to the many overlapping states or to broad structures which exist at those excitation energies in the residual nucleus. Moreover, reactions with three or more particles in the final state, of which only one particle is detected, will give rise to a continuous energy distribution similar to that observed in electron spectra from β decay. This is a direct consequence of a kinematically incomplete measurement even if the residual nucleus is left in a well-defined state.

Over the last few years there has been a growing interest in the continuum part of energy spectra. This in-

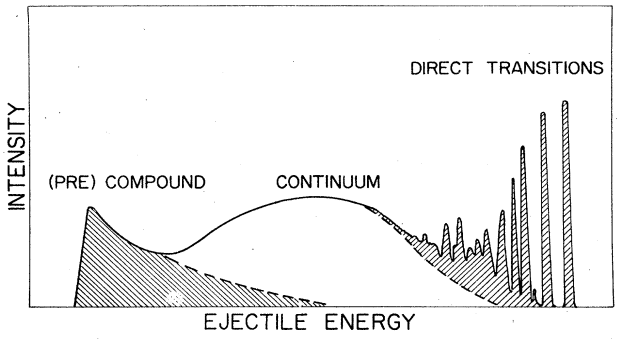

FIG. 1. A schematic particle energy spectrum at a forward angle (Aarts, 1983).

terest is mainly motivated by the increase of the cross section to this region by going to higher incident energies and heavier projectiles. Moreover, a better understanding of the underlying reaction mechanisms will also facilitate the study of collective phenomena as giant resonances and of deeply bound hole states, since these nuclear structure studies involve the subtraction of this continuum "background."

This paper deals primarily with those processes leading to three bodies in the final state in which the projectile and/or the ejectile are involved. In particular, we will focus on reactions induced by ^{3}He and ^{4}He in the energy range of 10—40 MeV per nucleon. The reaction processes are separated in sequential and direct processes according to the time scales involved, *direct breakup* with a time scale corresponding to the nuclear reaction time, and *sequential breakup* in which the lifetime of the unstable system is characteristic. In sequential breakup the ejectile is produced in a particle unstable state which will subsequently decay. In this process the properties of the breakup remnants are determined by the state to which the ejectile is excited. Information on the reaction mechanism is lost to a large extent due to the relatively long lifetime of those states. In direct breakup the projectile breaks up due to the interaction with the target nucleus. In such a process the two (light) ejectiles are related to the projectile and hence exhibit the properties of the projectile. It will be clear that the kinematics of the reaction process will play an important role in the interpretation of the experiments; therefore this paper starts with a section on three-body kinematics.

Sequential breakup has been observed for the first excited state of the deuteron (d^*), excited states of the α particle, the Li isotopes, ^{8}Be, and other light heavy ions. In addition, reactions have been observed with two outgoing protons in a relative $S=0$, $T=1$ state. This "ejectile" will be named ^{2}He and refers to the proton-proton final-state interaction at low relative energies. Aside from studies directed to the final-state interaction, studies of this type of reaction started with the investigation of the (^{9}Be,^{8}Be) reaction by Brown *et al.* (1965) and were continued about ten years later by Wozniak (1974) and Wozniak *et al.* (1976). In this reaction the outgoing ^{8}Be is unbound with respect to the decay in two α particles by only 90 keV. Reactions with ^{2}He and α^* (the first excited state of the α particle) as ejectiles were first studied by Jahn, Wozniak *et al.* (1976) and Jahn, Stahel *et al.* (1976). The data of the various reaction with unbound ejectiles and their description are presented in Sec. IV for ^{3}He- and ^{4}He-induced reactions.

Direct breakup has been observed for deuterons, ^{3}He, ^{4}He, and heavier ions in interactions with nuclei. It is probably a phenomenon that occurs in reactions between target nuclei and all energetic complex projectiles. Deuteron projectile breakup was the first and most generally studied breakup process. In 1935 Oppenheimer and Phillips (Oppenheimer, 1935; Oppenheimer and Phillips, 1935) investigated deuteron breakup. They proposed a model in which the Coulomb field causes the deuteron to break up. The experiments of Helmholz *et al.* (1947) were carried out at incident energies where the nuclear field became the main cause for the deuteron breakup. These results have led Serber (1947) to develop a simple model that still forms the basis for the present understanding of this type of reaction. Since Serber's work deuteron breakup was studied for many target nuclei at various bombarding energies. For a review of the deuteron-projectile breakup work we refer to the paper of Baur and Trautmann (1976).

Compared to the case of deuteron breakup little was known of the breakup properties of ^{3}He and ^{4}He until quite recently. The investigations on ^{3}He-induced direct breakup started with an investigation of the properties of the continuum region in the inclusive (^{3}He,d) reactions by Matsuoka *et al.* (1978). Studies on the breakup of the α particle were started by Budzanowski *et al.* (1978) and Wu *et al.* (1978). Since then detailed work by several groups have revealed different reaction processes contributing to this continuum. The experimental data and their interpretation for ^{3}He and ^{4}He are reviewed in Sec. V.

The advantage of He-induced reactions for the study of the reaction mechanisms is that the structure of these projectiles is still rather simple. Therefore, the number of reaction processes is limited and they can be recognized in coincidence measurements. A common feature of all these processes is that the interaction between the projectile and the target nucleus seems to take place between only one constituent of the projectile (the participant), whereas the other part continues undisturbed by the nuclear interaction (the spectator). It was found that the interaction between the participant and the target nucleus resembles the interaction in "conventional" nuclear collisions: elastic and inelastic scattering, nucleon transfer, and particle capture. This finding is the basis of the various models which are reviewed in Sec. VI. This section starts with a summary of the formal reaction theory. In order of increasing complexity the model of Serber (1947), the plane-wave Born approximation, the quasifree break-

up model (QFBM), and the distorted-wave breakup model (DWBM) are presented. Conceptually these models may be considered refinements of the Serber model. The Serber model, however, is restricted to the calculation of the shape of the bump in inclusive spectra only.

In the last section the conclusions and perspectives are presented. Besides a summary of the results for the various reactions this section contains a description of possible relations with heavy-ion–induced reactions and some suggestions for future research.

II. THREE-BODY KINEMATICS AND PHASE-SPACE ASPECTS

A. Kinematics

The understanding of kinematics plays an essential role in the analysis of three-body breakup processes. Three particles in a final state correspond to nine degrees of freedom. Since conservation of momentum imposes three conditions, the number of degrees of freedom is reduced to six. Therefore, experimentally a measurement is defined as being kinematically complete if six independent kinematical quantities are determined. An example is the measurement of the masses, energies, and emission angles of two of the three particles in the final state. In such an experiment the corresponding properties of the third undetected particles can be calculated exactly. Breakup processes leading to a discrete final state (with a fixed Q value) gives an additional constraint which decreases the number of degrees of freedom to five. This implies that, e.g., the energies of the two detected particles are correlated.

In this paper the notation will be used in which E, $\mathbf{p}$, $\mathbf{v}$, μ, θ, and φ stand for the kinetic energy, momentum, velocity, reduced mass, polar, and azimuthal angle, respectively (Ohlsen, 1965; Fuchs, 1982). The quantities describing the motion of the particles are denoted by an index in the usual way. The relative motion of two particles i and k is indicated by i-k, whereas three indices i-lk refer to the motion of fragment i relative to the center of mass of the fragments l and k. Masses are given by m_i. A reaction with three particles in the final state can be written as

$$a+A\rightarrow 1+2+3\ . \tag{2.1}$$

A division will be made in reactions in which the three final particles are produced simultaneously [Fig. 2(a)], referred to as *direct breakup,* and in reactions which proceed through the formation of an intermediate state in one of the subsystems; an intermediate state subsequently decays into two particles [Figs. 2(b)–2(d)]. This last process will be called *sequential breakup,* and three different intermediate unbound states (indicated with an asterisk) might exist

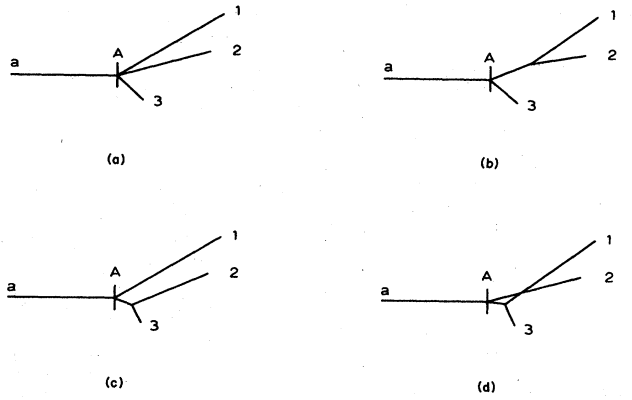

FIG. 2. Schematic presentation of direct breakup (a) and sequential breakup (b), (c), (d).

$$a+A\rightarrow 12^*+3\ , \tag{2.2}$$

$$a+A\rightarrow 23^*+1\ , \tag{2.3}$$

$$a+A\rightarrow 13^*+2\ . \tag{2.4}$$

This separation in the two extremes (direct and sequential) is based on the different time scales involved (see Secs. IV.A.1 and VI). The three-body ground-state–ground-state Q value is defined as

$$Q_3^{gg}=m_a+m_A-m_1-m_2-m_3\ . \tag{2.5}$$

For sequential processes it is often convenient to use the two-body ground-state–ground-state Q value, Q_2^{gg}, given by

$$Q_3^{gg}=Q_2^{gg}+Q_{th}\ , \tag{2.6}$$

in which Q_{th} is the threshold energy for the breakup of the intermediate system. In the decay, the difference between the excitation energy of the intermediate system and the Q_{th} is converted into the relative kinetic energy (ε) of the breakup remnants. For example, for the breakup of the intermediate state 12^* with an excitation energy $E(12^*)$, one can then write

$$\varepsilon=E(12^*)+Q_{th}\ . \tag{2.7}$$

In a kinematically complete experiment, in which two particles (1 and 2) are detected in coincidence at angles $\theta_1,\varphi_1,\theta_2,\varphi_2$, the laboratory energies E_1 and E_2 are dependent variables for a given Q value Q_3. For nonrelativistic energies their relation is given by (Ohlsen, 1965; Stahel, 1979)

$$1/m_3[E_1(m_1+m_2)+E_2(m_2+m_3)-2(m_a m_1 E_a E_1)^{1/2}\cos\theta_1-2(m_a m_2 E_a E_2)^{1/2}\cos\theta_2 +2(m_1 m_2 E_1 E_2)^{1/2}\cos\theta_{1\text{-}2}]=Q_3+E_a(1-m_a/m_3) \tag{2.8}$$

in which

$$\cos\theta_{1\text{-}2}=\cos\theta_1\cos\theta_2+\sin\theta_1\sin\theta_2\cos(\varphi_1-\varphi_2)\ . \qquad (2.9)$$

Due to the fact that the recoiling nucleus is unobserved, an infinite number of E_1,E_2 pairs fulfill Eq. (2.8), even if all other variables are kept fixed. To be more precise, each E_1,E_2 pair corresponds to a different energy and emission angle of the unobserved nucleus. Equation (2.8) describes a closed curve in the E_1,E_2 space (an ellipse in $E_1^{1/2},E_2^{1/2}$ space) resulting in a solution which is in general double valued. In the reactions that will be discussed in this paper we will restrict ourselves to reactions in which particle 3 is much heavier than particles 1 and 2.

In Fig. 3 this is illustrated for the reaction $\alpha+{}^{12}\mathrm{C}\rightarrow p+p+{}^{14}\mathrm{C}^*$ at $E_\alpha=65$ MeV with an E_2 vs E_1 diagram. The calculated kinematic loci for events corresponding to the ground state and the two first excited states in ^{14}C at 6.73 and 10.72 MeV, respectively, are represented by the solid lines. For $m_1,m_2\ll m_3$ and at high incident energy, these kinematic loci are single valued and almost straight lines except near the maximum values of E_1 and E_2. This is due to the fact that for a fixed excitation energy in ^{14}C the recoil energy of ^{14}C is almost independent of E_1 and E_2. For heavier targets the above-mentioned recoil effects will be even smaller.

Direct information on the occurrence of intermediate states can be obtained by calculating for each point on the kinematic locus the relative energies $E_{1\text{-}2}$, $E_{1\text{-}3}$, and $E_{2\text{-}3}$. Peaks in these relative energies are connected with states above the breakup threshold in the respective composite systems. The relative energies, ε, follow straightforwardly from their definition (see Fig. 4):

$$\varepsilon=E_{1\text{-}2}=\tfrac{1}{2}\mu_{1\text{-}2}v_{1\text{-}2}^2=\frac{1}{m_1+m_2}[m_2E_1+m_1E_2-2(m_1m_2E_1E_2)^{1/2}\cos\theta_{1\text{-}2}]\ . \qquad (2.10)$$

Usually ε is a small number corresponding to the difference between two large energies, one being weighted by $\cos\theta_{1\text{-}2}$. Therefore, the determination of ε is especially sensitive to the spread in the value of the relative angle $\theta_{1\text{-}2}$ due to the finite size of each of the detectors. This sensitivity has two major consequences: a broadening of the width of states in an ε distribution and a selection of a region in relative energy. The averaging over the experimental range of $\theta_{1\text{-}2}$ gives a width much larger than the intrinsic one. An example is given in Fig. 5 for the reaction $^{28}\mathrm{Si}(\alpha,\alpha t)^{25}\mathrm{Al}(gs)$ at $E_\alpha=65$ MeV (de Meijer *et al.*, 1983), which shows the results of an analysis of the sequential decay of the $E_x=4.63$ MeV level in ^{7}Li. This state corresponds to a resonance in the t-α channel with a $\Gamma=93$ keV. The solid line represents the result of the analysis in which realistic values for $\theta_{1\text{-}2}$ (see inset) have been used, whereas the dashed line corresponds to a δ function for the $\theta_{1\text{-}2}$ distribution. The dramatic effect of the geometry is evident.

A selection of a region in relative energy will enhance certain aspects of the reaction process. For instance, small values of $E_{1\text{-}2}$ are kinematically restricted to a small angle $\theta_{1\text{-}2}$. Therefore, an experiment in which particles 1 and 2 are detected at a small relative angle will enhance the observation of resonances or states just above the threshold in the (12) system. Since particle 3 is emitted in the 123 c.m. system in the opposite direction from 1 and 2, the relative energies $E_{1\text{-}3}$ and $E_{2\text{-}3}$ are fairly large and would correspond to structures at high excitation energy. Such structures are unlikely and have a strongly reduced probability of detection in this geometry; therefore peaks observed along the kinematical locus will in general correspond to states in the (12) system.

For a fixed geometry and certain detector thicknesses

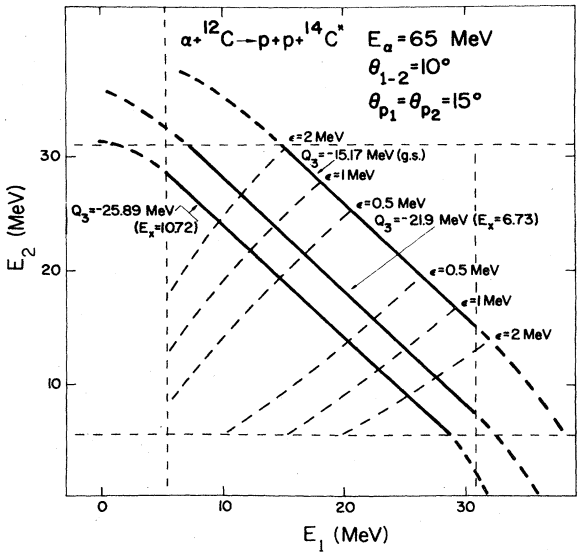

FIG. 3. An E_1 vs E_2 diagram for the $^{12}\mathrm{C}(^4\mathrm{He},^2\mathrm{He})^{14}\mathrm{C}$ reaction at $E_\alpha=65$ MeV. The dashed lines indicate the experimental detection limitations (van Driel, 1980).

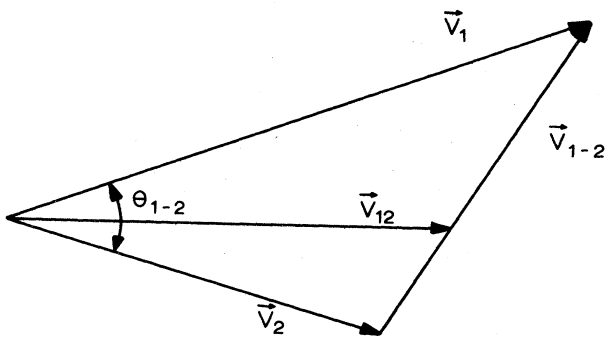

FIG. 4. Velocity diagram for a sequential breakup reaction.

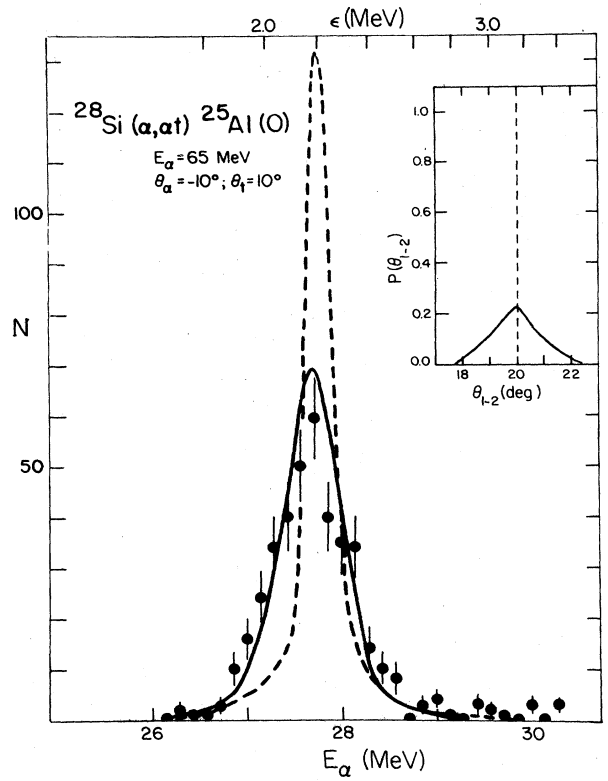

FIG. 5. Example of the strong effect of the geometry of the detection system on the experimental data for the ^{28}Si($\alpha,\alpha t$)^{25}Al (gs) reaction.

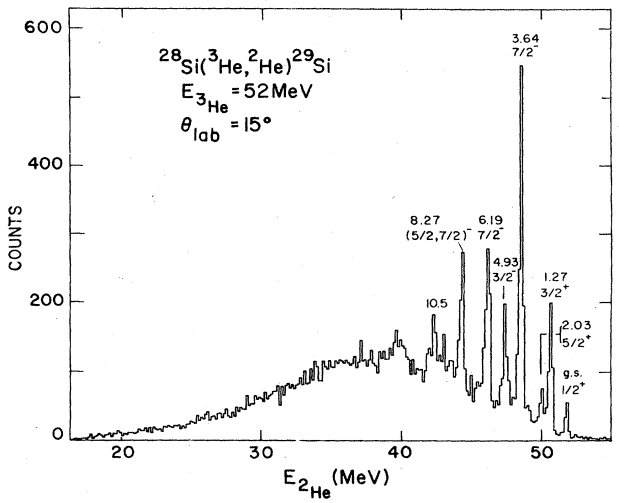

FIG. 6. The total kinetic energy spectrum for the reaction ^{28}Si(^{3}He, ^{2}He)^{29}Si at $E_{^3He}$=52 MeV. The good energy resolution is due to the fact that the loci of constant Q value are almost straight lines (van Driel, Kamermans, de Meijer, and Dieperink, 1980).

the experimental limitation in the ε-energy range are indicated in Fig. 3. The dashed lines correspond to constant values of ε. The upper limit of ε is determined by the maximum energy of the protons that can be detected (ground state and first-excited state in ^{14}C) or by the minimum detectable proton energies (E_x=10.72 MeV state in ^{14}C). The lower limit of ε is determined by the minimum relative angle between the two counters. For $\varepsilon \ll E_1+E_2$ this lower limit occurs at the point on the locus for which $m_1E_2=m_2E_1$. It should be noted that for a given locus each value of ε corresponds to two sets of E_1,E_2 values, one with $E_1>E_2$ and one with $E_1<E_2$, corresponding to forward and backward emission of particle 1, respectively. For the $\alpha+^{12}C\rightarrow p+p+^{14}C^*$ reaction this results in slightly different angles in ^{2}He emission.

The analysis of the correlation data depends on the type of information one wants to extract. If the major interest of the measurement concerns nuclear structure information of the residual nucleus, for instance, from sequential breakup (see Sec. IV.B) the so-called total kinetic energy spectra (TKE) equal to E_1+E_2 are created. These spectra can be considered as a projection of the data onto a line perpendicular to the straight loci of constant Q value. In the case of the detection of ^{2}He ($m_1=m_2$) this line is the diagonal ($E_1=E_2$) in the E_2 vs E_1 diagram. Due to the fact that the loci are to a good approximation straight lines these energy spectra show a good energy resolution. An example of such a projected energy spectrum is shown in Fig. 6 for the one neutron transfer reaction ^{28}Si(^{3}He,^{2}He)^{29}Si at $\theta=15°$ and $E_{^3He}$=52 MeV (van Driel, Kamermans, de Meijer, and Dieperink, 1980). The resulting energy resolution full width at half maximum (FWHM) equal to 250 keV, for small ε values, is hardly affected by the curvature of the kinematic loci but is mainly determined by energy straggling in the target and kinematical broadening due to the angular range which is accepted by the finite opening angles of the counter telescopes. In general, a better energy resolution will be obtained by calculating the Q-value spectrum from Eq. (2.8).

Some care must be taken in the interpretation of the TKE or Q-value spectra especially in the low-energy continuum part. This is illustrated by Fig. 7 (de Meijer *et al.*, 1983). The shape of the proton energy spectrum [Fig. 7(c)] seems to be in contrast with the TKE spectrum at the lowest energies [Fig. 7(b)]. This apparent discrepancy is simply due to the fact that the projection path at lower energies is much shorter than at, e.g., TKE equal to 30 MeV. The relative energy range that can contribute to low TKE values is reduced due to phase-space limitation in the E_1,E_2 plane.

A major drawback of this type of analysis is the fact that no information on the relative-energy distribution is obtained. Therefore, the use of this projection technique is quite limited; for the investigation of the final-state interaction in the intermediate state another way of analyzing the data has been employed. A given locus in the two-dimensional diagram indicates that E_1 and E_2 are dependent quantities and hence that no information is lost

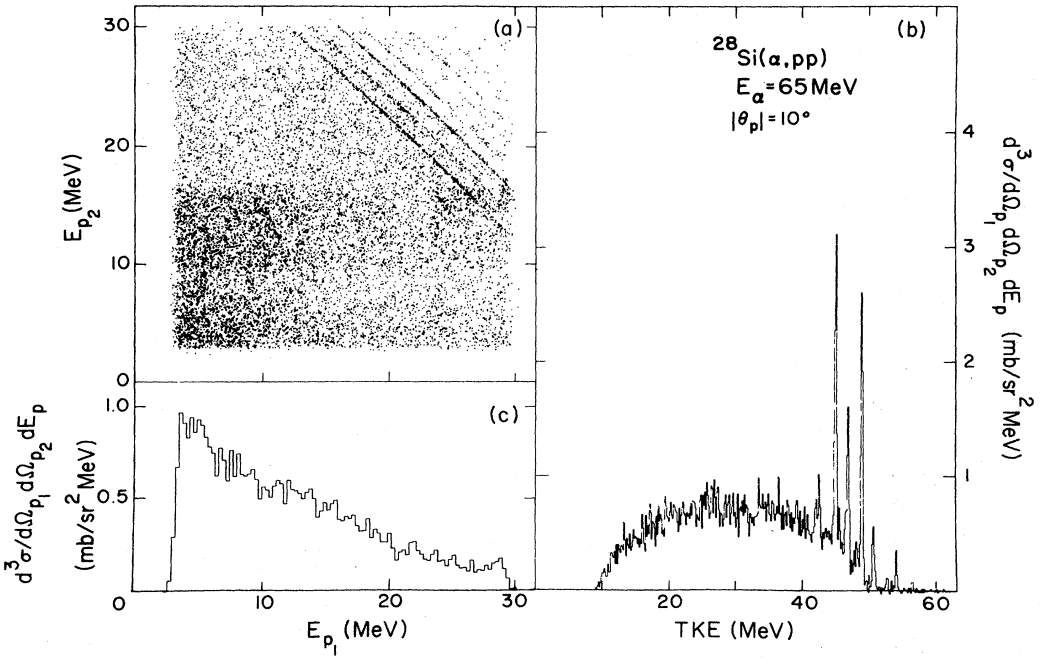

FIG. 7. The effect of phase-space limitations in the E_1,E_2 plane on the total kinetic energy spectrum (de Meijer *et al.*, 1983).

when the data are projected onto either the E_1 or the E_2 axis. Such projections provide detailed information on the relative-energy distribution along the locus and consequently on the intermediate state the reaction goes through. Figure 8 shows an example for correlated proton emission in the ^{13}C(^{3}He,^{2}He)^{14}C reaction to the $E_x=6.73$ MeV state. The data clearly reveal a structure consisting of two bumps. As indicated in Fig. 8, this structure corresponds to an intermediate state in the $(p+p)$ system, namely, the $^1S_0$ state of ^{2}He (see also Sec. IV.A.5). Note that the ε is a nonlinear function of E_{p_1}. The curves in the figure are the results of calculations discussed in Sec. IV.A.5. This way of presenting the data is also the most commonly used technique in the analysis of direct-breakup processes for which there is no clear energy correlation between the two emitted particles. The projection, however, of (part of) the two-dimensional diagram onto one of the axes gives information on the underlying reaction mechanisms (see Sec. V).

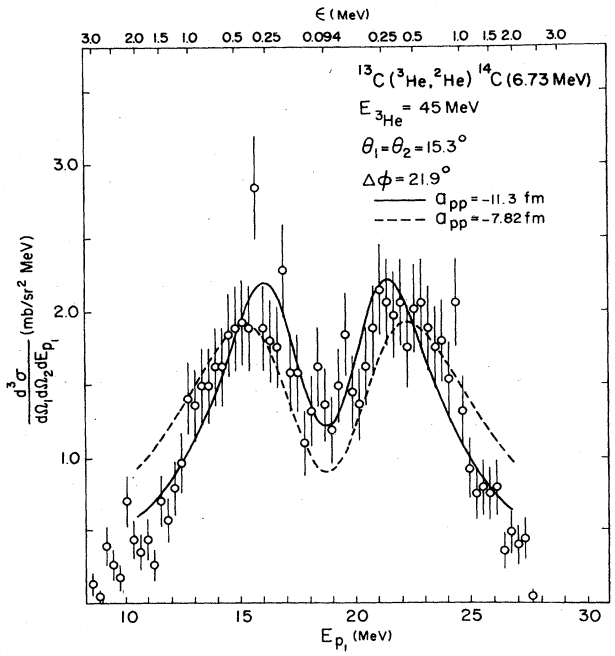

FIG. 8. Relative-energy distribution of the two protons emitted in the ^{13}C(^{3}He,^{2}He)^{14}C reaction. The nonlinear ε distribution is also shown. The curves are discussed in Sec. IV (after Stahel, 1979).

An alternative approach for deducing the relative-energy spectra in sequential breakup is to calculate ε from Eq. (2.10). The major contribution to the ε resolution is the accuracy with which the angle $\theta_{1\text{-}2}$ can be determined. Only a few experiments have been performed with a very narrow collimation system (e.g., Stahel, 1979) due to the drawback of the considerably reduced count rate. The best way is of course to measure the angle with position-sensitive detectors. For light-ion–induced reactions the thickness of the available position-sensitive detectors is insufficient to stop the protons; therefore to our knowledge, this technique has been applied only in heavy-ion reaction studies (e.g., van Driel, Gonggrijp *et al.*, 1981; Rae *et al.*, 1981).

It is worthwhile to mention at this point a recently introduced way to present the data from heavy-ion reaction studies (Ho *et al.*, 1980). Correlation data are transformed in Galilean invariant "velocity plots." These are contour plots of the triple differential cross section $d^3\sigma/d\mathbf{v}^3_{1_{\text{lab}}}$ in the plane subtended by any two of the $\mathbf{v}_{1_{\text{lab}}}$

components, having a constraint on the velocity vector distribution of particle 2. Although these plots have not yet been used in the analysis of light-ion breakup reactions, they may be useful in order to extract the emission source of the light particle (Ho *et al.*, 1981).

In the analysis or interpretation of the experimental results one has to convert the data to the appropriate c.m. system. For the sequential breakup of the 12* system the transformation will be made to the systems in which the interactions take place: the 3-12 and the 1-2 system. The first one represents the c.m. system for the reaction $a+A\rightarrow 12^*+3$ and the second one is the c.m. system for the decay. The relation for both systems relative to the laboratory coordinates are presented in Fig. 9. On the other hand, calculations for direct breakup, carried out in the c.m. system for which the T matrix is defined, are in general transformed to the laboratory system. For sequential breakup the six variables measured in a two-detector coincidence experiment have to be transformed to the six variables describing the relative and center-of-mass motion of the two fragments. These transformations are easily obtained by calculating the Jacobian J. These transformations have been worked out by, e.g., Ohlsen (1965) and more recently by Fuchs (1982). As pointed out by Fuchs, the transformation of the laboratory system to the 3-12,1-2 system presented by Ohlsen yields the correct answer despite an erroneous derivation (Fuchs, 1982).

We will apply their results for the sequential breakup, assuming that several loci in the E_1 vs E_2 plane can be observed. In this situation only one E_i is an independent variable. This means that all information contained in the density distribution along the locus will be conserved in a projection of the events in the locus onto, e.g., the E_1 axis. The experimental cross section obtained from the projection may be transformed to the 3-12,1-2 system by

$$\frac{d^3\sigma}{d\Omega_1 d\Omega_2 dE_1}=J\frac{d^3\sigma}{d\Omega_{3\text{-}12}d\Omega_{1\text{-}2}d\varepsilon}\ , \tag{2.11}$$

where $d\Omega_{1\text{-}2}$ is the solid angle of the relative motion of 1 and 2 with respect to their centers of mass and $d\Omega_{3\text{-}12}$ the solid angle of the c.m. system 12 with respect to the c.m. system 123 of the total reaction (see Fig. 9). The Jacobian J for this transformation is given by (Fuchs, 1982)

$$J=\frac{\partial(\Omega_{3\text{-}12},\Omega_{1\text{-}2},\varepsilon)}{\partial(\Omega_1,\Omega_2,E_1)}$$
$$=\frac{1}{p_{3\text{-}12}\mu_{3\text{-}12}\mu_{1\text{-}2}p_{1\text{-}2}}\frac{m_1m_2m_3p_1p_2}{m_2+m_3+\dfrac{m_2(\mathbf{p}_1-\mathbf{P})\cdot\mathbf{p}_2}{p_2^2}} \tag{2.12}$$

with the reduced masses $\mu_{1\text{-}2}=m_1m_2/m_1+m_2$ and $\mu_{3\text{-}12}=m_3(m_1+m_2)/m_1+m_2+m_3$, and $p_{3\text{-}12},p_{1\text{-}2}$ the associated momenta. $\mathbf{P}$ is the total momentum.

As for reactions with bound ejectiles one might like to deduce from the observed cross section $d^3\sigma/d\Omega_1 d\Omega_2 dE_1$ the differential cross section $d\sigma/d\Omega_{3\text{-}12}$ for the unbound

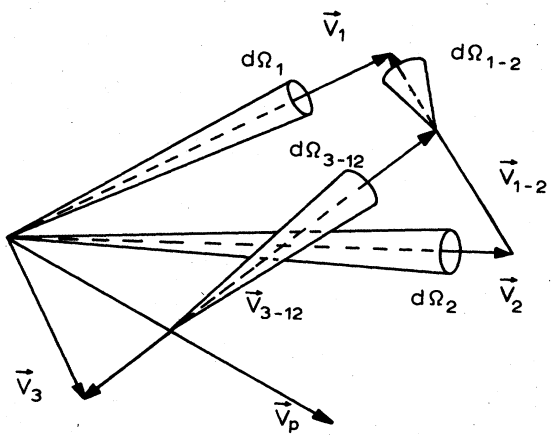

FIG. 9. Relation between the measured quantities in the laboratory system ($\mathbf{v}_1$, $d\Omega_1$, $\mathbf{v}_2$, $d\Omega_2$) and the quantities in the (1-2) and (3-12) systems (see text). Note the asymmetry in the definition for velocities and solid angles. $d\Omega_{1\text{-}2}$ denotes the solid angle of particle 1 with respect to the center of mass of the (1-2) system, whereas $\mathbf{v}_{1\text{-}2}$ describes the relative motion of particle 1 with respect to particle 2.

system 12*. After the transformation to the 3-12,1-2 system [Eq. (2.11)] one integrates over $d\Omega_{1\text{-}2}$ and ε. If the angular distribution of the breakup remnants is isotropic in their own c.m. system (e.g., the proton and triton from the decay of the $J^\pi=0^+$; $E_x=20.1$ MeV state in ^{4}He or both protons of ^{2}He in a relative S state) the integration over $d\Omega_{1\text{-}2}$ can easily be performed, yielding

$$\frac{d^2\sigma}{d\Omega_{3\text{-}12}d\varepsilon}=\frac{4\pi}{J}\frac{d^3\sigma}{d\Omega_1 d\Omega_2 dE_1}\ . \tag{2.13}$$

Due to the fact that experimentally only a limited relative energy range can be observed ($\varepsilon_1,\varepsilon_2$), the differential cross section reads

$$\frac{d\sigma}{d\Omega_{3\text{-}12}}=\int_{\varepsilon_1}^{\varepsilon_2}\frac{4\pi}{J}\frac{d^3\sigma}{d\Omega_1 d\Omega_2 dE_1}d\varepsilon\ . \tag{2.14}$$

In a few cases this process is considered a simple two-step process with two-body kinematics for the (12)* formation. An effective solid angle of the detection system for a given relative energy is then calculated and absolute experimental cross sections can be extracted. This procedure, which originates from studies with ^{8}Be in the exit channel (Wozniak *et al.*, 1976), has for He-induced reactions been applied only in order to obtain absolute cross sections in the (α,α^*) reaction (Kamermans *et al.*, 1979) and will not be discussed in detail.

B. Phase-space aspects

In this paper the experimental results on both sequential and direct breakup are compared with calculations in the framework of direct reaction theory. According to Fermi's golden rule, the transition probability per unit time for a system going from an initial (i) to a final state

(f) is given in first-order perturbation theory by

$$W_{fi}=\frac{2\pi}{\hbar}\,|\,T_{fi}\,|^2\rho\ , \tag{2.15}$$

where $T_{fi}=\langle f\,|\,V\,|\,i\,\rangle$ is the matrix element of the perturbation operator V (see also Sec. VI.B) that causes the transition and ρ the (momentum) phase-space factor which represents the number of final states per energy interval. The reaction cross section follows from Eq. (2.15) as

$$d\sigma=\frac{2\pi}{\hbar}\frac{\mu_i}{p_i}\,|\,T_{fi}\,|^2\rho\ , \tag{2.16}$$

with μ_i and p_i being the reduced mass and momentum in the incident channel, respectively. For two-body kinematics the phase-space factor in standard notation is given by

$$\rho=\frac{d\mathbf{p}_f}{dE_f(2\pi\hbar)^3}=p_f\mu_f d\Omega_f/(2\pi\hbar)^3\ . \tag{2.17}$$

This leads to the well-known expression of the differential cross section:

$$\frac{d\sigma}{d\Omega_f}=\frac{\mu_i\mu_f}{(2\pi\hbar^2)^2}\frac{k_f}{k_i}\,|\,T_{fi}\,|^2\ . \tag{2.18}$$

The phase-space factor for sequential breakup of the (12)* intermediate state in the 3-12 system can be written as (Stahel, 1979)

$$\rho=\frac{d\mathbf{p}_{3\text{-}12}d\mathbf{p}_{1\text{-}2}}{d\varepsilon(2\pi\hbar)^6}$$

$$=p_{3\text{-}12}\mu_{3\text{-}12}p_{1\text{-}2}\mu_{1\text{-}2}d\Omega_{3\text{-}12}d\Omega_{1\text{-}2}d\varepsilon/(2\pi\hbar)^6\ . \tag{2.19}$$

Therefore, the triple differential cross section for sequential breakup reads

$$\frac{d^3\sigma}{d\Omega_{3\text{-}12}d\Omega_{1\text{-}2}d\varepsilon}=\frac{\mu_i\mu_{3\text{-}12}}{(2\pi\hbar^2)^2}\frac{k_{3\text{-}12}}{k_i}\,|\,T_{fi}\,|^2\frac{\mu_{1\text{-}2}p_{1\text{-}2}}{(2\pi\hbar)^3}\ . \tag{2.20}$$

The phase-space factor for direct breakup has been evaluated by several authors (see, e.g., Ohlsen, 1965; Baur *et al.*, 1976; Fuchs, 1982). For a given Q value this leads to

$$\rho(E_1)dE_1d\Omega_1d\Omega_2=\frac{h^{-6}m_1m_2m_3p_1p_2}{(m_2+m_3)+m_2\dfrac{(\mathbf{p}_1-\mathbf{P})\cdot\mathbf{p}_2}{p_2^2}}$$

$$\times dE_1d\Omega_1d\Omega_2\ . \tag{2.21}$$

Note that the cross-section calculations require the evaluation of T_{fi} for three final particles. Because this is not incorporated in existing reaction models, one is forced to make some approximations. The reduction to a calculation of a two-particle matrix element is performed both in the description of sequential breakup as in direct breakup and will be discussed in Secs. IV and VI, respectively. It is important to remark that the reactions discussed in this paper are limited to the class with three particles in the final state. However, at higher energies and especially with increasing projectile mass, multiparticle processes will occur, which will require the evaluation of phase-space factors for more than three particles in the final state. This extremely complex problem was already attacked by high-energy physicists some decades ago in the description of multipion production (e.g., Block, 1956). We foresee that in the near future, the interest of nuclear physicists for this problem will strongly increase, especially in the field of intermediate-energy heavy-ion physics.

III. EXPERIMENTAL SETUPS

Breakup processes induced by ^{3}He and ^{4}He beams have been investigated over a wide range of incident energies and target nuclei. Experimental data for ^{3}He exist in the energy range between 8 MeV (Bohne *et al.*, 1970) and 130 MeV (Bojowald *et al.*, 1981; Djaloeis *et al.*, 1983). Reaction studies with α particles have been performed between 55 MeV (Stahel, 1979) and 175 MeV (Budzanowski *et al.*, 1979). In studies which are based on a systematic approach, reactions on a large variety of target nuclei ranging from ^{12}C sometimes up to ^{208}Pb (e.g., Budzanowski *et al.*, 1979; Stahel, 1979; van Driel, Kamermans, and de Meijer, 1980) have been measured.

The common feature of all these experiments is the requirement that highly energetic light particles (p,d,t) have to be detected. Therefore, rather thick targets can be tolerated. In general, target thicknesses are in the order of a few mg/cm^2. Beam currents are essentially limited by the maximum tolerable count rate in the ΔE counters. The count rate predominantly originates from elastically scattered ^{3}He or ^{4}He particles.

Both in the inclusive experiments and in the kinematically complete correlation measurements relatively simple detection systems have been employed. The detector telescopes consist of up to four counters (Budzanowski *et al.*, 1979), in which the signal of the last detector is often used to reject particles which have traversed all the other detectors. For the detection at the lower incident energies conventional Si detectors with various thicknesses are the constituents of the detector systems (e.g., Jahn, Wozniak *et al.*, 1976; Congedo *et al.*, 1980; van Driel, Kamermans, de Meijer, and Dieperink, 1980; van Driel, Kamermans, and de Meijer, 1980). At higher energies the particles (especially the protons) cannot be stopped in commercially available Si detectors (thicknesses $\lesssim 5$ mm). For these higher energies a combination is employed of Si detectors with Ge detectors and/or of Si detectors with NaI(Tl) detectors (Budzanowski *et al.*, 1979; Wu *et al.*, 1979; Matsuoka *et al.*, 1980; Koeslag *et al.*, 1983). The advantage of the use of Ge detectors compared to NaI(Tl) crystals is the better energy resolution. The Ge detectors, however, have to be cooled to liquid-nitrogen temperature, which complicates the experimental setup.

In He-induced reactions neutrons have been detected only in one isolated case. In order to investigate the

(^{3}He,$\vec{d}$) reaction via the breakup of the $\vec{d}$ ($J=0$, $T=1$) in a proton and a neutron (Janetzki *et al.*, 1976), the neutrons were detected in a liquid scintillator (NE213). In this experiment the energy of the neutrons was deduced from the flight time over 1 m. In this p-n correlation measurement one has the unique possibility to detect both emitted particles at relative angle $\theta_{1\text{-}2}=0°$.

There is little advantage in the use of magnetic spectrographs for the investigation of unbound ejectiles (Aarts *et al.*, 1980). Although a high-energy resolution can be achieved, the momentum bite covered in one field setting is often too small to be of any value for the reaction studies discussed in this paper. Furthermore, it is applicable only to the decay into two identical particles.

A major point of interest for kinematically complete experiments with three particles in the final state, is the geometry of the two-particle detection setup. For the study of sequential breakup, in-plane and out-of-plane detector geometries have been employed. In order to obtain nuclear structure information one has to measure angular distributions of the unbound ejectile, which means that data have to be taken at different angles with respect to the incoming beam while keeping the relative angle between the two emitted fragments fixed. This can be achieved in-plane (Janetzki *et al.*, 1976) or by placing the two detector telescopes at a fixed out-of-plane angle (see Fig. 10) (Jahn, Wozniak *et al.*, 1976; Jahn, Stahel *et al.*, 1976; van Driel, Kamermans, de Meijer, and Dieperink, 1980; van Driel, Kamermans, and de Meijer, 1980). This last concept originates from earlier ^{8}Be studies and was introduced for the He-induced breakup reactions by Jahn, Wozniak *et al.* (1976). The out-of-plane geometry has been used most frequently in a large number of sequential decay experiments (e.g., Jahn, Wozniak *et al.*, 1976; Jahn, Stahel *et al.*, 1976; de Meijer *et al.*, 1977; Kamermans *et al.*, 1979; Stahel, 1979; van Driel, Kamermans, de Meijer, and Dieperink, 1980; van Driel, Kamermans, and de Meijer, 1980). Such a setup with a large vertical opening angle has the advantage that a relatively large opening angle can be combined with a limited spread in the horizontal emission angle. With such a geometry the effects of kinematical broadening on the energy resolution are reduced. Moreover, with this setup one can measure at extremely small emission angles, even at zero degrees, for ejectiles that break up symmetrically (van Driel, Kamermans, and de Meijer, 1980).

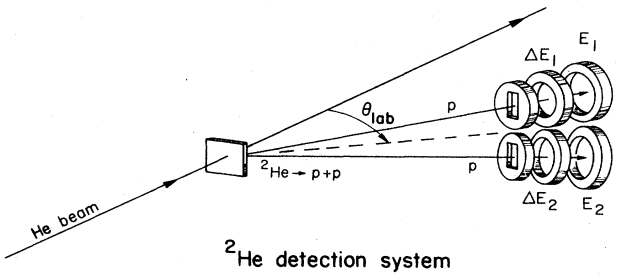

FIG. 10. Schematic drawing of a ^{2}He detection system (van Driel, Kamermans, de Meijer, and Dieperink, 1980; van Driel, Kamermans, and de Meijer, 1980).

For studies of the final-state interaction (FSI) between the two breakup fragments in the decay stage of the sequential breakup process, measurements of the dependence on the relative angle between the breakup products at one (or a few) fixed emission angle(s) of the composite system have been performed. These experiments have been carried out for in-plane (van Driel, Kamermans, de Meijer, and Dieperink, 1980) and out-of-plane (Congedo *et al.*, 1980) geometries. Both measurements concern the FSI of ^{2}He studied in the (^{3}He,^{2}He) reaction, where for the in-plane geometry at a fixed angle $\theta_{^2\text{He}}=20°$ the relative angle between the two protons was varied between 8.6° and 20.6°. In the out-of-plane setup a much larger relative angular range (between 5° and 170°) could be covered.

The main requirement for the two detector telescopes in correlation experiments of direct breakup studies is that a wide angular range on both sides of the beam direction can be covered. Only in this way, as will be discussed extensively in Sec. V, may the different reaction processes contributing to the inclusive spectra be identified. Data acquisition in the exclusive experiments is normally performed on an event-by-event basis. This enables the construction of two-dimensional spectra, which is a necessary prerequisite for the full three-body kinematical treatment of the primary data. Examples of such an analysis are the construction of relative-energy spectra from the measured ejectile energies and emission angles, and the calculation of Q-value spectra for systems where the loci of constant Q value are not completely straight.

IV. SEQUENTIAL BREAKUP

A. Description of sequential breakup processes

1. Introduction

In sequential breakup reactions a distinct separation is assumed between the production process of the unbound ejectile and its subsequent decay. This means that the properties of the breakup remnants are independent of the formation process; they are determined by the unbound system itself. In general this process will take place if the decay occurs outside the (nuclear) interaction region of the nucleus. The Coulomb interaction is considered to be of minor importance in this respect, since its corresponding wavelength is much longer than the distance between the two participants in the breakup. Therefore, the question whether sequential breakup will occur is directly related to the question whether the half-life of the unbound ejectile is long compared to the nuclear reaction time. For particles with a long half-life like ^{8}Be (3×10^{-16} s) it is well known by now that analysis of the data can be done with standard reaction theory (Wozniak *et al.*,

1976). For laboratory energies in the order of 10–20 MeV per nucleon, ejectiles in a state with a width of 1 MeV will decay at a distance of 5–10 fm from the production area. So also for ^{2}He or the deuteron in the singlet state, one expects these reactions to take place in two independent steps. In this paper the first step will be governed by standard distorted-wave Born approximation (DWBA), whereas the second part is described in the framework of a final-state interaction (FSI). This separation is a relatively old problem that has been addressed by several groups (e.g., Cohen *et al.*, 1967; Henley and Lacey, 1967; Bohne *et al.*, 1970; Congedo *et al.*, 1980). For instance, Henley and Lacey (1967) have published a zero-range DWBA calculation of the (^{3}He, *pp*) reaction for two extreme cases: (i) the two protons are strongly correlated; their final-state interaction is taken into account explicitly, whereas their interaction with the nucleus is approximated by the interaction between the residual nucleus and the center of mass of the two protons (sequential breakup); (ii) the protons interact with the residual nucleus individually whereas their mutual interaction is neglected (nonsequential breakup).

The strong similarity between the angular distributions observed in (α,^{2}He) and (α,*d*) reactions and the early successes of straightforward DWBA calculations of the (α,^{2}He) reaction (de Meijer *et al.*, 1977), using a deuteron optical model potential for the ^{2}He exit channel, stimulated the research of sequential breakup processes. It was hoped that, in addition to obtaining information on the reaction mechanism (e.g., the validity of the separation of the formation and decay process), a powerful tool could be developed for nuclear structure research.

In this section a DWBA description will be presented of one- and two-nucleon transfer reactions and inelastic scattering. From the reaction mechanism point of view, the one-nucleon transfer reaction is the most extensively studied process, in which via the absolute normalization also information on the final-state interaction has been obtained.

The sequential breakup reaction may be written as

$$a+A\rightarrow B+b\rightarrow B+x+y\ , \tag{4.1}$$

where b is the unbound ejectile which decays into particles x and y. Assuming that the outgoing channel can be described by an optical model potential acting on the c.m. coordinates of the unbound ejectile only [the so-called (**R**,**r**) formalism given by Henley *et al.* (1967)], we can write the DWBA cross section as [see Eq. (2.18) or Jackson (1970) for the notation]

$$\frac{d^2\sigma}{d\Omega_f d\varepsilon}=\frac{\mu_f\mu_i}{(2\pi\hbar^2)^2}\frac{k_f}{k_i}\,|\,T_{fi}^{\mathrm{DW}}(\varepsilon)\,|^2\ . \tag{4.2}$$

The transition amplitude $T_{fi}^{\mathrm{DW}}(\varepsilon)$, which is dependent on the relative energy of the breakup fragments x and y, is given by

$$T_{fi}^{\mathrm{DW}}(\varepsilon)=\sqrt{\rho(\varepsilon)}\int d\mathbf{r}_i d\mathbf{r}_f \chi^{(-)}(\mathbf{k}_f,\mathbf{r}_f) \times\langle\psi_B\varphi_b(\varepsilon)\,|\,V\,|\,\psi_A\varphi_a\rangle\chi^{(+)}(\mathbf{k}_i,\mathbf{r}_i)\ . \tag{4.3}$$

With κ being the relative momentum between the two breakup fragments, the phase-space factor is simply given by $\rho(\varepsilon)=\mu\hbar\kappa/(2\pi\hbar)^3$. The form factors appearing in Eq. (4.3) for one- and two-nucleon transfer reactions and for inelastic scattering will be discussed in the next three sections separately. In Eq. (4.3) $\chi^{(-)}$ represents the outgoing wave function of the unbound ejectile. Such a wave function follows from the optical model parameters; in the case of ^{2}He a set of deuteron optical model parameters was successfully used (de Meijer *et al.*, 1977; van Driel, Kamermans, de Meijer, and Dieperink, 1980; van Driel, Kamermans, and de Meijer, 1980).

The formalism presented in this section is in principle applicable only for the description of transitions leading to bound states in the final nucleus B. Some of the examples given in this paper and in its references are transitions to unbound states. However, the absolute magnitude of the cross section was found to be mainly determined by the width of these resonance states (Vincent and Fortune, 1970). Therefore, if the width of the resonance is sufficiently small, the cross section may be approximated by the cross section on the resonance. Moreover, for sequential breakup no systematic deviations in the description of the shape and the absolute magnitude between transitions to bound and unbound states have been observed (van Driel, Kamermans, de Meijer, and Dieperink, 1980; van Driel, Kamermans, and de Meijer, 1980).

In principle, the methods that will be discussed here are also applicable to heavier ejectiles like ^{14}N* and ^{16}O*, as observed in heavy-ion reactions (Rae *et al.*, 1981; van Driel, Gonggrijp *et al.*, 1981). Many simplifications, however, like the zero-range approximation, can no longer be made.

2. One-nucleon transfer reactions

The form factor for one-nucleon transfer, e.g., the (^{3}He,^{2}He) reaction, can be expressed as (van Driel, Kamermans, de Meijer, and Dieperink, 1980)

$$\sqrt{\rho(\varepsilon)}\langle\psi_B\varphi_{^2\mathrm{He}}(\varepsilon)\,|\,V_{^2\mathrm{He},n}\,|\,\psi_A\varphi_{^3\mathrm{He}}\rangle=[C^2S\rho(\varepsilon)]^{1/2}\varphi_B^*(\mathbf{r}_n)\int d\xi\,\varphi_{^2\mathrm{He}}^*(\xi,\varepsilon)V(\mathbf{r},\xi)\varphi_{^3\mathrm{He}}(\mathbf{r},\xi) \equiv(C^2Sc^2{}_S)^{1/2}\varphi_B^*(\mathbf{r}_n)D(\mathbf{r},\varepsilon)\ , \tag{4.4}$$

where ξ is the internal coordinate of ^{2}He, **r** the coordinate of the neutron relative to the ^{2}He center of mass and $\varphi_B(\mathbf{r}_n)$ the bound-state wave function of the transferred neutron. The factor C^2S is the usual spectroscopic factor and c^2s is the

light-particles spin-isospin coupling constant. All the ε dependence of the transition-matrix element is contained in $D(\mathbf{r},\varepsilon)$. Assuming in ^{3}He an $l=0$ motion for the neutron relative to the two-proton center of mass (Bassel, 1966) and applying the zero-range approximation, $D(\mathbf{r},\varepsilon)=D_0(\varepsilon)\delta(\mathbf{r})$, we can reduce the six-dimensional integral to two three-dimensional ones in the usual way. Comparing Eqs. (4.2)—(4.4) with the differential cross section calculated by a standard DWBA code as DWUCK4 (Kunz, 1974) gives

$$\frac{d^2\sigma^{lsj}}{d\Omega_f d\varepsilon}=N(\varepsilon)C^2S^{lsj}\sigma^{lsj}_{\mathrm{DWUCK}}(\varepsilon,\theta)\ . \tag{4.5}$$

The normalization function depends on the relative energy:

$$N(\varepsilon)=10^{-4}c^2s\rho(\varepsilon)\langle\varphi_{^2\mathrm{He}}(\varepsilon)\,|\,V_{^2\mathrm{He},n}\,|\,\varphi_{^3\mathrm{He}}\rangle^2=10^{-4}c^2sD_0^2(\varepsilon)\ . \tag{4.6}$$

The $\sigma^{lsj}_{\mathrm{DWUCK}}$ depends on the relative energy in two ways. First, a trivial dependence via the reaction Q value, because the kinetic energy available in the exit channel is determined not only by the two-body reaction Q value, but also by the energy going into the relative motion of both breakup fragments. Second, the interaction in the exit channel, approximated by an optical model description, will also depend on this relative energy. Normally, an ε-independent deuteron optical model potential has been used for the interaction in the ^{2}He exit channel. For the real part of this potential, the validity of this assumption has been investigated by a folding-model calculation (van Driel, Kamermans, de Meijer, and Dieperink, 1980), following the method of Watanabe (1958) and Johnson and Soper (1970,1972). Since the ^{2}He wave function extends to infinity, a reasonable cutoff radius ($r_{\max}$) has to be chosen. For ^{2}He with proton energies E_{p_1} and E_{p_2}, respectively, one obtains

$$V_{^2\mathrm{He}}(\mathbf{R},\varepsilon)=\int_0^{r_{\max}}d\xi\,\varphi^*_{^2\mathrm{He}}(\varepsilon,\xi)[V_p(E_{p_1},\mathbf{R}+\tfrac{1}{2}\xi)+V_p(E_{p_2},\mathbf{R}-\tfrac{1}{2}\xi)]\varphi_{^2\mathrm{He}}(\varepsilon,\xi)\rho(\varepsilon)\ , \tag{4.7}$$

with E_{p_1} and E_{p_2} given by

$$E_{p_1,p_2}=\tfrac{1}{2}[E_{^2\mathrm{He}}+\varepsilon\pm2\cos\varphi(E_{^2\mathrm{He}}\varepsilon)^{1/2}]\ , \tag{4.8}$$

where φ is the angle between ξ and $\mathbf{R}$ and $E_{^2\mathrm{He}}$ is the c.m. energy of the two protons. For the nucleon-nucleus potential the parametrization according to Perey and Perey (1976) has been taken. This type of folding potential has been used in the analysis of the (^{3}He,^{2}He) (van Driel, Kamermans, de Meijer, and Dieperink, 1980) and the (α,^{2}He) reactions (van Driel, Kamermans, and de Meijer, 1980). A comparison between the behavior of the folding optical model potential and the deuteron optical model potential shows only a small (10%) difference in the absolute cross section and no noticeable change in the fits of the angular distribution data for single-nucleon transfer. At least for the cases investigated, the use of the deuteron optical model parameters for the ^{2}He exit channel seems justified. The fact that the ε dependence of the DWBA cross section was found to be small has the important consequence that *relative* spectroscopic factors can be deduced in a simple way. This is illustrated for the ^{28}Si(^{3}He,^{2}He)^{29}Si reaction at $E_{^3\mathrm{He}}=52$ MeV in Fig. 11 (van Driel, Kamermans, de Meijer, and Dieperink, 1980). For different relative-energy bites (different β's) the relative yields and so spectroscopic factors of seven peaks are, within experimental uncertainties, the same.

So far, the discussion of the description of sequential-breakup processes has been limited to zero-range DWBA, which was justified, since the main component of the ejectile wave function (d or ^{2}He) is an s wave. However, some experimental work has been published on unbound Li nuclei as ejectiles in α-induced pickup (Saha *et al.*, 1978). In particular, the (α,^{5}Li) proton pickup reaction has been studied at $E_\alpha=65$ MeV for the target nuclei ^{12}C and ^{24}Mg. In this case the main component in the ejectile (^{5}Li) wave function is a p wave, which requires a DWBA calculation in full finite range. In the post formalism the interaction between the transferred proton and the α particle gives the necessary convergence factor, which allows the integrations to be done by the usual techniques (Kunz *et al.*, 1979). Analyzing the ^{12}C(α,^{5}Li)^{11}B reaction at $E_\alpha=65$ MeV, Kunz *et al.* found a rather good agreement for the relative-energy dependence of the cross section (Kunz *et al.*, 1979).

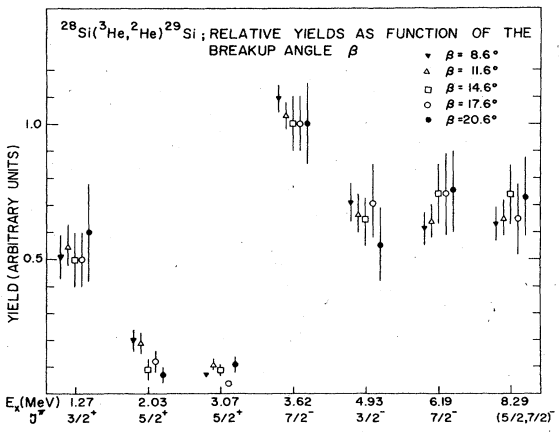

FIG. 11. Relative yields of seven transitions normalized such that the sum of these yields is the same at each of the five measurements (van Driel, Kamermans, de Meijer and Dieperink, 1980).

3. Two-nucleon transfer reactions

The more complicated DWBA description of two-nucleon transfer with an unbound ejectile has been worked out only for the $(\alpha,{}^2\text{He})$ reaction. The transition amplitude for two-nucleon transfer reactions can be factorized into a part containing the nuclear structure information and a part that depends on the kinematics of the reaction (Glendenning, 1965). All structure information will be contained in the factor G that depends on the wave functions of the target and the final level in the residual nucleus. The factor G is equivalent to the spectroscopic amplitude S used in single-nucleon transfer. The kinematical part therefore describes the transfer amplitude of a structureless nuclide into the orbital state N,L of a structureless residual nucleus, resulting in a normalized bound-state cluster wave function U. The form factor appearing in Eq. (4.3) can—for example, for the $(\alpha,{}^2\text{He})$ reaction—be expressed as

$$\sqrt{\rho(\varepsilon)}\langle\varphi_B\varphi_{^2\text{He}}(\varepsilon)\,|\,V_{^2\text{He},2n}\,|\,\psi_A\varphi_\alpha\rangle=\sum_{NL}[C^2\rho(\varepsilon)]^{1/2}U^*_{NL}(\mathbf{R})G_{NLSJT}\int d\xi\int d\eta\,\varphi^*_{^2\text{He}}(\varepsilon)V(\mathbf{r},\xi,\eta)\varphi_\alpha(\mathbf{r},\xi,\eta)$$
$$\equiv\sum_{NL}(C^2c^2s)^{1/2}U^*_{NL}(\mathbf{R})G_{NLSJT}D(\mathbf{r},\varepsilon)\ . \tag{4.9}$$

The phase-space factor $\rho(\varepsilon)=\mu\hbar\kappa/(2\pi\hbar)^3$ with κ the relative momentum between the two protons. ξ is the internal coordinate of the ^{2}He, η the internal coordinate of the two neutrons, $\mathbf{r}$ the relative coordinate of the two-proton and two-neutron centers of mass in the α particle, and $\mathbf{R}$ the coordinate of the c.m. of the two transferred neutrons. Since the quantum indices N, L, S, J, and T refer to the transferred neutron pair, the actual values for S and T are 0 and 1, respectively, and consequently $J=L$. The factors C^2 and c^2s are the heavy-particle isospin Clebsch-Gordan and the light-particle spin-isospin coupling constants, respectively. All ε dependence of the transition-matrix element is again contained in $D(\mathbf{r},\varepsilon)$. Assuming $L=0$ motion for the neutron pair in the α particle and applying the zero-range approximation the six-dimensional integral can be simplified in the same way as in Sec. IV.A.2.

Calculations have been performed with the microscopic form-factor option of the program DWUCK4 (Kunz, 1974). By making the same assumptions as for the $(^3\text{He},{}^2\text{He})$ reaction, which are less well founded here, cross sections have been obtained for $\varepsilon=0$, and by using a deuteron optical-model parameter set to generate the outgoing ^{2}He distorted waves. It was found (van Driel, Kamermans, and de Meijer, 1980) that the use of an optical model potential derived by the folding model as described in the preceding section did slightly deteriorate the quality of the fits to the angular distributions. Although it is clear that the DWBA description for two-nucleon transfer is less satisfactory than for one-nucleon transfer, it will be shown (see Sec. IV.B.2) that valuable nuclear structure information can still be deduced from these processes.

Some experimental work has been performed on the $(\alpha,{}^{6,7}\text{Li})$ reaction (Saha *et al.*, 1978); however, no description of these pickup processes has been presented.

4. Inelastic scattering

The DWBA description of these processes was initiated by the investigation of the (α,α^*) reaction. In this reaction the α projectile is excited to its first excited state at $E_x=20.1$ MeV; $J^\pi=0^+$, whereas the target nucleus stays either in its ground state (single excitation) or is excited, too (mutual excitation) (Jahn, Stahel *et al.*, 1976; Kamermans *et al.*, 1979; van Driel, Harakeh *et al.*, 1981). The one-step excitation mechanism of both processes has been described with a microscopic calculation of the form factor using a double-folding method (Kamermans *et al.*, 1979). The general form of the inelastic form factor in a scattering system $(a+A)$ can be written as

$$F(\mathbf{R})=\langle\psi'_a(\mathbf{r}_a)\psi'_A(\mathbf{r}_A)\,|\,V(\mathbf{R}+\mathbf{r}_a-\mathbf{r}_A)\,|\,\psi_a(\mathbf{r}_a)\psi_A(\mathbf{r}_A)\rangle\ , \tag{4.10}$$

where $\psi_k(\mathbf{r}_k)$ and $\psi'_k(\mathbf{r}_k)$ are nuclear wave functions for the two nuclei in their initial and final channel, respectively, and $V(\mathbf{R}+\mathbf{r}_a-\mathbf{r}_A)$ is the nucleon-nucleon interaction between the nucleons of nuclei a and A.

If we replace the nuclear wave functions for both nuclei by transition densities given by $\rho_k(\mathbf{r}_k)=\langle\psi'_k(\mathbf{r}'_k)\delta(\mathbf{r}'_k-\mathbf{r}_k)\psi(\mathbf{r}'_k)\rangle$, the inelastic form factor becomes

$$F(R)=\int\int\rho_a(r_a)\rho_A(r_A)[Y_{L_a}(\Omega_a)Y_{L_A}(\Omega_A)]V(\mathbf{R}+\mathbf{r}_a-\mathbf{r}_A)d^3r_a d^3r_A\ . \tag{4.11}$$

This expression can be used for the description of elastic scattering, single and mutual excitation. For the description of elastic scattering, $\rho_a(r_a)$ and $\rho_A(r_A)$ are the ground-state densities for target and projectile, whereas for inelastic excitation the corresponding density is replaced by the transition density describing the excitation of the final state.

Assuming a simple microscopic structure for the states

in the residual nucleus and a transition density for the α^* deduced from inelastic electron scattering, these calculations fail to describe the unexpected strong mutual excitation observed in scattering from ^{24}Mg and ^{28}Si. Moreover, only the shape of the single excitation could be reproduced. The absolute magnitude of the differential cross section for single excitation was overestimated by almost an order of magnitude. A much better description of the experimental data can be obtained if coupled channel effects are taken into account (van Driel, Harakeh *et al.*, 1981). Since it was not possible with available coupled-channel codes to treat a reaction process that involves simultaneous excitations in both final nuclei, it was assumed that the excitation of the projectile can be considered as a loss of kinetic energy into the excitation of the total system without any dramatic modifications of the optical model geometrical parameters. Form factors used were the one proposed by Satchler for the monopole excitation (Satchler, 1972) and the normal collective one for angular momentum transfer $L \geq 2$. With these coupled-channel calculations it was possible to describe both single and mutual excitations in the same framework with parameters that were obtained from or found to be in agreement with other experiments. The results of these calculations and the comparison with the experimental data are shown in Fig. 12. This observation of strong coupled-channel effects in the description of mutual excitations has been shown to be important for the understanding of inelastic heavy-ion scattering (Bond *et al.*, 1982).

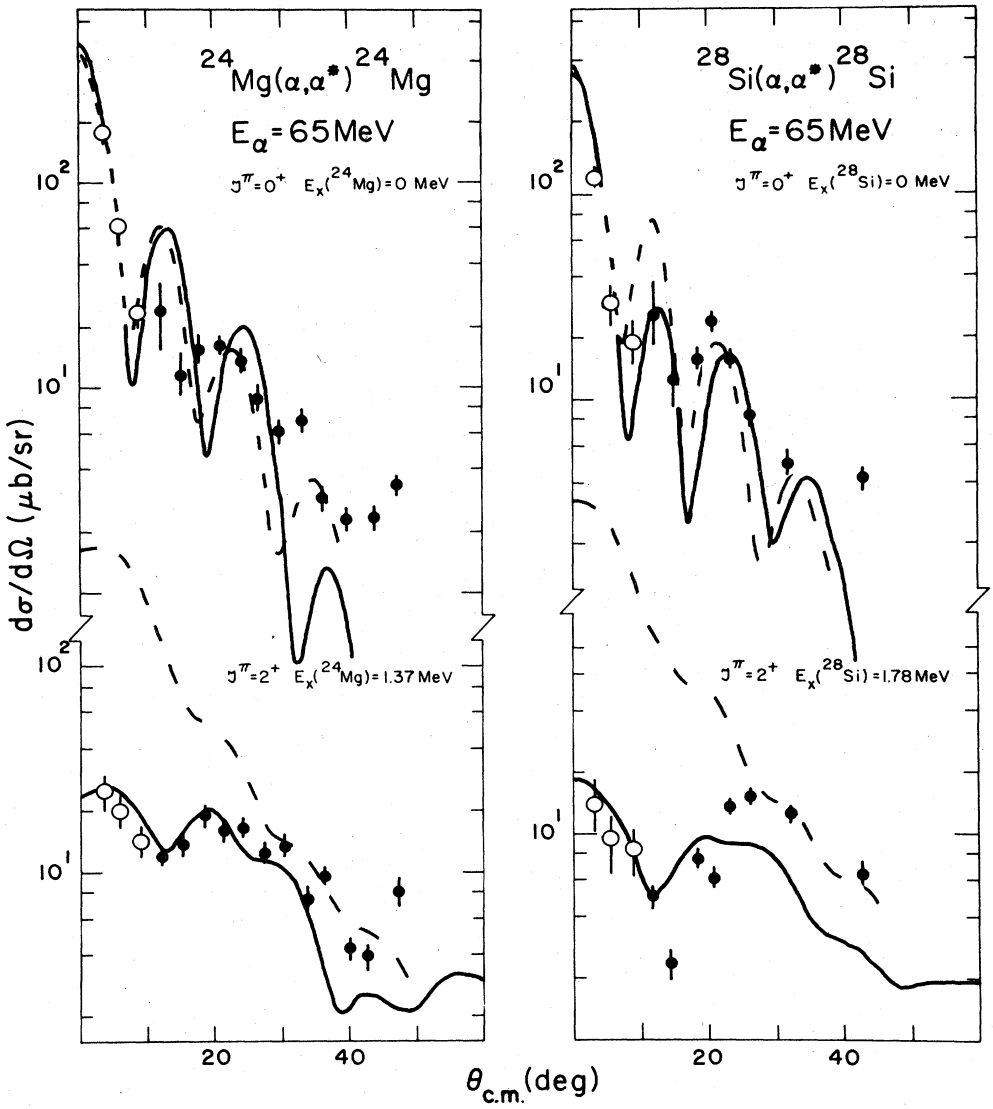

FIG. 12. Angular distributions for the ^{24}Mg$(\alpha,\alpha^*)^{24}$Mg and ^{28}Si$(\alpha,\alpha^*)^{28}$Si reactions. Data for the single and mutual excitation are shown together with the results from the CCBA calculation (solid lines) and from the microscopic folding-model calculations (dashed lines) (van Driel, Harakeh *et al.*, 1981).

5. Final-state interaction

The relative-energy spectra of the breakup remnants show an enhancement, which is due to the final-state interaction. This is clearly shown in Fig. 8 of Sec. II for the $^{13}C(^3He,^2He)^{14}C$ reaction leading to the $E_x=6.73$ MeV state in ^{14}C. The dip in this spectrum at low relative energies results from the Coulomb repulsion which is counteracting and dominating the nuclear attractive force. In this formalism the relative-energy dependence is mainly contained in the normalization function, which for the $(^3He,^2He)$ reaction is given by Eq. (4.6). The smaller effect of the dependence of the production cross section on the relative energy has already been discussed in Sec. IV.A.2.

Early calculations of the enhancement have been performed in the Watson-Migdal formalism (Watson, 1952; Migdal, 1955), and it was shown that these calculations hardly differ from the ones in which no approximations for the Coulomb wave functions have been made. However, as can be seen in Fig. 8, the experimental data are more peaked than the results of the Watson-Migdal calculations (dashed curve). Fitting the data by varying the scattering length in the Watson-Migdal formalism (solid line) results in a large effective scattering length of $a_{pp}=-11.3$ fm. Similar effects have also been observed in our analysis of the projected proton spectra from the $^{12}C(\alpha,^2He)^{14}C$ and $^{12}C(d,^2He)^{12}C$ reaction measured by Stahel (1979). These effects raise the question whether they are due to ε dependences in the calculation of the formation cross section or if we are observing a modification of the free p-p FSI due to the presence of nuclear matter. The first effect is a more or less trivial one, while the second one would indicate that the assumption of the independence of formation and decay is not valid.

Experimentally the absolute normalization constant $N(\varepsilon)$ is deduced from the data by using Eqs. (2.13) and (4.5). The calculation of the theoretical absolute normalization involves the FSI in a direct way. This requires the evaluation of an integral which contains one unbound wave function. For light-ion–induced single-nucleon transfer reactions with bound particles in the outgoing channel a similar integral has been evaluated by Thompson and Hering (1970) and Bassel (1966). Thompson and Hering assume that the wave function of the transferred particle can be parametrized by a Hulthén function. Their method is too simple and the fact that they use a fixed value for the Hulthén parameter for different reactions has been seriously criticized by Kok and Rinat (1973). Bassel's method consists of reducing the integral to a simpler one by replacing $V(\mathbf{r},\xi)$ by $-E_{sep}$, where $-E_{sep}$ is the separation energy of the transferred particle in the projectile. However, this procedure is not reliable for unbound particles. The normalization factor for the $(^3He,\vec{d})$ reaction has been calculated by Lim (1972) and Janetzki *et al.* (1976). In the calculations of Lim a continuum wave function given by Arenhövel *et al.* (1971) for the singlet deuteron was taken. However, as has been pointed out by Janetzki *et al.* (1976), this wave function does not have the proper energy dependence and is normalized in finite space. Janetzki *et al.* find a satisfactory agreement with their $(^3He,\vec{d})$ data at $E_{^3He}=13$ MeV by writing the wave function for the singlet s state in terms of a Jost function.

A more detailed calculation of the normalization factor has been presented by van Driel, Kamermans, de Meijer, and Dieperink (1980). As a starting point they take the Reid soft core (RSC) interaction (Reid, 1968). The ^2He wave function was constructed by numerically solving the Schrödinger equation using the $L=0$, $S=0$ RSC potential. The ^3He wave function was obtained by taking the $L=0$, $S=0$ component of a Faddeev wave function obtained with the RSC interaction (Brandenburg *et al.*, 1975). Assuming only s-state contributions, they described the interaction between the transferred neutron and the ^2He by the sum of the $L=0$, $S=0$ RSC potential and the diagonal part of the $L=0$, $S=0$ 1RSC potential (Reid, 1968). Coulomb effects were taken into account in a way analogous to the method of Phillips (1964). The normalization factor calculated by this procedure is given in Fig. 13. The figure shows clearly the effect of the Coulomb repulsion between the two protons. Without the Coulomb effects (the case of $2n$ or $\vec{d}$) the low-ε region is strongly enhanced due to the $l=0$ nucleon-nucleon interaction. For larger ε, where the nuclear interaction dominates, the difference gradually disappears. A comparison between the experimental and calculated relative-energy dependence of the cross section is presented in Fig. 14. In the calculation the above-discussed effects of (i) the normalization factor, (ii) the Q-value dependence, and (iii) the folding optical model potential are included. The ε dependence of the cross section is nicely reproduced, and even the absolute values are in reasonable agreement: $N_{^2He}=0.47\pm0.20$ and $N_{^2He}=0.76$ MeV^2 fm^3 for experi-

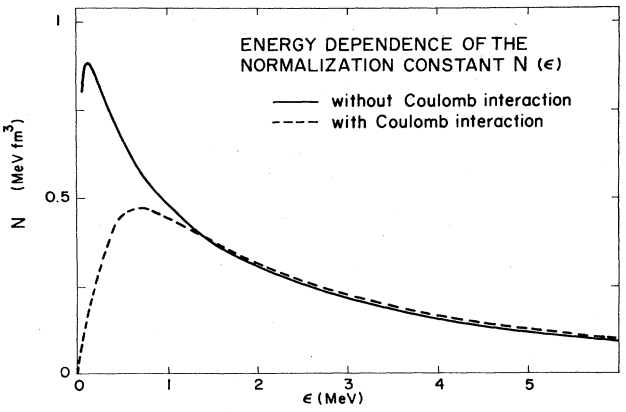

FIG. 13. Energy dependence of the normalization constant $N(\varepsilon)$. The solid line represents the case without Coulomb interaction; the dashed curve is calculated from the solid one by making a correction for the Coulomb interaction using the asymptotic behavior of the wave functions (van Driel, Kamermans, de Meijer, and Dieperink, 1980).

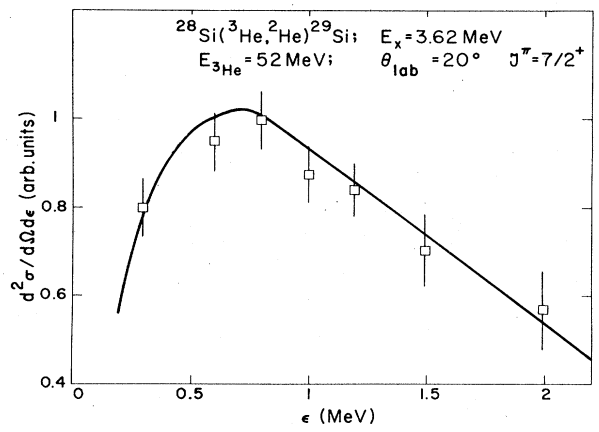

FIG. 14. Comparison of the shape of the normalization constant $N(\varepsilon)$, which is corrected for the ε dependence of the DWBA cross section, with the double differential cross section as function of the relative energy for the $J^\pi=\frac{7}{2}^-$, $E_x=3.62$ MeV state in ^{29}Si (after van Driel, Kamermans, de Meijer, and Dieperink, 1980).

ment and theory, respectively. It should be noted that the calculated value is quite sensitive to the imaginary well depth. An increase of 30% in this well depth will bring both values into perfect agreement without changing the shape of the angular distributions.

The agreement observed in Fig. 14 between the experimental and calculated relative-energy spectrum underlines the validity of the separation of the reaction into a formation and a decay process. The only connection between the two is the trivial relation between the reaction Q value and the relative energy in the decay [see Eqs. (2.6) and (2.7)]. The result also shows that the FSI observed in these type of reactions is well described by the calculation with realistic wave functions as described above. Such calculations show that the apparent discrepancy in Fig. 8 can be completely removed. So in this type of reaction one observes the free p-p FSI modified by the ε dependence of the normalization constant in the formation cross-section description.

B. Structure information from sequential breakup

1. One-nucleon transfer reactions

He-induced one-nucleon transfer reactions with unbound ejectiles have been studied for quite some time. At low incident energy the ^{10}Be(^{3}He,d)^{11}C reaction was performed at 8, 10, and 11 MeV (Bohne *et al.*, 1970), the ^{13}C(^{3}He,d)^{14}N reaction at 13 MeV (Janetzki *et al.*, 1976), and the (^{3}He,^{2}He) reaction at 13 and 17 MeV on the target nuclei ^{9}Be, ^{51}V, ^{65}Cu, and ^{87}Y (Congedo *et al.*, 1980). At higher incident energy, data are available for the ^{28}Si(^{3}He,^{2}He)^{29}Si reaction at 52 MeV (van Driel, Kamermans, de Meijer, and Dieperink, 1980) and the ^{12}C,^{24}Mg(α,^{5}Li)^{11}B,^{23}Na reactions at 65-MeV incident energy (Saha *et al.*, 1978).

Although in most cases spectroscopic information could be extracted, the main emphasis of these studies was directed towards the reaction mechanism. Investigations have focused on states for which (reliable) spectroscopic information exists, and the agreement between the nuclear structure information obtained in the sequential breakup reactions and the conventional single-nucleon transfer reactions is taken as evidence for the understanding of the reaction process. Two examples will shortly be discussed in order to indicate the quality of information that can be obtained. Figure 15 shows the angular distributions of three states in ^{14}N excited in the ^{13}C(^{3}He,$\vec{d}$)^{14}N reaction at 13 MeV (Janetzki *et al.*, 1976), which are compared with the result of the ^{13}C(^{3}He,d)^{14}N reaction. The experimental angular distributions of both reactions are very similar and the DWBA description is satisfactory. The different curves in the figure correspond to different optical model potential sets in the DWBA calculations (Janetzki *et al.*, 1976). The relative spectroscopic factors normalized to the ^{14}N ground state are, for

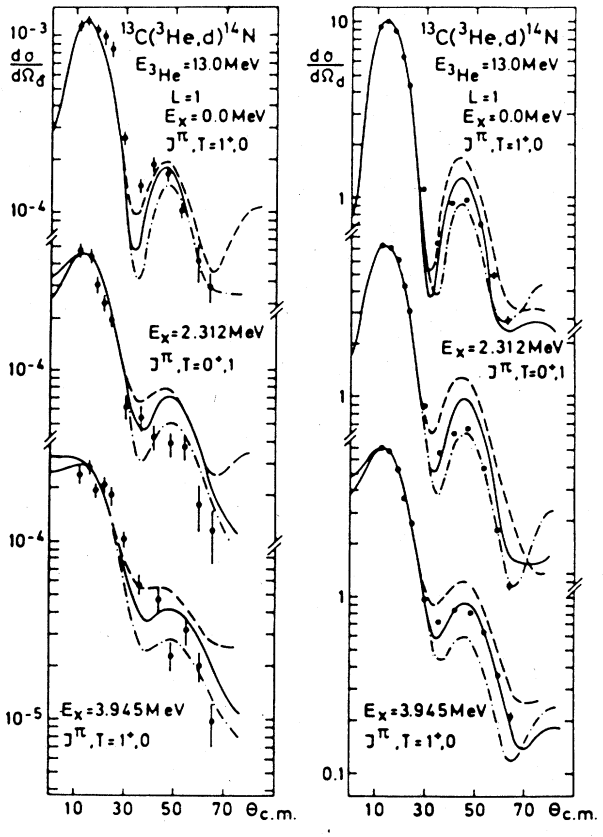

FIG. 15. Angular distributions of deuteron and singlet deuteron for transitions leading to the ground state and the first two excited states of ^{14}N with the ^{13}C(^{3}He,d)^{14}N and ^{13}C(^{3}He,$\vec{d}$)^{14}N reactions. The curves are the results of calculations using various optical model potentials (Janetzki *et al.*, 1976).

$E_x = 2.312$ MeV, 1.50 and 1.57 and for the $E_x = 3.945$ MeV state 0.43 and 0.41, for the (^{3}He,d) and (^{3}He,$\bar{d}$) reaction, respectively. Angular distributions and the results from DWBA calculations for the ^{28}Si(^{3}He,^{2}He)^{29}Si reaction (van Driel, Kamermans, de Meijer, and Dieperink, 1980) are shown in Fig. 16. The dashed curves correspond to calculations with a folding optical model potential and the solid lines represent the fit with a deuteron optical model potential (see Sec. IV.A.2). The deduced spectroscopic factors are compared in Fig. 17 with the results of the ^{28}Si(d,p)^{29}Si reaction and the (^{3}He,d) reaction leading to the mirror nucleus ^{29}P. These results indicate that sequential breakup processes in which a single nucleon is transferred are potentially a good spectroscopic tool. However, up to now no new nuclear structure information has been obtained with this type of reaction.

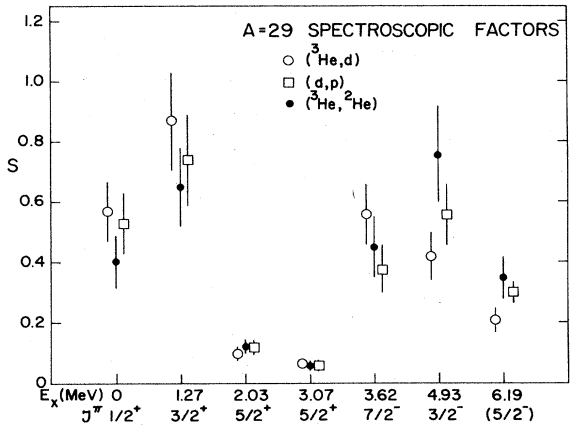

FIG. 17. Comparison between spectroscopic factors in $A = 29$ for the reactions ^{28}Si(^{3}He,d)^{29}P, ^{28}Si(d,p)^{29}Si, and ^{28}Si(^{3}He,^{2}He)^{29}Si (van Driel, Kamermans, de Meijer, and Dieperink, 1980).

2. Two-nucleon transfer reactions

From the sequential breakup reactions in which two nucleons are transferred, the (α,^{2}He) reaction has been studied at relatively high incident energies in order to obtain spectroscopic information. An extensive systematic survey on the $1p$- and $2s1d$-shell nuclei ^{12,13}C, ^{14,15}N, ^{16,18}O, ^{20,22}Ne, ^{26}Mg, ^{28,29}Si, ^{32}S, and ^{36,38}Ar at $E_\alpha = 65$ MeV and on ^{24}Mg and ^{40}Ca at 55 MeV has been presented by Jahn *et al.* (1978). More detailed angular distribution measurements on ^{12}C, ^{24,26}Mg, ^{28}Si, ^{40}Ca, ^{58}Ni, ^{90}Zr, and ^{208}Pb have been published by van Driel, Kamermans, and de Meijer (1980) at $E_\alpha = 65$ MeV.

It was realized in 1976 (Jahn, Wozniak *et al.*, 1976) that the (α,^{2}He) reaction on light nuclei selectively populated two-neutron states of high spin in the final nuclei. This selectivity is analogous to the one observed in the (α,d) reaction where the transfer of $(1d_{5/2})^2_5$ and $(1f_{7/2})^2_7$ pairs is highly favored due to the large negative Q values, the good overlap of the relative s motion of the neutron-proton pair with the relative s motion in the projectile, and the large spectroscopic factors. Therefore, one expects for the (α,^{2}He) reaction at comparable bombarding energies a strong population of states in which two neutrons are coupled to $(1d_{5/2})^2_4$ and $(1f_{7/2})^2_6$. At 65-MeV bombarding energy the angular momentum mismatch for a surface reaction is about $(4-5)\hbar$ for $1p$-shell targets and $(5-6)\hbar$ for $2s1d$-shell targets. Indeed, in the survey of Jahn *et al.* (Jahn *et al.*, 1978) it was found that the only states strongly populated in reactions on p-shell nuclei were those of a $(p_{1/2}d_{5/2})_3$ and $(d_{5/2})^2_4$ character, whereas for $2s1d$-shell nuclei $(d_{3/2}f_{7/2})_5$ and $(f_{7/2})^2_6$ transition are strongly favored and have a maximum cross section almost independent of the target mass. An example is shown in Fig. 18 for the ^{40}Ca(α,^{2}He)^{42}Ca reaction (Jahn *et al.*, 1978). The only strongly populated peak corre-

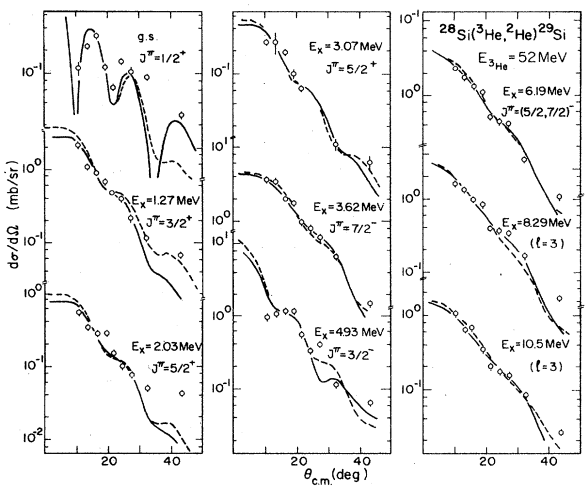

FIG. 16. Angular distributions and DWBA calculations for the ^{28}Si(^{3}He,^{2}He)^{29}Si reaction. The solid lines are the results of a calculation with the deuteron optical model potential, whereas the dashed curves correspond to a folding optical model calculation at $\varepsilon = 1.0$ MeV (van Driel, Kamermans, de Meijer, and Dieperink, 1980).

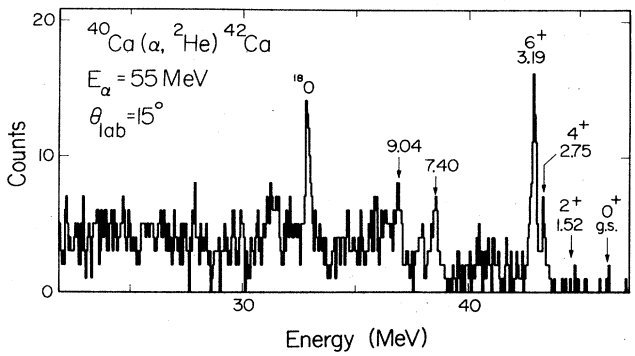

FIG. 18. Total kinetic energy spectrum of the ^{40}Ca(^{4}He,^{2}He)^{42}Ca reaction at an incident energy of 55 MeV (Jahn *et al.*, 1978).

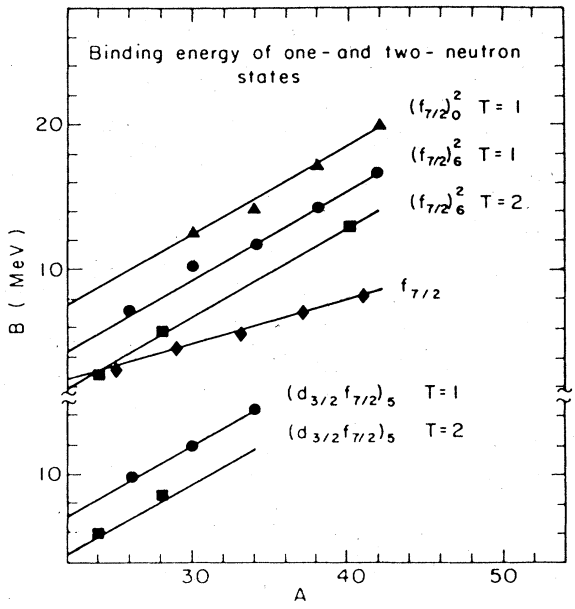

FIG. 19. Binding energies B for some one- and two-neutron states as a function of the mass of the final nucleus A (Jahn *et al.*, 1978).

sponds to a transition to the $J^\pi=6^+$; $E_x=3.19$ MeV state, which is known to be a $2n$ state of $(f_{7/2})^2_6$ character (Kanestrøm and Koren, 1969). Although spin assignments in the work of Jahn *et al.* are mainly based on excitation strengths, the authors were able to deduce the A dependence of the binding energies of two-neutron states with a $(f_{7/2})^2_6$ and $(d_{3/2}f_{7/2})_5$ character. This A dependence (see Fig. 19) nicely agrees with values obtained for other configurations, and with calculations employing the Bansal-French method (solid lines) (Bansal and French, 1964). At the same time it became clear that a reliable description of the ^{28}Si$(\alpha,^2$He$)^{30}$Si angular distributions could be obtained with standard DWBA using a deuteron optical model parameter set for the outgoing ^{2}He (de Meijer *et al.*, 1977). Full angular distributions for reactions on ^{12}C, ^{24,26}Mg, ^{28}Si, ^{40}Ca, and ^{58}Ni were measured by van Driel, Kamermans, and de Meijer (1980) and described with DWBA calculations. In order to judge the quality of this spectroscopic information an example is shown in Fig. 20 for the ^{24}Mg$(\alpha,^2$He$)^{26}$Mg reaction. It is interesting to notice (see Sec. III) that for these systems, which break up symmetrically, cross sections at very small angles (even zero degrees) can be obtained. The deduced spectroscopic information is condensed in Table I. Contrary to the (^{3}He,^{2}He) reaction the description of the shape of the $(\alpha,^2$He) angular distributions was found to be sensitive to the optical potential that generates the outgoing ^{2}He waves. The best fits were obtained with a deu-

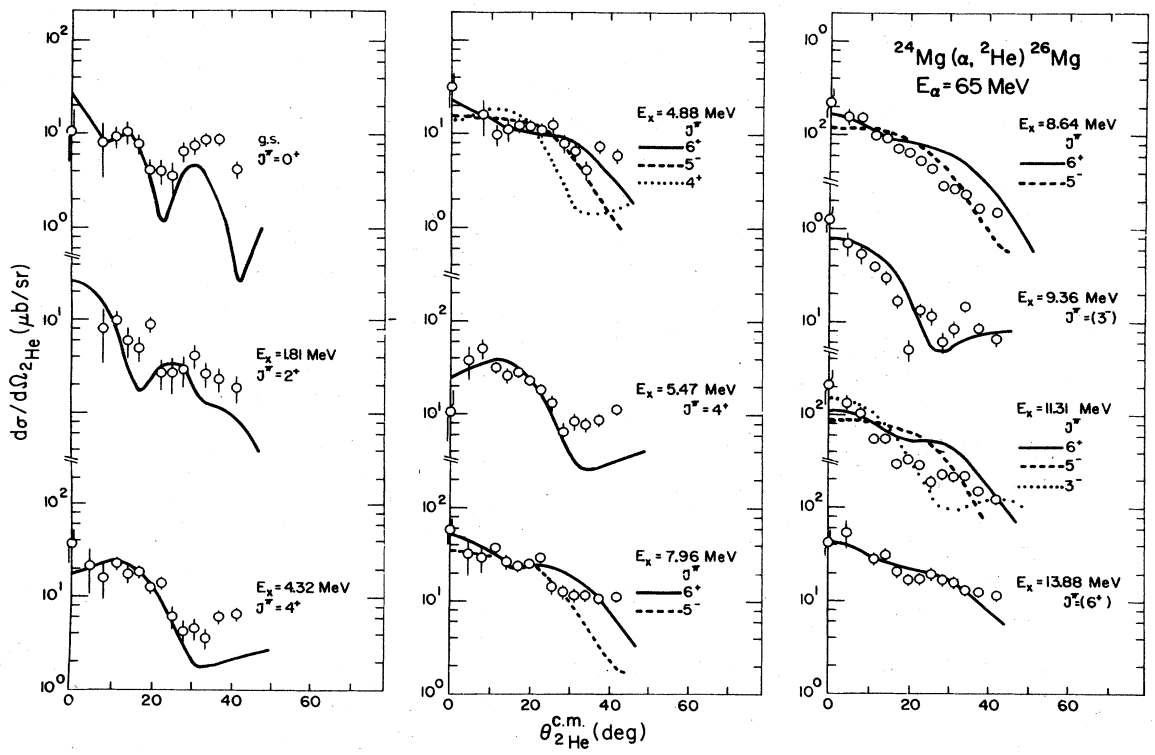

FIG. 20. Angular distributions for transitions observed in the ^{24}Mg$(\alpha,^2$He$)^{26}$Mg reaction. The curves in the figure are the results of DWBA calculations for the different L transfers (van Driel, Kamermans, and de Meijer, 1980).

TABLE I. Excitation energies, spins, parities, transfer amplitudes, and normalization constants for transitions in the ^{24}Mg(α,^{2}He)^{26}Mg reaction. For details of the assignments see van Driel, Kamermans and de Meijer (1980).

E_x (MeV)	E_x (MeV)	J^π	Transfer amplitudes	N
−0.03±0.09	*gs*	0^+	$1.0(d_{5/2})^2$	140 ± 40
			$0.733(d_{5/2})^2+0.284(s_{1/2})^2+0.297(d_{3/2})^2$	90 ± 30
1.77±0.08	1.809	2^+	$1.0(d_{5/2})^2$	50 ± 20
			$-0.168(d_{5/2})^2-0.028(d_{5/2}s_{1/2})+0.034(d_{5/2}d_{3/2})$ $-0.057(s_{1/2}d_{3/2})+0.054(d_{3/2})^2$	$(3.8\pm1.3)\times10^4$
4.27±0.06	4.318	4^+	$1.0(d_{5/2})^2$	28 ± 7
			$1.0(d_{5/2}d_{3/2})$	9 ± 3
4.88±0.07	4.900	4^+	$1.0(d_{5/2})^2$	21 ± 10
		5^-	$1.0(d_{5/2}f_{7/2})$	6.2± 1.6
		6^+	$1.0(f_{7/2})^2$	9.0± 1.5
5.51±0.08	5.474	4^+	$1.0(d_{5/2})^2$	42 ± 10
			$1.0(d_{5/2}d_{3/2})$	14 ± 5
7.96±0.08		5^-	$1.0(d_{5/2}f_{7/2})$	13 ± 3
		6^+	$1.0(f_{7/2})^2$	22 ± 10
8.64±0.03	8.62	5^-	$1.0(d_{5/2}f_{7/2})$	48 ± 12
9.36±0.04		3^-	$1.0(d_{5/2}f_{7/2})$	80 ± 20
11.31±0.07	11.23	6^+	$1.0(f_{7/2})^2$	50 ± 20
		5^-	$1.0(d_{5/2}f_{7/2})$	35 ± 12
		3^-	$1.0(d_{5/2}f_{7/2})$	230 ±100
			$1.0(d_{5/2}p_{3/2})$	90 ± 30
			$1.0(s_{1/2}f_{7/2})$	100 ± 30
13.88±0.09		6^+	$1.0(f_{7/2})^2$	20 ± 4

teron optical model parameter set, whereas a folding optical model gave a somewhat worse description. With a deuteron optical model parameter set the zero-range DWBA description works reliably and consequently likely J^π values could be determined for states which are otherwise hardly accessible. However, this statement is mainly confined to the $2s1d$-shell nuclei; for heavier nuclei a strong increase of the continuum structure hinders the extraction of spectroscopic information.

V. DIRECT BREAKUP

A. Introduction

Pronounced, bell-shaped enhancements (*bumps*) are observed at forward angles in the continuum part of ^{3}He-induced spectra of protons, deuterons, and tritons. Figure 21 presents as an example (^{3}He,d) spectra at several angles at $E_{^3\mathrm{He}}=130$ MeV (Djaloeis *et al.*, 1983). As shown in Fig. 22 bumps also occur in the inclusive spectra of protons, deuterons, tritons, and ^{3}He from α-induced reactions on ^{27}Al at $E_\alpha=160$ MeV (Wu *et al.*, 1979). In all these spectra the bump occurs near an energy which corresponds to the beam velocity (*beam velocity energy*). The data illustrate that the relative importance of the bump decreases rapidly with increasing detection angle. In addition to the bump component, one observes in the continuum part of the spectra (see Figs. 21 and 22) a component at the low-energy side. This component is present at all angles and has at backward angles, where the bump has disappeared, the shape of an exponential tail. We therefore will refer to this component of the continuum as the *tail.*

These components of the continuum have been studied over a wide range of incident energies. For ^{3}He projectiles the investigations were carried out at $E=52$ MeV (Aarts, Bhowmik *et al.*, 1981; Aarts, Grasdijk *et al.*, 1981; Aarts, 1982,1983; Aarts, Malfliet, de Meijer, and van der Werf, 1984), 68 MeV (Bousshid *et al.*, 1980), 70 MeV (Matsuoka, 1978), 90 MeV (Matsuoka *et al.*, 1978,1980), 110 MeV (Matsuoka *et al.*, 1978), and 130 MeV (Bojowald *et al.*, 1981; Djaloeis *et al.*, 1983). Inclusive spectra from α-induced reactions have been investigated at $E=65$ MeV (de Meijer *et al.*, 1983), 80 MeV (Wu *et al.*, 1979), 120 MeV (Koeslag *et al.*, 1983,1984), 140 MeV (Wu *et al.*, 1978; Koontz, 1980), 160 MeV (Wu *et al.*, 1979), and 172.5 MeV (Budzanowski *et al.*, 1978; Shyam *et al.*, 1983). This vast amount of data shows in general a large similarity between processes observed for ^{3}He and α projectiles. The most salient systematic information obtained for the bump part and the tail part will be discussed in Secs. V.B.1 and V.B.2, respectively.

The occurrence of a bump at beam velocity suggests that it is due to a fast reaction process in which the observed particle has left the interaction region between projectile and target practically undisturbed. This particle thus behaved as a *spectator.* Consequently the interaction has occurred between the other constituent of the projectile (the *participant)* and the target. To establish the characteristics of the participant-target interaction, correlation experiments are essential.

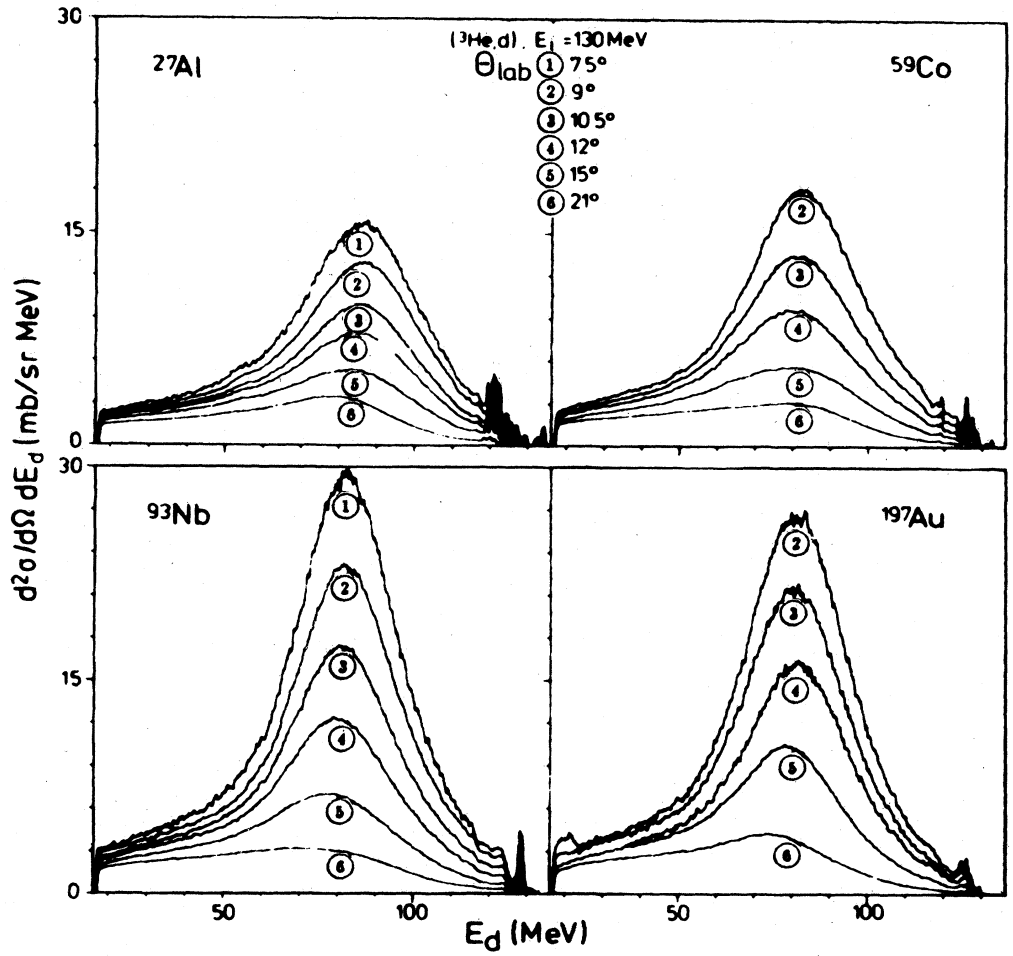

FIG. 21. Examples of d spectra from the (^{3}He,d) reaction at $E_{^3\mathrm{He}} = 130$ MeV (Djaloeis *et al.*, 1983).

Detailed coincidence studies for ^{3}He-induced reaction measurements have been carried out at 33 MeV (Drumm *et al.*, 1983) for p-d coincidences, at 52 MeV (Aarts, Grasdijk *et al.*, 1981; Aarts, 1982,1983; Aarts, Malfliet, de Meijer, and van der Werf, 1984) for p-p, p-d, p-t, and p-^{3}He combinations, and at 90 MeV (Matsuoka *et al.*, 1980) for p-d coincidences. The p-d correlation experiment at 33 MeV has been carried out with a polarized beam and analyzing powers have been measured. The p-d coincidences, especially at 52 MeV, have played an important role in the understanding of the various processes. Correlation data for α projectiles have been obtained at 65 MeV (de Meijer *et al.*, 1983), 120 MeV (Koeslag *et al.*, 1983,1984), 140 MeV (Koontz, 1980), and 172.5 MeV (Budzanowski *et al.*, 1979). All measurements involve coincidences between charged particles.

From all these studies a rather simple picture emerges. In general, it was found that the participant-target interaction corresponds to the one responsible for well-known reaction processes like elastic scattering, inelastic scattering, particle transfer, and absorption. This allows a schematic classification of the breakup processes as is given, e.g., in Fig. 23 for 52-MeV ^{3}He on ^{28}Si (de Meijer, 1982). According to this scheme, *elastic breakup* is the process in which the ^{3}He projectile breaks up into p and d, while the target nucleus ^{28}Si remains in its ground state. If instead the target nucleus is left in an excited state, the process is named *inelastic breakup*. *Absorptive breakup* is the process in which the participant is absorbed by the target nucleus. In Fig. 23 this process is presented for a proton participant absorbed by ^{28}Si; the compound system ^{29}P decays subsequently by the emission of a proton. In addition to the p-d coincidences from ^{3}He-induced reactions p-t, p-^{3}He, and d-d coincidences have also been observed. It was found that these coincidences could be explained by the *breakup-transfer* process. In this process the participant picks up a nucleon from the target. For deuteron participants this leads to triton or ^{3}He ejectiles. For proton participants this results in d-d coincidences. This process is kinematically distinguishable from the *transfer-breakup* process, in which the ^{3}He projectile as an entity picks up a nucleon and forms an unstable state of ^{4}He or ^{4}Li, which subsequently decays via sequential breakup.

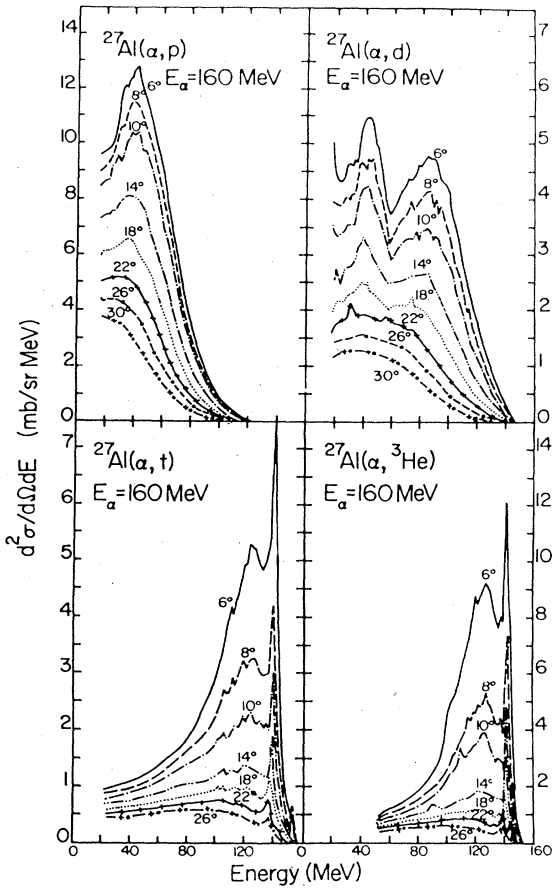

FIG. 22. The differential energy spectra of p, d, t, and ^{3}He resulting from the bombardment of 160-MeV α particles on ^{27}Ar (Wu *et al.*, 1979).

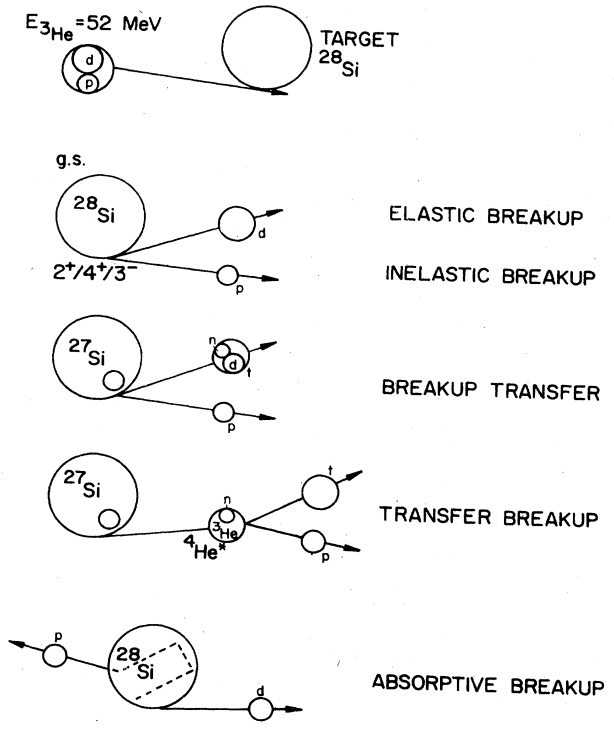

FIG. 23. Schematic representation of various breakup processes (de Meijer, 1982).

The identification of elastic breakup, inelastic breakup, and absorption breakup is illustrated in Fig. 24. This two-dimensional E_p vs E_d spectrum (Aarts, Grasdijk *et al.*, 1981) is obtained with a detection geometry in which deuterons are detected at $-10°$ and protons at a backward angle of $-145°$. In this spectrum one observes loci corresponding to events belonging to the ^{28}Si(^{3}He,pd)^{28}Si reaction (see Sec. II). As has been discussed before, the presence of a locus implies that the reaction has been measured kinematically complete and that the loci correspond to transitions to states in the residual nucleus ^{28}Si. At relatively low proton energies, there is an intense concentration of uncorrelated events which do not belong to a particular locus. Aarts (1983) and Aarts, Malfliet, de Meijer, and van der Werf (1984) showed that the main difference between the spectra for various targets is the number and the position of the loci and the intensity of the uncorrelated events. At more forward angles the intensity of the loci increases relative to the uncorrelated events and at very forward angles the ground-state transition dominates the spectrum. The events in Fig. 24 there-

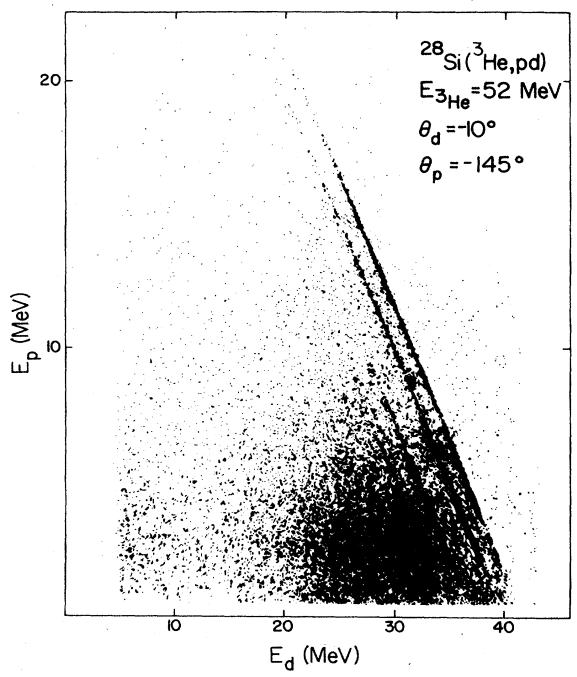

FIG. 24. Two-dimensional E_p vs E_d spectrum of the reaction ^{28}Si(^{3}He,pd) at $\theta_p=-145°$ and $\theta_d=-10°$ (Aarts, Grasdijk *et al.*, 1981).

fore may be categorized in the above-defined classes.

(i) The events belonging to the ground-state locus. In these reactions all particles (proton, deuteron, and target nucleus) are left in their ground state, and the process is called *elastic breakup.*

(ii) The events on the other loci. In these reactions only the target is excited, and the process is called *inelastic breakup.*

(iii) The uncorrelated events which mainly result from absorptive breakup, as will be discussed in Sec. V.C.1.

We like to note that we follow here the nomenclature used by Aarts, Grasdijk *et al.* (1981), Aarts (1983), and Aarts, Malfliet, de Meijer, and van der Werf (1984) and not the one introduced by Baur (1976), Baur and Trautmann (1976), Baur *et al.* (1976), and Baur *et al.* (1980), who use the name *inelastic breakup* for all reactions except for elastic breakup. To avoid confusion we will refer to this family of processes as *nonelastic breakup* [(ii) and (iii)]. This may sometimes lead to confusion with the nomenclature used in heavy-ion physics. However, where possible we will indicate the names used in heavy-ion physics for processes corresponding to those observed in the light-ion—breakup reactions.

The specific properties of the reaction processes, their experimental identification, and their relative contribution to the inclusive yields are discussed in Secs. V.C.1, V.C.2, and V.D. In Sec. V.C.4 an additional process is described, in which two particles with spectator characteristics (both with beam velocity energies) are observed. This process was found in proton-proton correlation measurements in both ^{3}He- and α-induced reactions. The main part of the bump in the inclusive proton spectrum is due to this process. For ^{3}He-induced reactions the neutron is the participant in the process leading to two spectator protons. Since the neutron itself is not detected in these coincidence measurements, it is not yet clear what the contributions of elastic, inelastic, and absorptive breakup are. This situation, with more than three particles in the final state, is comparable to that of inclusive measurements (kinematically incomplete). Therefore, the breakup with two spectator particles is discussed separately.

So far we have discussed those processes which lead to common features in the reactions with ^{3}He and α projectiles. Especially at the lower α energies, however, there exist some distinct differences. In contrast to, e.g., the inclusive (^{3}He,d) spectra at $E_{^3\mathrm{He}}=52$ MeV, the inclusive (α,t) and ($\alpha,^3$He) spectra at comparable beam velocity ($E_\alpha=65$ MeV) do not show pronounced enhancements around beam velocity energies (spectator characteristics). Also, the coincidence measurements at $\theta_1=10°$ and $\theta_2=-10°$ show hardly any cross section for direct-breakup reactions but indicate that the dominant contributions come from sequential breakup processes (de Meijer *et al.*, 1983). The absence of spectator bumps in the (α,t) and ($\alpha,^3$He) spectra can be understood by considering the phase space available for this type of reaction.

In Fig. 25 the three-particle phase spaces for projectile breakup in the (d,p), (^{3}He,d), and (α,t) reactions have been presented schematically. From this figure one sees that in the case of the deuteron, where the bump will occur at approximately $\frac{1}{2}E_b$, the phase space is rather flat. This is still true for the (^{3}He,d) reaction, where the bump will occur at about $\frac{2}{3}E_b$. However, in the case of the (α,t) reaction at $E_\alpha=65$ MeV (de Meijer *et al.*, 1983) the spectator energy of $\frac{3}{4}E_b$ lies outside the available phase space, explaining why hardly any direct breakup can be expected at this beam energy. So it is because of the larger ejectile/projectile mass ratio and the much larger binding energy of the α projectile that this mismatch occurs for the (α,t) reaction and not for the (^{3}He,d) reaction. For deuteron spectators in the (α,d) reaction such a mismatch does not occur and the spectrum at $E_\alpha=65$ MeV shows a bump. From phase-space arguments one expects the onset of breakup processes with tritons and ^{3}He particles as spectator in the energy range $80<E_\alpha<100$ MeV.

At higher energies marked differences also occur. Contrary to the bell-shaped enhancements observed in the (^{3}He,d) and (^{3}He,p) reactions, which are predominantly due to spectator particles, the bumps in the (α,t) and

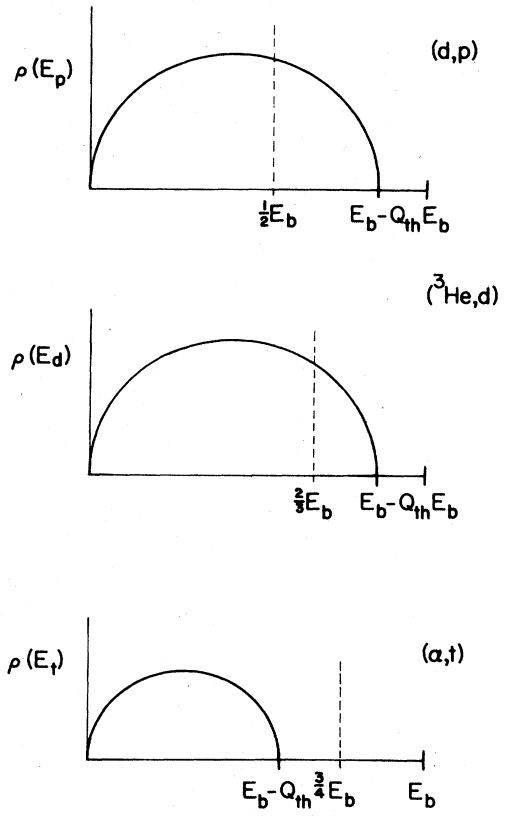

FIG. 25. Schematic representation of phase-space distributions, $\rho(E)$, and beam velocity energies for the reactions (d,p), (^{3}He,d), and (α,t). In this figure E_b represents the beam energy and Q_{th} follows from Eq. (2.6).

(α,^{3}He) spectra arise almost exclusively from particle unbound states populated in these single-nucleon transfer reactions (Koeslag *et al.*, 1983). Furthermore, one observes a contribution to the triton tail from *t-p* coincidences which is strongly forwardly peaked. The corresponding process in ^{3}He-induced reactions should be observed in *d-p* coincidences; no evidence for such a process is found in the tail of the (^{3}He,*dp*) spectra.

B. Systematics of the continuum

1. Bump part

a. Position of the bump

The bump near beam velocity energies is most prominently observed at forward angles (see Figs. 21 and 22). Its position varies slightly with the target mass due to the Coulomb field of the target nucleus. With increasing scattering angle the cross section for the bump decreases rapidly and the peak of the bump also shifts to slightly lower energies. The angular dependence of the bump cross section for protons and deuterons produced by 52-MeV ^{3}He on ^{12}C, ^{28}Si, and ^{58}Ni is shown in the upper part of Fig. 26. The decrease of the cross section for deuterons is even stronger than for protons (Aarts, 1983).

For the same systems the centroid position of the bump as function of the scattering angle is given in Fig. 27. The energy shift can be understood in a relatively simple geometrical model that assumes the projectile to break up at the point of closest approach along a Coulomb trajectory for both the projectile and the spectator. Without relative motion (Fermi motion) between the constituents in the projectile, the detection angle θ^{spec} and the energy E^{spec} can be easily calculated from classical mechanics. In this picture the occurrence of a spectator at $\theta \neq \theta^{\text{spec}}$ is due to the Fermi motion in the projectile. The probability for a certain value of the relative velocity follows from the momentum distribution of the constituents. For ^{3}He and α particles the momentum distribution peaks at small relative momenta. The velocity diagram in Fig. 28 shows schematically the spectator angle θ^{spec}, the spectator velocity v^{spec}, and the velocities at other angles that correspond to a minimum relative velocity. In this simple spectator model, the centroid position of the bump will change with $\cos^2(\theta - \theta^{\text{spec}})$. The solid line in Fig. 27, which is arbitrarily normalized to the data, indicates the bump positions in the proton and deuteron spectra calculated with this geometrical model. At forward angles this

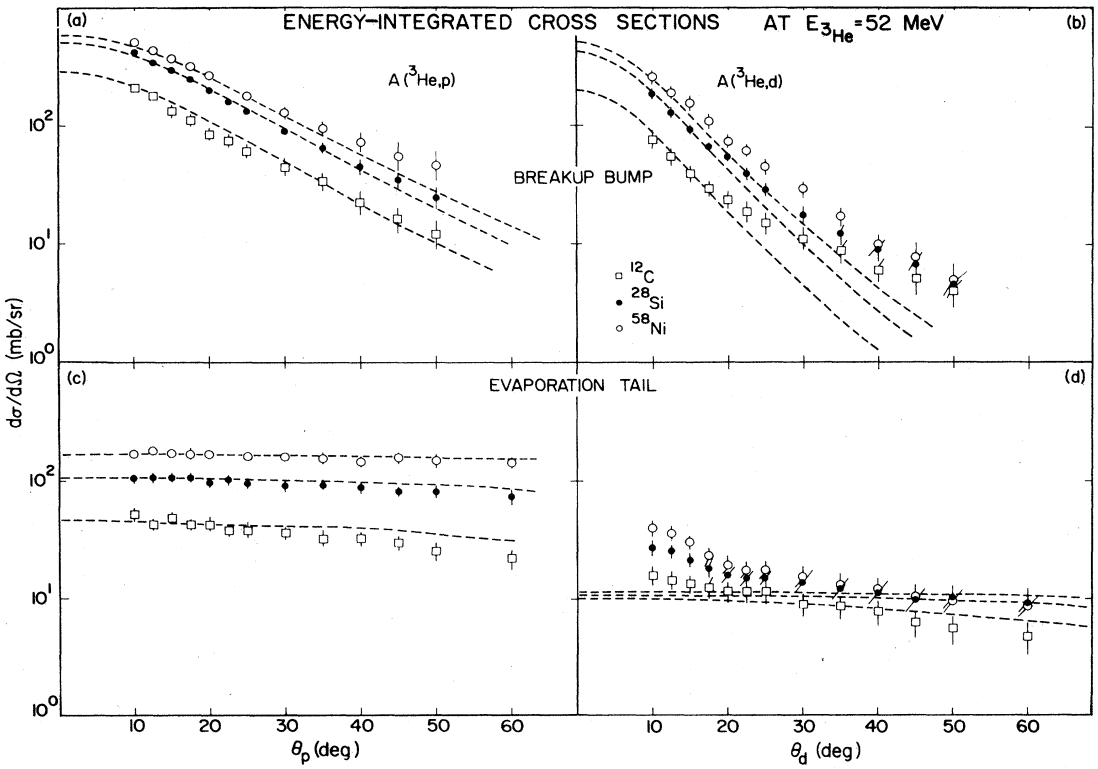

FIG. 26. The angular distribution for the energy-integrated continuum cross sections for the bump and the tail in the inclusive proton and deuteron spectra induced by 52-MeV ^{3}He at various targets. The curves in (a) and (b) represent the QFBM calculations (see Sec. VI); the curves in (c) and (d) the calculations with the Fermi-gas model (Aarts, 1983; Aarts, Malfliet, de Meijer, and van der Werf, 1984).

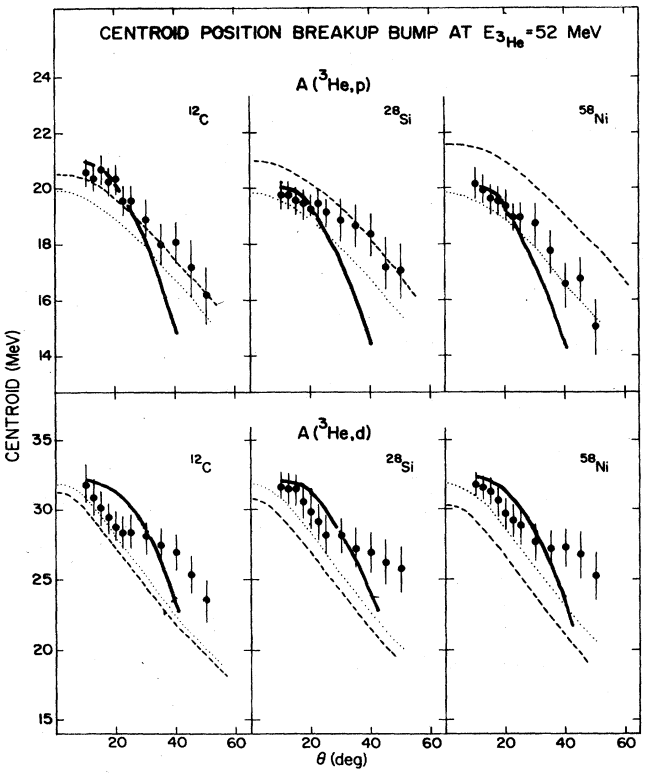

FIG. 27. Centroid positions of the continuum bump in the inclusive spectra for protons and deuterons as a function of the detection angle θ. The dashed and dotted curves represent QFBM calculations (see Sec. VI) with and without Coulomb corrections, respectively (Aarts, 1983; Aarts, Malfliet, de Meijer, and van der Werf, 1984). The solid curves represent the angular dependence according to $\cos^2(\theta-\theta^{\rm spec})$ as discussed in Sec. V.B.1.a.

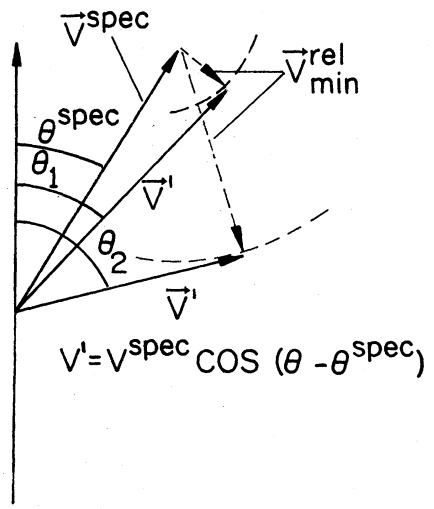

FIG. 28. Schematic representation of the velocities in a simple spectator model.

model reproduces the change in position rather well. At $E_{^3He}=130$ MeV the deuteron peak positions, observed in the range $\theta_d=7°-25°$ (Bojowald *et al.*, 1981), also follow the $\cos^2(\theta-\theta^{\rm spec})$ dependence quite well.

At α energies of 120 MeV and higher the experimental results are consistent with the ^{3}He data. However, at $E_\alpha=65$ MeV a bump is observed only in the deuteron spectrum (de Meijer *et al.*, 1983). The absence of the bump in the t and ^{3}He spectra at $E_\alpha=65$ MeV has been explained before in terms of a mismatch between the spectator energy and the available phase space (Sec. V.A). The data at $E_\alpha=80$ MeV have not been measured with energy resolution accurate enough to rule out the possibility that the bump observed in the t and ^{3}He spectra is due to unresolved transitions to discrete states in the final nucleus (Wu *et al.*, 1979).

In the (α,d) spectra at $E_\alpha=160$ MeV (see Fig. 22) two bumps are observed at around $E_d=40$ and 80 MeV, respectively (Wu *et al.*, 1979). This observation is made over a wide range of target masses, and only the relative intensity for the bump near $E_d=40$ MeV with respect to the one at $E_d=80$ MeV decreases with increasing A. The origin of the bump at 40 MeV is not yet clear. Wu *et al.* (1979) have suggested that it arises from a process in which the proton (or neutron) resulting from the projectile breakup picks up a neutron (or proton) from the target nucleus (breakup transfer). The resulting average deuteron energy, however, would then be roughly at $E_d=\frac{1}{4}E_\alpha+Q$, with Q being the Q value for the (α,dt) or $(\alpha,d\,^3\text{He})$ reactions, respectively. For an Al target those ground-state Q values are -31 and -26 MeV, respectively, and consequently the second deuteron peak is expected at $E_d\sim12$ MeV, much lower than observed. Therefore the suggestion of Wu *et al.* seems unlikely. Based on the Q values involved, an explanation in terms of a proton or neutron spectator and a triton or ^{3}He participant can also be ruled out. A reaction that could lead to a deuteron peak at about 40 MeV is the $(\alpha,^6\text{Li}^*)$ reaction. In this sequential breakup reaction one might expect that the resulting α and d will share the kinetic energy proportional to their mass. Coincidence measurements are necessary to reveal the origin of this additional bump.

Finally, a remark should be made on the position of the triton bump observed in ^{3}He-induced reactions around $E_t=\frac{2}{3}E_{^3He}$ (Bousshid *et al.*, 1980; Aarts, Bhomik *et al.*, 1981). Although the triton is not a constituent of the ^{3}He projectile, the main characteristics for the triton bump are the same as those for the proton and deuteron bump. This is the reason why the triton bump has been related to breakup processes. As will be discussed in Sec. V.C.3 the tritons in the bump arise partly from the breakup-transfer process.

b. Width of the bump

The width of the bump has been studied systematically for ^{3}He-induced reactions (Matsuoka *et al.*, 1978; Bousshid *et al.*, 1980; Aarts, Bhowmik *et al.*, 1981; Aarts, 1983; Aarts, Malfliet, de Meijer, and van der Werf, 1984). In this section we report on these studies. It was found that for protons and deuterons the width of the bump is almost independent of the target mass. For tritons, however, a target dependence is observed: the bumps for ^{12}C, ^{28}Si, and ^{58}Ni are not as broad as for the other target nuclei. Especially for ^{12}C there may be contributions from discrete states to the continuum that are not resolved. The dependence of the width of the bump on the emission angle is weak. Only at the highest energy studied, $E_{^3\mathrm{He}}=130$ MeV, are the widths at very forward angles smaller than at more backward angles (see Fig. 29). From the Serber model (Serber, 1947), developed for deuteron breakup reactions at high energy, one expects the width to vary with the incident energy E as $\sqrt{E}$. In this model the average relative velocity, Δv, of the constituents in the projectile is related to the binding energy ($\Delta v^2 \sim \varepsilon$). The width of the bump then corresponds to the energy difference between the cases where Δv and v^{spec} are parallel and antiparallel:

$$\Gamma \sim (v^{\mathrm{spec}}+\Delta v)^2-(v^{\mathrm{spec}}-\Delta v)^2 = 4v^{\mathrm{spec}}\Delta v \sim \sqrt{E\varepsilon}\ . \tag{5.1}$$

The experimental data for ^{3}He-induced reactions, presented in Fig. 30, are not consistent with such an $\sqrt{E}$ dependence (dashed line). The deviations from the $\sqrt{E}$ dependence might be attributed to the available phase space as illustrated in Fig. 25. From this figure one sees that in the case of deuteron-induced reactions the bump will occur in the region where the phase space is rather flat and the Serber model is expected to work well. For the (^{3}He,d) reaction the bump occurs in a domain of the phase space which varies considerably with particle energy. The rate of variation depends on the distance between $\frac{2}{3}E_b$ and E_b-Q_{th}. Hence in the case of ^{3}He one might expect smaller values than given by Eq. (5.1). A simple calculation (solid line in Fig. 30) in which the phase space is multiplied by the momentum distribution of ^{3}He reproduces these widths. The fact that a linear fit (dotted line) reproduces the data must be considered accidental.

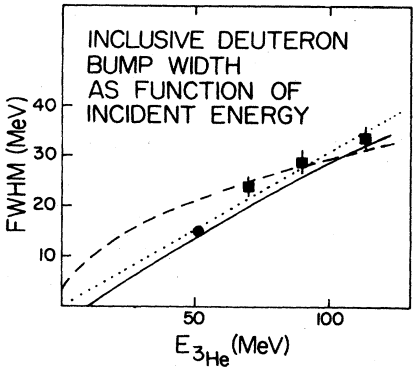

FIG. 30. The width of the bump in the inclusive deuteron spectrum as function of projectile energy: ●, value taken from (Aarts, 1983; Aarts, Malfliet, de Meijer, and van der Werf, 1984); ■, values taken from (Matsuoka *et al.*, 1978). The curves represent the square-root dependence (dashed line), the linear dependence (dotted line), and the QFBM calculations (solid line) discussed in Sec. VI (Aarts, 1983; Aarts, Malfliet, de Meijer, and van der Werf, 1984).

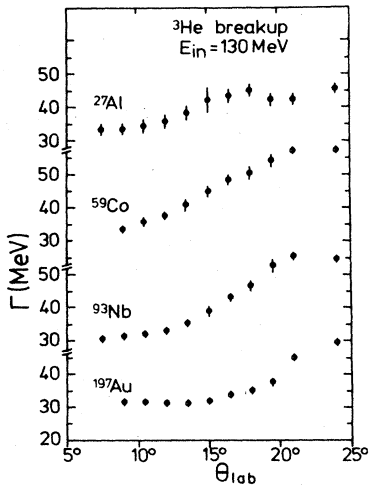

FIG. 29. Angular distribution of the width Γ of the bump in the inclusive deuteron spectrum at $E_{^3\mathrm{He}}=130$ MeV (Bojowald *et al.*, 1981).

c. Target dependence of the bump cross section

An important quantity is the cross section for the bump as a function of the target mass. This quantity has been studied for both ^{3}He and α projectiles. A problem is the subtraction of the continuum background. For their α-induced spectra Wu *et al.* (1979) have used a plane-wave projectile breakup calculation (see also Sec. VI) to determine at each angle the shape of the bump. The magnitude of the cross section was obtained by normalizing the calculations to the spectra at $\theta=6°$. The total cross sections at $E_\alpha=80$ and 160 MeV, presented in Fig. 31, have been obtained by integrating these calculated bumps over energy and angle. The results show that the bump cross sections follow an $A^{1/3}$ dependence.

For ^{3}He-induced reactions the dependence of the bump cross section on the target mass has been studied in more detail. At forward angles the production cross section nicely follows an $A^{1/3}$ dependence at 90 MeV (Matsuoka *et al.*, 1978; Bousshid *et al.*, 1980) and at 130 MeV (Djaloeis *et al.*, 1983). But at 70 MeV a deviation from

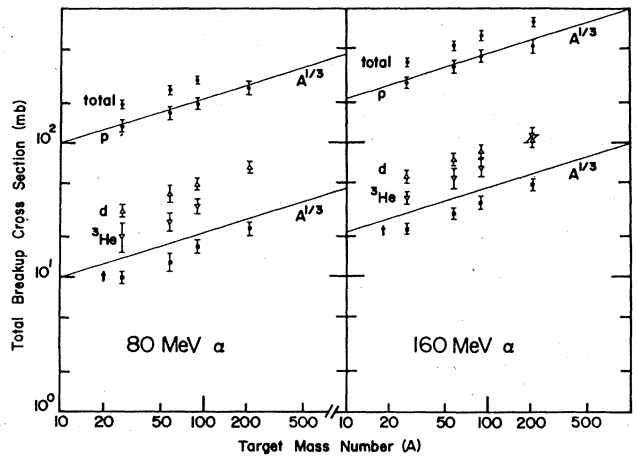

FIG. 31. The total breakup yield and breakup yield of each channel as a function of target mass for 80- and 160-MeV alpha. It should be noted that the proton yield is distributed over a much larger region of phase space than the triton and ^{3}He yields, resulting in a significantly greater yield than indicated by comparisons of the peak cross sections at 6° (Wu *et al.*, 1979).

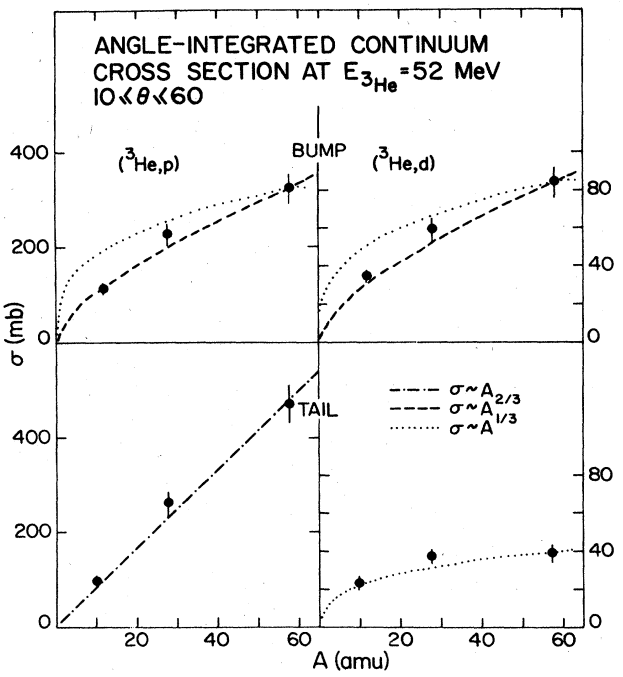

FIG. 32. Angle-integrated ($10° \leq \theta \leq 60°$) continuum cross sections as a function of target mass A for bumps and tails in inclusive proton and deuteron spectra from 52-MeV ^{3}He-induced reactions on C, Si, and Ni (Aarts, 1983; Aarts, Malfliet, de Meijer, and van der Werf, 1984).

this $A^{1/3}$ behavior is observed for targets heavier than ^{118}Sn (Matsuoka *et al.*, 1978). This effect has been attributed to the Coulomb repulsion that prevents the nuclei from touching (Matsuoka *et al.*, 1978). At 52 MeV for the heaviest target, ^{58}Ni, no deviations were observed (Aarts, 1983; Aarts, Malfliet, de Meijer, and van der Werf, 1984). If one, however, integrates the cross section over an angular range between 10° and 60° (Aarts, 1983; Aarts, Malfliet, de Meijer, and van der Werf, 1984), the cross sections for both the proton and deuteron bump show a dependence somewhere between $A^{1/3}$ and $A^{2/3}$ (see the upper part of Fig. 32).

For the inclusive triton spectra at $E_{^3\mathrm{He}}=68$ and 90 MeV from ^{27}Al, ^{nat}Fe, ^{59}Co, ^{93}Nb, ^{197}Au, and ^{209}Bi (Bousshid *et al.*, 1980) the energy-integrated cross sections also follow an $A^{1/3}$ dependence. The data of Aarts, Bhowmik *et al.* (1981), however, show that the cross sections for the closed-shell nuclei ^{12}C, ^{28}Si, and ^{58}Ni are considerably lower than for the neighboring nuclei. This effect for ^{12}C, ^{28}Si, and ^{58}Ni is opposite to the so-called Nemets effect observed in deuteron breakup, where larger cross sections for deuteron breakup were observed for closed-shell nuclei (Nemets, 1968; Jarczyk *et al.*, 1973).

The characteristics of the bumps may be summarized as follows.

(i) The bump occurs at about beam velocity energies. Deviations from this position near the grazing angle, θ_{gr}, can be explained in terms of the energy difference between the slowdown of the projectile and the acceleration of the ejectile. For $\theta > \theta_{gr}$ the bump position will shift to lower energies approximately proportional to $\cos^2(\theta - \theta_{gr})$.

(ii) The width of the bump is in first order proportional to $\sqrt{E}\varepsilon$, with E being the bombarding energy and ε the binding energy of the projectile. Deviations occur due to the effects of phase space.

(iii) At forward angles the cross sections vary with target mass as $A^{1/3}$. At lower energies and with heavier targets deviations may occur due to the Coulomb barrier.

(iv) We like to add that there is yet little information on the energy dependence of the cross section. So far there are indications that there is a threshold for spectator breakup processes due to a mismatch of spectator energies and phase space. Above this threshold the cross section seems to increase gradually with energy (see, e.g., Fig. 31).

(v) Furthermore, the bumps for α-induced reactions have an apparent smaller cross section (see Figs. 21 and 22). This might be due to the broader momentum distribution, the number of possible partitions, and the smaller spectroscopic factors for partitions of the α projectile.

2. Tail part

Besides the bump the continuum part of the spectra usually contains a tail. This tail is present at all angles and is clearly observed at large angles. So far the properties of the tail have been studied for ^{3}He projectiles only at an incident energy of 52 MeV. In this study Aarts (1983) and Aarts, Malfliet, de Meijer, and van der Werf (1984) determined the shape of the tail at $\theta = 70°$, where the bump cross section is small, and assumed that its

shape remained identical for the other angles. The decomposition was made by scaling the magnitude of the cross section of the $\theta=70°$ spectrum so that the height at the low-energy side of the spectrum matched the spectrum studied. A different behavior of the tail for protons and deuterons was observed in the angular distributions of the energy-integrated cross section, as presented in the lower part of Fig. 26. For the protons the cross sections scale approximately with A. For the deuterons the cross sections are almost independent of A and show a forward peaking.

If one integrates the cross sections of the tail part of the spectrum over the angular range one obtains a cross section for protons which is linearly dependent on A and one for deuterons proportional to $A^{1/3}$ (see the bottom part of Fig. 32). In the case of full equilibration the shape of the tail spectra may be reproduced by a standard Fermi-gas model calculation for the recoiling compound system. The results of such a calculation for protons and deuterons assuming compound nucleus formation (Aarts, Malfliet, de Meijer, and van der Werf, 1984) are indicated in Figs. 26(c) and 26(d), respectively. In these calculations the value for the temperature T has been taken as a free parameter determined from the best fit to the spectra at $\theta_{\text{lab}}=70°$. These values are listed in Table II together with the values calculated with a standard Fermi-gas model. A comparison between the calculations and the experimental data in Fig. 26 shows a qualitative agreement for protons. The results for deuterons indicate that the deuteron-tail spectra cannot be described in this way. Furthermore, a comparison between the experimental and calculated values for the temperature (presented in Table II) shows for the deuterons an increase of the experimental values with A, whereas a decrease is expected from the Fermi-gas model. This, together with the forward peaking of the angular distribution of the deuteron tail [Fig. 26(d)], suggests that the deuteron is emitted from the projectile at an early stage of the collision (preequilibrium process).

C. Processes contributing to the continuum

1. Absorptive breakup

Absorptive breakup is found to be the major contributing reaction process to the continuum for spectra induced by ^{3}He projectiles. A good example of how to decompose

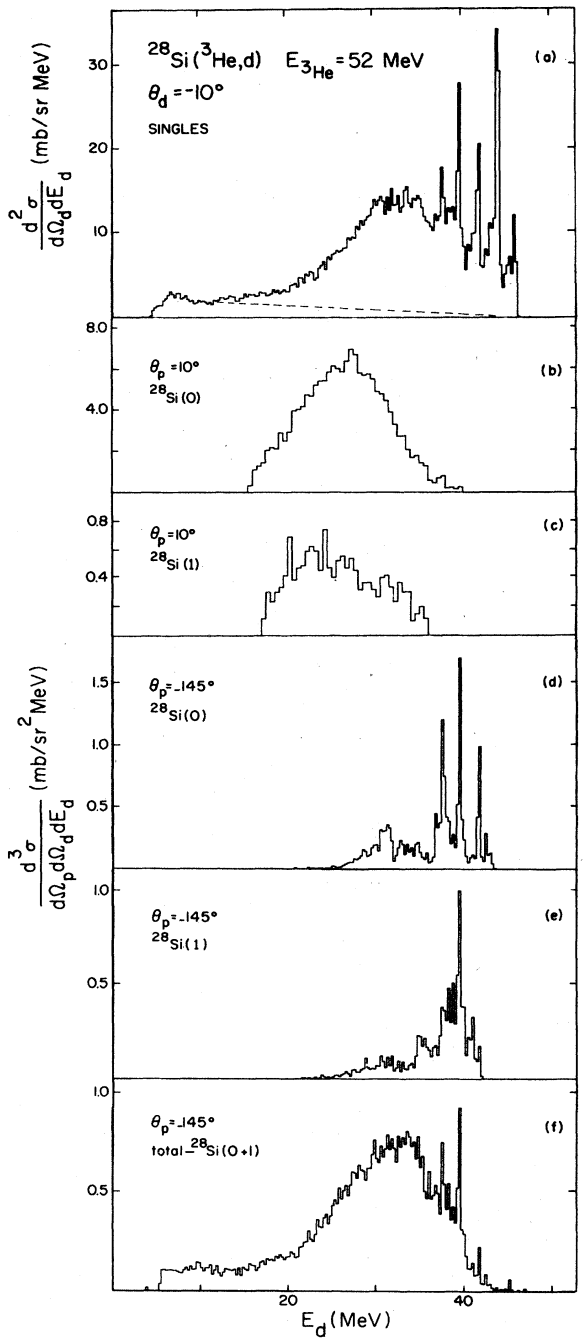

FIG. 33. Comparison among (a) the singles deuteron spectra at $\theta_d=-10°$ and the projected deuteron spectra from the (^{3}He,pd) at $\theta_d=-10°$, (b) gated on the ground-state transitions at $\theta_p=+10°$, (c) gated on the transitions to the first excited state at $\theta_p=+10°$, (d) gated on the ground-state transitions at $\theta_p=+145°$, (e) gated on the transitions to the first excited state at $\theta_p=+145°$, and (f) gated on the TKE spectrum excluding the transitions to the ground and first excited state at $\theta_p=+145°$ (Aarts, 1983; Aarts, Malfliet, de Meijer, and van der Werf, 1984).

TABLE II. Comparison between the temperatures calculated for a Fermi gas of nucleons (T_{calc}) and the experimental values (T_{exp}) (Aarts, Malfiet, de Meijer, and van der Werf, 1984).

Target	T_{calc} (MeV)	T^p_{exp} (MeV)[a]	T^d_{exp} (MeV)[b]
^{12}C	6.6	5.2±0.8	6 ±2
^{28}Si	4.9	4.0±0.6	7.0±1.5
^{58}Ni	3.8	3.5±0.6	8 ±2

[a]Obtained from the inclusive proton spectrum at $\theta_p=70°$.
[b]Obtained from the inclusive deuteron spectrum at $\theta_d=70°$.

the inclusive (^{3}He,d) cross section is presented in Fig. 33. The contribution to the inclusive deuteron yield at $\theta_d = 10°$ of elastic, inelastic, and absorptive breakup can be obtained from p-d coincidences by setting gates in the TKE spectrum on the ground state, on the strongly excited 2^+ state, and on the remainder. By projecting the events in each gate on, e.g., the E_d axis, one obtains for each angle θ_p the corresponding deuteron spectra, which one may compare with the inclusive spectrum. In Fig. 33 a comparison is given for ^{28}Si at $E_{^3\mathrm{He}} = 52$ MeV between the inclusive deuteron spectra at $\theta_d = -10°$ and various θ_p. Figures 33(b) and 33(c) show the projected deuteron spectra at $\theta_p = 10°$ for the loci of the ground state and the first excited state, respectively. Corresponding spectra at $\theta_p = +145°$ are presented in Figs. 33(d) and 33(e). Figure 33(f) shows the projections onto the deuteron energy axis of all events with a TKE smaller than the energy of the transition to the first excited state.

At $\theta_p = 10°$ the spectrum gated with the ground-state locus shows a broad bump and no contribution to the tail. The bump is shifted to lower energies with respect to the bump in the inclusive spectrum by about 5.5 MeV. This energy shift corresponds to the binding energy of the deuteron in ^{3}He. For the gate on the first excited state the bump has shifted even more towards lower energies. This is consistent with a breakup process in which the proton is a spectator (Aarts, Grasdijk *et al.*, 1981; Aarts *et al.*, 1982). At $\theta_p = +145°$ the bump has almost completely disappeared [Figs. 33(d) and 33(e)] and only sharp peaks remain, which are also present in the inclusive spectra. Thus these peaks are due to (^{3}He,d) transitions to states which have an excitation energy above the proton decay threshold.

The observation that the bumps, generated with the gates on the loci, show up at different energies than the bump in the inclusive spectra indicates that elastic and inelastic breakup are not the major contributors to the inclusive bump. Figure 33(f) suggests that the main contribution to the inclusive bump arises from uncorrelated events: the deuteron spectrum contains a tail and a bump and the bump is centered on energies corresponding to beam velocity ($\frac{2}{3}E_{^3\mathrm{He}}$). For ^{28}Si it has been shown that the corresponding proton spectra have a shape in which the intensity decreases exponentially for energies above the Coulomb barrier. Such a shape is characteristic for statistical emission. Aarts, Bhowmik *et al.* (1981), Aarts (1983), and Aarts, Malfliet, de Meijer, and van der Werf (1984) have identified this process as *absorptive breakup*. The definition of this process was given earlier (Koontz *et al.*, 1979) as "a reaction in which a subset of projectile nucleons suffers strong interaction with the target nucleus resulting in either evaporation or non-statistical emission of particles from the residual nucleus, leaving the remaining subset of projectile nucleons to continue with essentially their initial momentum prior to the interaction." In heavy-ion reactions the corresponding process has been named incomplete fusion (Inamura *et al.*, 1977; Wilzcyński *et al.*, 1980).

We should like to point out that in the case discussed above the deuteron is spectator and the proton is participant, absorbed by ^{28}Si to form ^{29}P. At the bombarding energy of 52 MeV the compound nucleus is formed such that it almost exclusively decays by protons. For higher energies and medium-heavy targets, also decay by neutrons and α particles might occur, depending on the thresholds. For very heavy nuclei the compound system is likely to fission.

In addition to the proton being participant there is absorptive breakup in which the proton is spectator and the deuteron as participant is absorbed. The compound system will again predominantly decay by proton, neutron, α-particle emission, or fission. So for the case of ^{28}Si this process will not be observed in d-p coincidences but in p-p coincidences. This process has been observed as the one-proton spectator breakup (Aarts, 1983; Aarts, Malfliet, de Meijer, and van der Werf, 1984).

For α-induced reactions absorptive breakup was also found to be important. Figure 34 shows the p-d coincidence data at $\theta_p = 10°$, $\theta_d = -10°$ for the α-induced reaction on ^{28}Si at $E_\alpha = 65$ MeV (de Meijer *et al.*, 1983). In addition to the loci, which correspond to the proton decay of proton unstable states populated in the (α,d) reaction, the data show events which seem to concentrate at low E_p. The projected deuteron spectrum in Fig. 34 has been obtained by selecting events with TKE less than 41.4 MeV (i.e., excluding the strong loci). The proton spectrum has an exponential shape, whereas the deuteron spectrum seems to consist of a bump and a tail. The bump part might be associated with absorptive breakup of the α particle with one deuteron being spectator and the

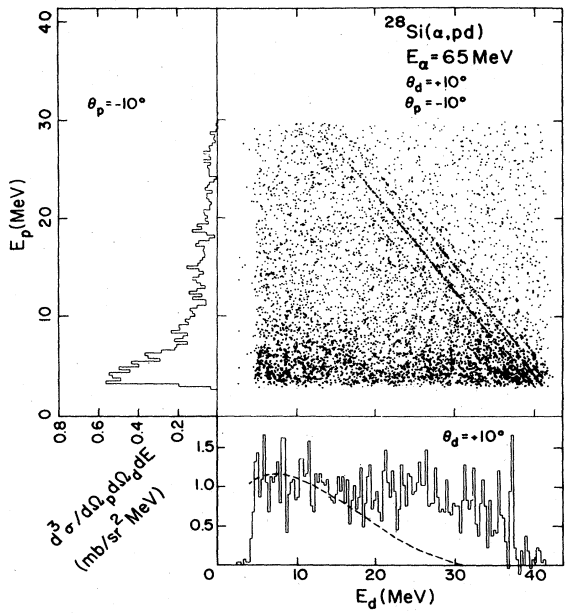

FIG. 34. Coincidence p-d spectra for the (α,pd) reaction: (a) the two-dimensional spectrum, (b) the projected proton spectrum, and (c) the projected deuteron spectrum. The spectra (b) and (c) are for events with TKE <41.4 MeV. The dashed line indicates the separation of the projected deuteron spectrum into a tail and a bump (de Meijer *et al.*, 1983).

other being absorbed to form a compound system which subsequently evaporates a proton. The bump in the inclusive deuteron spectrum at $\theta_d = 10°$ and $E_\alpha = 65$ MeV originates mainly from absorptive breakup (de Meijer *et al.*, 1983). The interpretation of the results at the higher α energy of 140 MeV (Koontz, 1980) is not unique. From their proton-deuteron correlation data it is not clear whether we are dealing with a process in which both the proton and the deuteron have approximately energies corresponding to beam velocities or if there is a combination of proton bump—deuteron tail and deuteron bump—proton tail, as possibly observed at $E_\alpha = 65$ MeV.

2. Elastic and inelastic breakup

Elastic and inelastic breakup have been extensively studied for ^{3}He- and α-induced reactions. For ^{3}He-induced reactions we illustrate these processes via *p-d* coincidence measurements at 52 MeV (Aarts, Grasdijk *et al.*, 1981; Aarts *et al.*, 1982). As was already mentioned in the introduction (Sec. V.A), these processes can be identified via the loci in a two-dimensional energy spectrum (see Fig. 24). From the projected deuteron energy spectra of the loci it was found (Sec. V.C.1) that these spectra were bell shaped and shifted towards lower energies compared to the inclusive data [see Figs. 33(b) and 33(c)]. These results suggest a process in which the proton is a spectator and the deuteron, as a participant, is elastically or inelastically scattered. The shift in the centroid position corresponds to the Q value for the reaction.

At $E_\alpha = 140$ MeV (Koontz, 1980) the elastic-breakup reactions have been investigated for the reactions (α,pt) and (α,dd). Three correlations were measured: the proton angle fixed at $\theta_p = 15°$ and the triton angle variable, the triton angle fixed at $\theta_t = 15°$ and the proton angle variable, and one deuteron angle fixed and the other deuteron angle variable. It is remarkable that in the correlation with the tritons detected at the fixed angle $\theta_t = 15°$ for all proton angles the triton bump centers at about 70 MeV and the proton at about 50 MeV. This result is consistent with a breakup process in which the proton is the spectator and the triton the participant, which scatters elastically with the target nucleus. The projected proton and triton spectra for the case θ_p fixed at $\theta_p = 15°$ are similar to the ones described above and indicate as expected a breakup with a proton spectator.

The elastic-breakup data obtained at 120 MeV (Koeslag *et al.*, 1983,1984) have been measured with a higher energy resolution than those of Koontz. The projected energy spectra show, in addition to the breakup bump, sharp states belonging to (α,t) transitions to proton unstable states. Also, these data indicate that in the forward-angle domain the proton is the spectator. For θ_t fixed at $\theta_t = -10°$ the triton spectra tend to shift gradually to higher energies with increasing $|\theta_p|$. At large angles they become difficult to distinguish from discrete transitions.

The data at $E_\alpha = 140$ MeV have been integrated over angle and energy assuming no dependence on the azimuthal angle. The contributions to the inclusive proton, deuteron, and triton yields are 4 ± 1, 7 ± 2, and 7 ± 2 mb/sr, respectively, corresponding to 1%, 3%, and 7% of the inclusive yields. From these values it can be concluded that elastic breakup is only a minor contributor to the total inclusive spectrum.

Analyzing powers of deuterons originating from elastic breakup of polarized ^{3}He have been measured at 33 MeV for the reactions on ^{12}C, ^{27}Al, and ^{58}Ni (Drumm *et al.*, 1983). For ^{12}C, the elastic-breakup component has a large negative analyzing power, the magnitude of which depends on the deuteron energy. This means that the analyzing power depends on the ratio in which the total energy is shared between the proton and the deuteron and hence on their relative energy. Figure 35 (Drumm *et al.*, 1983) presents the elastic-breakup differential cross sections and analyzing powers as functions of the deuteron angle for the three target nuclei. The solid lines represent the cross-section calculations with the distorted-wave breakup model (DWBM), described in Sec. VI. The solid and dashed lines for the analyzing powers in the ^{12}C experiment represent optical model calculations for elastic scattering of 27.5-MeV ^{3}He and 18-MeV deuterons, respectively. Drumm *et al.* (1983) relate the analyzing powers of the ^{3}He scattering to *p-d* coincidences at the same side of the beam and deuteron scattering to *p-d* coincidences at the opposite side. Moreover, they relate the ^{3}He scattering to sequential breakup and deuteron scattering to direct breakup. The optical model calculations for elastic deuteron scattering, however, have in the

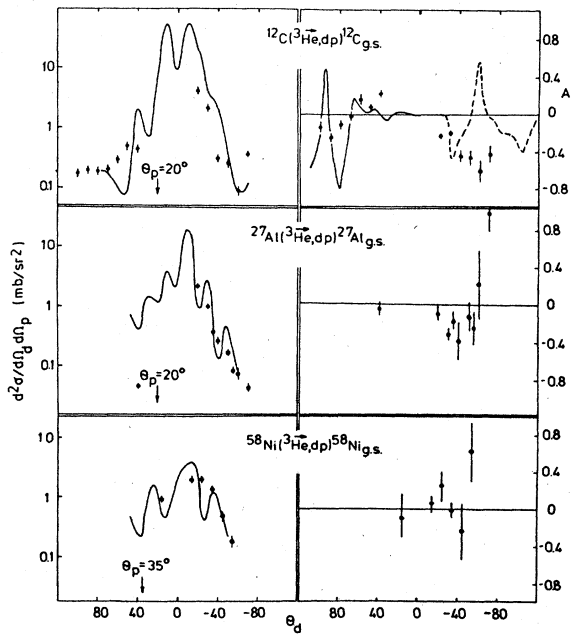

FIG. 35. The elastic-breakup differential cross section and analyzing powers for ^{12}C, ^{27}Al, and ^{58}Ni as a function of the deuteron angle at fixed proton angle given in the figure (Drumm *et al.*, 1983).

region of the maximum negative analyzing power the wrong sign.

In our opinion, a study of the analyzing powers in terms of elastic scattering is far too simple to provide a basis for valid conclusions. In addition, the energy resolution of about 1 MeV obscures the contribution of states which decay by proton emission to the ^{12}C ground state. So the large negative analyzing power might partly be due to transitions to these states, which in the case of ^{13}N also show negative analyzing powers.

The results of ^{3}He breakup did show that the cross section for inelastic breakup is 1—2 orders of magnitude weaker than elastic breakup. Since breakup cross sections are 1—2 orders of magnitude weaker in α-induced reactions, inelastic breakup has not been studied for α-induced breakup.

3. Breakup-transfer reactions

The breakup-transfer reaction has mainly been investigated via proton-triton coincidence measurements in the reaction ^{28}Si+^{3}He at 52 MeV (Aarts, Bhowmik *et al.*, 1981). The cross section for this process is about 2 orders of magnitude smaller than for elastic breakup. The fact that in general the elastic-breakup cross sections in α-induced reactions are about an order of magnitude weaker than in ^{3}He-induced reactions makes the observation of a breakup-transfer process in α-induced reaction almost impossible. As mentioned in the introduction (Sec. V.A), the inclusive (^{3}He,t) spectra at forward angles show a bump, which has been attributed to breakup processes. It has been suggested by Nomura (1978) that this bump may arise from a combined *breakup-transfer* reaction in which the ^{3}He breaks up into a deuteron and a proton followed by neutron pickup from the target by the deuteron. Besides this mechanism Bousshid *et al.* (1980) point out that the reaction might also proceed by sequential breakup via the (^{3}He,α^*) reaction subsequently followed by the decay of α^* into $t+p$ (see Sec. IV). This process via sequential decay will be named *transfer breakup* (see also Fig. 23). In this case α^* represents any excited state of the ^{4}He nucleus. It was also argued that ^{4}Li* production would be likely.

Figure 36 shows for ^{3}He projectiles the coincidence spectra gated on the ground state and/or first excited state in the $A=27$ nuclei in the TKE spectra at $\theta_1=-10°$ and $\theta_2=10°$. The bottom scale represents the energy of the heavier particle, the top scale the excitation energy in the nuclei ^{4}He and ^{4}Li together with the position of known resonances. These data clearly show that for this reaction the main contribution comes from the breakup-transfer process. The dashed curve for the d-d coincidences is calculated assuming that the reaction proceeds via the 25.5-MeV state in ^{4}He. Clearly the curve does not fit the data eliminating the transfer-breakup process as the main contributor. Even stronger evidence for breakup transfer is provided by the p-^{3}He coincidences which show a peak at a relative energy corresponding to an excitation energy lower than the ^{4}Li(gs). For the $p+t$

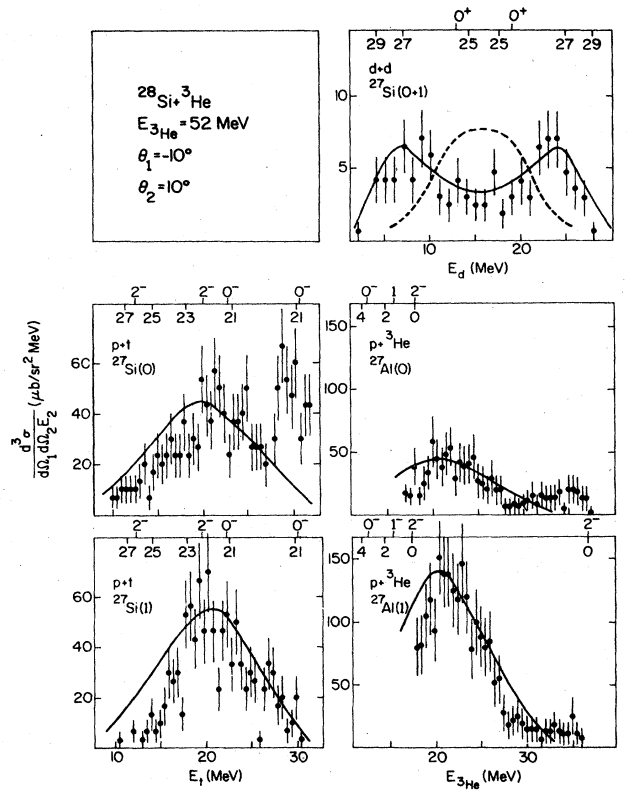

FIG. 36. Projected spectra gated on the ground state and/or first excited state in the final nucleus for the (^{3}He,dd), (^{3}He,pt), and (^{3}He,p^3He) reactions on ^{28}Si at $\theta_1=-10°$ and $\theta_2=10°$. The solid curves indicate the QFBM calculations (see Sec. VI). Excitation energies relative to the ground state in ^{4}He and ^{4}Li are indicated above each spectrum together with known resonances. The dashed line in the (^{3}He,dd) spectrum corresponds to ^{4}He* decay into $d+d$. The structures observed in the high-energy part of the triton spectrum [^{27}Si(gs)] arise from proton decay states in ^{28}P (Aarts, 1983).

data sequential decay cannot be ruled out easily. However, changes in the relative angle between proton and triton $\theta_{1\text{-}2}$ (see Sec. II) would change the correspondence between particle energy and relative energy. This change was not observed, and evidently the transfer-breakup mechanism can be excluded as the dominant process. The projected triton spectra show a bump around 20 MeV and for the ground-state transition some sharp states. The bump is situated at an energy $E_t \sim \frac{2}{3}E_{^3\text{He}}+Q(^3\text{He},pt)$. Similarly, the p-^{3}He data show a bump at an energy $E_{^3\text{He}} \sim \frac{2}{3}E_{^3\text{He}}+Q(^3\text{He},p^3\text{He})$. These observations are consistent with a reaction mechanism in which the proton is the spectator and the interaction of the deuteron with the target nucleus is a single-nucleon pickup process. The (^{3}He,dd) data are consistent with a process in which the deuteron acts as spectator ($E_d \sim 25$ MeV) and the proton picks up a neutron from the target nucleus ($E_d \sim 10$ MeV).

4. Breakup with two spectator particles

Both in ^{3}He- and α-induced reactions, a process was observed in which two ejectiles (protons) were emitted with beam velocity energies: the two-proton spectator breakup. The data at $E_\alpha = 140$ MeV on ^{90}Zr, for instance, taken with both proton detectors at $\theta_p = 15°$, show a cluster of events centered on beam velocity energy for both protons (Koontz *et al.*, 1980). This process diminishes rapidly with increasing detection angles. In Fig. 37 p-p coincidence data at $\theta_{p_1} = -10°$ and $\theta_{p_2} = +10°$ are shown from the reaction ^{28}Si + ^{3}He at $E = 52$ MeV (Aarts, 1983; Aarts *et al.*, 1983). In Fig. 37(a) one can observe a number of loci, corresponding to the (^{3}He,^{2}He) reaction (see Sec. IV) and a concentration of uncorrelated events centered on proton energies of about 18 MeV. This indicates that at this angle combination there is an appreciable number of proton pairs traveling with approximately beam velocity (*two-proton spectators*). The intensity of this cluster decreases rapidly with increasing $|\theta_{p_2}|$. The projections on the E_{p_1} and E_{p_2} axes have been made for events with TKE less than 45 MeV in order to exclude a large contribution from the (^{2}He,^{2}He) events on the loci. The projected spectra in Figs. 37(b) and 37(c) have the same shape as the inclusive proton spectra. From Fig. 37(a) it is also clear that there is no concentration of events at low proton energies. This implies that at $\theta_{p_1} = -10°$, $\theta_{p_2} = 10°$ the tail part is mainly arising from bump-tail coincidences with only a small part from tail-tail coincidences. In addition to two-spectator events one observes at this angle combination also one-proton spectator events, because one proton travels with beam velocity, whereas the other probably originates from an absorptive process. At more backward angles the two-dimensional spectra look quite different, as can be seen in Fig. 38. In this geometry particle 2 has been detected at $\theta_{p_2} = 70°$. In Fig. 38(a) the loci have disappeared and a concentration of uncorrelated events shows up as a band at low E_{p_2}. The projection of these events on the E_{p_1} axis yields a spectrum that might be divided into a tail and a bump centered near beam velocity. Comparison with the corresponding spectrum at $\theta_{p_2} = 10°$ shows that the intensity ratio between bump and tail has changed in favor of the tail. The projection on the E_{p_2} axis results in a pure evaporationlike spectrum. So, as expected and in agreement with the α-induced reactions, at the more backward angles one predominantly observes one- and no-proton spectator events.

The reaction mechanism involved in these two-, one-, and no-proton spectator processes is not yet as well determined as in the processes discussed before. This is due to the fact that not all constituents of the projectile have been detected. We will illustrate this for the case of ^{3}He-induced reactions where the neutron is not detected. In the two-proton spectator case the interaction between projectile and target has taken place between the neutron and the target. Since the two-proton coincidence measurement is kinematically incomplete, the individual contributions of elastic, inelastic, and absorptive breakup remain unknown. In the one-proton spectator process the ^{3}He projectile breaks up with one proton spectator, and the deuteron or the d^* (the virtual state of the deuteron with $S=0$ and $T=1$) is absorbed, leading to the statistical emission of a proton. The two statistically emitted protons in the no-spectator process are due to the absorption of either the full projectile (^{3}He) or ^{2}He. The ^{2}He absorption corresponds to absorptive breakup. Aarts (1983) and Aarts *et al.* (1983) have shown that the coincidence spec-

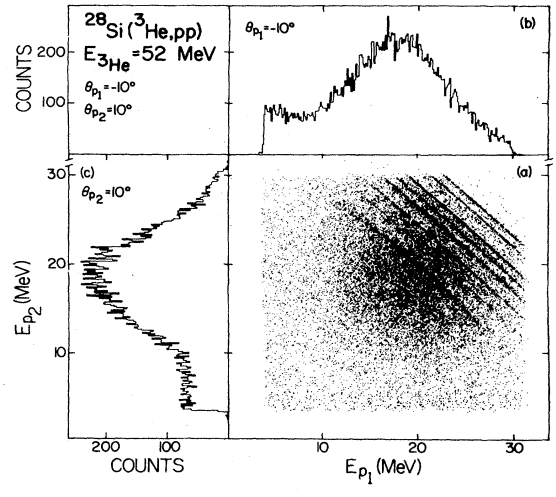

FIG. 37. A two-dimensional E_{p_2} vs E_{p_1} spectrum and the corresponding projections on the axes for events with TKE <45 MeV for the reactions ^{28}Si (^{3}He,pp) at $\theta_{p_1} = -10°$, $\theta_{p_2} = 10°$, and $E_{^3\mathrm{He}}$ MeV (Aarts *et al.*, 1983).

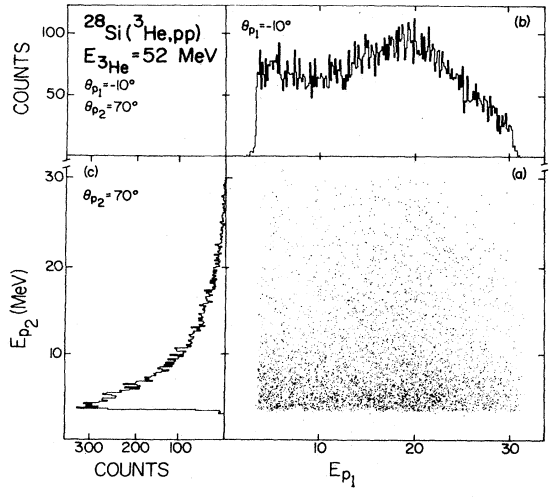

FIG. 38. A two-dimensional E_{p_2} vs E_{p_1} spectrum and the corresponding projectile spectra for the reaction ^{28}Si(^{3}He,pp) at $\theta_{p_1} = -10°$, $\theta_{p_2} = 70°$, and $E_{^3\mathrm{He}} = 52$ MeV (Aarts *et al.*, 1983).

TABLE III. Comparison between deuteron single cross sections at $\theta_d = 10°$ and cross sections derived from p-d coincidence measurements with the deuteron detection angle fixed at $\theta_d = -10°$ (Aarts, 1983; Aarts, Malfliet, de Meijer, and van der Werf, 1984).

Cross sections (mb/sr)		^{12}C	^{28}Si	^{58}Ni
Coincidence:	elastic breakup (0^+)	54±11	56±12	77 ±15
	inelastic breakup (2^+)	9±2	15± 3	3.4± 0.8
	absorptive breakup	25± 7	120±20	135 ±23
	total to the bump	88±13	190±30	220 ±30
	tail	22± 6	21± 5	15 ± 4
	total	110±15	210±30	230 ±30
Singles:	bump	80±20	192±20	270 ±30
	tail	15± 5	27± 5	40 ± 7
	total	95±20	220±20	310 ±30

tra at each angle combination might be unraveled into contributions from the three processes. The change in relative intensity between the three processes is also reflected in the shape of the TKE spectra as can be seen from Fig. 39. The spectra change from a bell-shaped continuum centered on 37 MeV with some sharp states superimposed on it at forward angles to a highly asymmetric continuum at backward angles and a centroid around 23 MeV.

D. Quantitative decomposition of the continuum cross section

By integrating the cross sections for the various processes over angle and energy one obtains their contribution to the inclusive spectra. For ^{3}He at 52 MeV this has been carried out for the targets ^{12}C, ^{28}Si, and ^{58}Ni (Aarts, 1983; Aarts *et al.*, 1983). Since the angular correlations have been measured in plane, the integration procedure has been carried out under the assumption of a linear dependence on the azimuthal angle (φ). This is equivalent to averaging the cross sections at $\varphi = 0°$ and 180°. Table III lists the contributions of elastic, inelastic, and absorptive breakup to the tail and bump part of the inclusive deuteron spectrum at $\theta_d = 10°$. It is clear that, except for ^{12}C, absorptive breakup is the dominant reaction process. Elastic and inelastic breakup contribute only to the bump part of the continuum. Table III also shows that for ^{12}C and ^{28}Si the inclusive deuteron yield for both the tail and the bump part is accounted for by the three kinds of p-d coincidence processes. For ^{58}Ni about 70% of the singles yield (bump ~80%, tail ~40%) is explained by the p-d coincidences. No significant coincidence yield was observed between deuterons and charged particles other than protons (Aarts, Bhowmik *et al.*, 1981; Aarts *et al.*, 1983). Calculations (Aarts, 1983; Aarts, Malfliet, de Meijer, and van der Werf, 1984) show that for ^{58}Ni the missing strength can be attributed to the neutron-decay channel, that is, to processes like absorptive breakup with the deuteron as spectator and for which the proton as participant is absorbed and a neutron reemitted.

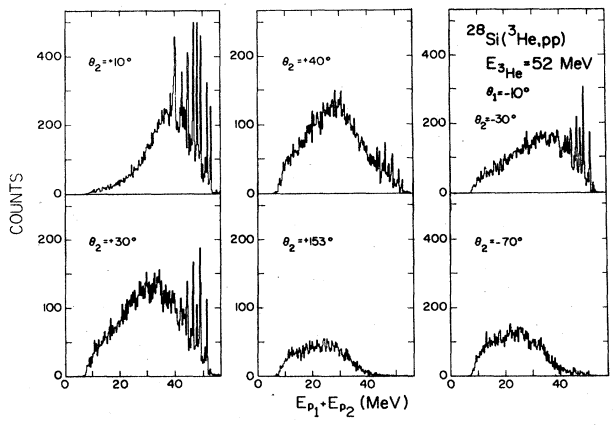

FIG. 39. TKE spectra for various angles of the moving telescope (θ_{p_2}) for the reaction ^{28}Si(^{3}He,pp) with $\theta_{p_1} = -10°$ (after Aarts, Malfliet, de Meijer, and van der Werf, 1984).

Figure 40 displays the target mass dependence of the elastic and absorption breakup contributions to the (^{3}He,d) yields. The contributions of absorptive breakup have been corrected for neutron decay by taking the difference between the singles cross section and the elastic-plus-inelastic breakup cross section. From Fig. 40 one can conclude that elastic breakup varies with target as $A^{1/3}$, indicating that elastic breakup is a peripheral process. For absorptive breakup where the cross section will depend on both the formation and the decay, the data indicate an $A^{2/3}$-A dependence. These results explain why their summed contribution leads to an A dependence somewhere between $A^{1/3}$ and $A^{2/3}$ for the inclusive bump cross sections. The fact that for higher energies an $A^{1/3}$ dependence is observed for the singles deuterons (Matsuoka *et al.*, 1978; Djaloeis *et al.*, 1983) might indicate that either elastic and inelastic breakup become more important or that in the absorptive breakup the nonstatistical emission of particles will increase.

The same procedure has been employed to reconstruct

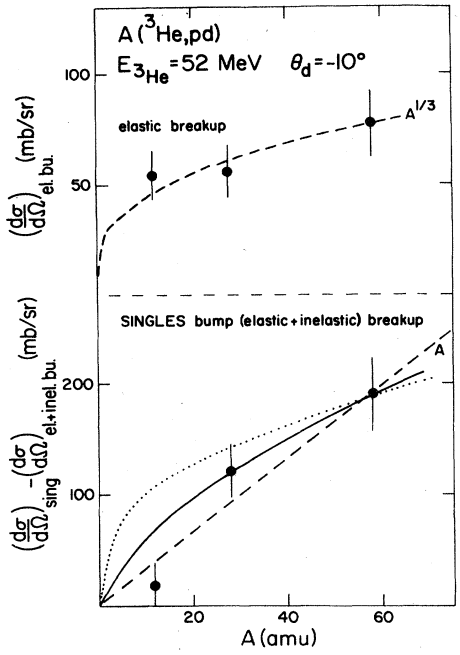

FIG. 40. The mass dependence of elastic breakup and absorptive breakup [singles bump—(elastic + inelastic) breakup] in p-d coincidence measurements at $\theta_d = -10°$ (Aarts, 1983; Aarts, Malfliet, de Meijer, and van der Werf, 1984).

the inclusive (^{3}He,p) cross sections from the various coincidence data. Table IV presents the contributions of p-d and various p-p cross sections, which have been integrated over angle and energy (Aarts, 1983; Aarts, Malfliet, de Meijer, and van der Werf, 1984). One observes that the inclusive proton yield for the bump is well reproduced by the coincidence data. There is no appreciable cross section going to an unobserved neutron channel. Or stated differently, if neutrons are produced in a (^{3}He,nxp) reaction, the processes with $x \geq 2$ are dominant.

Recently, Motobayashi *et al.* (1984) have investigated the importance of the neutron decay channel for medium-heavy nuclei. At $E_{^3\mathrm{He}} = 100$ MeV they investigated the breakup reaction via charged particle γ coincidences for the reaction on ^{165}Ho, ^{166}Er, and ^{167}Er. From the γ-ray spectra the final nucleus is identified. From their analysis they conclude that direct breakup accounts for about 60% of the angle-integrated cross sections in the proton and deuteron spectra. The contributions of elastic, inelastic, and absorptive breakup and preequilibrium emission (PEQ) to the breakup cross section at $\theta = 17°$ have been presented in Fig. 41 together with the decomposition of the cross sections at $E_{^3\mathrm{He}} = 52$ MeV. From the figure it is clear that absorptive breakup at $E_{^3\mathrm{He}} = 100$ MeV is still the main contributor to the inclusive (^{3}He,p) and (^{3}He,d) reactions. For the (^{3}He,d) case a direct comparison with the results of Aarts (1983) and Aarts, Malfliet, de Meijer, and van der Werf (1984) is possible if one assumes that the preequilibrium part corresponds to the tail. Both the particle-particle coincidences and the γ-ray method allow the decomposition in terms of the same breakup processes. The particle-particle method determines these contributions directly, while in the γ-ray method one strongly relies on the validity of exciton-model calculations. For the (^{3}He,p) case a direct comparison is not possible, since the p-p coincidences provide only two-, one-, and no-spectator yields. As mentioned before, the one-spectator process corresponds to absorptive breakup, and the two-spectator process contains elastic, inelastic, and absorptive breakup; their relative strength is unknown, because the neutron is not detected. The no-spectator process might be due to absorptive breakup and/or complete fusion.

As shown in Fig. 42, the results at $E_{^3\mathrm{He}} = 100$ MeV indicate that for these medium nuclei the major part of the cross section escapes via the dxn channel. For the protons their results confirm the results at 52 MeV that the

TABLE IV. Comparison between proton single cross sections at $\theta_p = -10°$ and cross sections obtained from p-d and p-p coincidence measurements with the proton detection angle fixed at $\theta_p = -10°$ (Aarts, 1983; Aarts, Malfliet, de Meijer, and van der Werf, 1984).

Cross sections (mb/sr)		^{12}C	^{28}Si	^{58}Ni
Coincidences:	two-proton spectator	75 ±10	175 ±20	205 ±35
	one-proton spectator (p_1)	100 ±20	220 ±40	270 ±50
	p-d coincidences	26 ± 5	21 ± 5	26 ± 5
	total to the bump	200 ±30	420 ±50	500 ±60
	one-proton spectator (p_2)	5 ± 3	10 ± 5	12 ± 5
	two-proton evaporation	30 ± 3	60 ± 8	150 ±30
	p-d coincidences	1.0± 0.5	3.3± 0.5	3.6± 0.5
	total to the tail	35 ± 4	75 ±10	165 ±30
	total	240 ±30	500 ±50	670 ±70
Singles:	bump	210 ±20	430 ±40	510 ±40
	tail	52 ± 6	105 ±10	170 ±20
	total	260 ±20	540 ±40	680 ±40

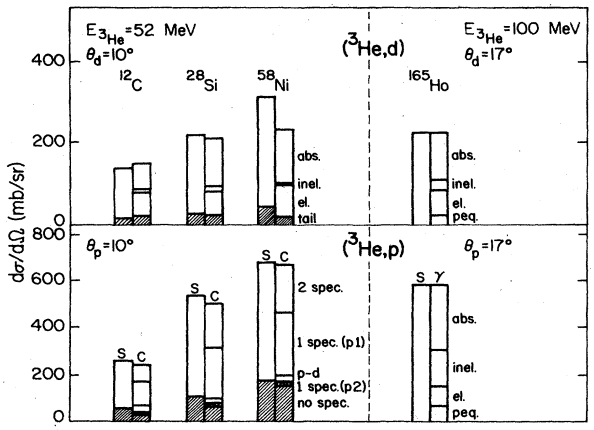

FIG. 41. Comparison of (^{3}He,d) and (^{3}He,p) inclusive cross sections (S) with those obtained in particle-particle coincidences (C) and the analysis of γ-ray spectra (γ). For details see text.

yield in $2pn$ channel is much larger than in the pn or $p2n$ channel.

The mass dependence for p-p coincidences has also been deduced (Aarts, 1983). An unambiguous dependence could be obtained only for the no-spectator component. Its linear dependence on A is consistent with that observed for the inclusive tail.

The relation between the coincidence cross sections and the inclusive yields has also been established for some of the α-induced data. At $E_\alpha = 65$ MeV the p-d cross sections were measured at $\theta_d = -10°$ and $\theta_p = 10°$ (de Meijer *et al.*, 1983). Assuming an isotropic angular distribution, de Meijer *et al.* found this absorptive breakup process to contribute 16 ± 7 mb/sr to the bump in the inclusive deuteron spectrum of 23 ± 6 mb/sr.

At higher energies, $E_\alpha = 140$ MeV, Koontz (1980) also analyzed the p-d correlations. Integration over angle and energy results in a contribution of 30 mb/sr to the total inclusive proton spectrum and of 40 mb/sr to the inclusive deuteron spectra. These contributions correspond to about 6% and 80% of the total inclusive yields, respectively (Koontz, 1980). At the same energy of $E_\alpha = 140$ MeV the tritons at forward angles were found to be mainly coincident with low energetic protons. These coincidences contribute 83 ± 6 mb/sr or 70% to the inclusive triton yield at $\theta_t = 15°$ (Koontz, 1980).

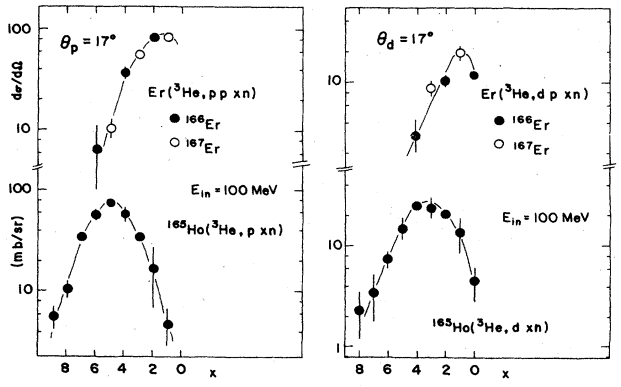

FIG. 42. Neutron multiplicity distributions of the reactions (a) ^{165}Ho(^{3}He,pxn)^{4}Er and ^{166,167}Er(^{3}He,$2pxn$)^{4}Er, and (b) ^{165}Ho(^{3}He,dxn)^{4}Er and ^{166,167}Er(^{3}He,$dpxn$)^{4}Er. Protons and deuterons were detected at 17°. Lines are intended only to guide the eye (Motobayashi *et al.*, 1981).

E. Conclusions

The analysis of the bumps in the continuum of inclusive spectra induced by ^{3}He or α projectiles reveals that these enhancements are partly due to breakup processes in which the detected particle is a spectator. This process is always present at those incident energies where the spectator energy (beam velocity energy) is allowed by the three-particle phase space. For some ejectiles these bumps also contain contributions from the decay of unresolved states populated by stripping reactions. For a fixed bombarding energy the bump cross section at forward angles shows a target-mass dependence given by $A^{1/3}$, whereas the width of the bump is determined by the product of the momentum distribution of the constituents in the projectile and the available phase space.

The measurements of particle-particle angular correlations in He-induced reactions reveal that the shape and magnitude of the continuum part of the inclusive particle spectra can be explained as the sum of contributions of various processes. The cross sections for those processes show very different dependences on detection angle and target mass. One therefore should be cautious in attempting to deduce information on reaction mechanisms of one apparent phenomenon in inclusive spectra from angular distributions and mass dependence only. Decomposition via detailed angular correlation measurements revealed that the following direct breakup processes contribute to the bump part: (i) elastic breakup, (ii) inelastic breakup, and (iii) absorptive breakup. Absorptive breakup is the dominant channel for at least the ^{3}He projectiles. Especially the measurements of ^{3}He-induced triton spectra have shown the existence of the breakup-transfer process. A common feature of all the breakup processes is the observation of a spectator particle. The reactions differ by the interaction of the participant and the target nucleus. These interactions resemble those responsible for processes in conventional nuclear reactions.

In addition to the reactions mentioned above, the p-p coincidence data show two-proton spectator and no-proton spectator processes for both projectiles, but the details of the reaction mechanisms contributing to these processes are not yet well determined.

The main differences between the ^{3}He- and α-induced breakup reactions are (i) the absence of direct breakup processes in the (α,t) and (α,^{3}He) channels at $E_\alpha = 65$ MeV, (ii) the fact that at higher energies ($E_\alpha = 120$ MeV) the bump in the (α,t) and (α,^{3}He) spectra was found to be exclusively due to sequential particle decay of states popu-

lated in the conventional transfer reactions, and (iii) the strongly forward peaked process in the α-induced t-p coincidences, which contribute to the inclusive triton tail spectrum.

VI. DESCRIPTION OF DIRECT BREAKUP PROCESSES

A. Introduction

Breakup data for various projectiles have been used to test a number of descriptions of the reaction mechanisms. In this section we will focus mainly on those approaches that have been applied to the analysis of ^{3}He and ^{4}He breakup reactions.

This section starts with a semiempirical model, based on the spectroscopic properties of the projectile, that relates the coincidence cross sections with the inclusive yields. In Sec. VI.C a summary is given of the formal reaction theory which forms the basis for the elaborate models. The transition-matrix elements from the formal reaction theory will be evaluated for the various models in order of increasing complexity. We will start with the Serber model, developed by Serber in 1947 for the description of deuteron projectile breakup data at $E_d = 190$ MeV. In this model the T-matrix element is a probability function given by the internal-momentum distribution of the projectile. Next, the inclusion of the wave functions will take place for both the entrance and exit channels. In the first stage we evaluate the matrix elements for the case of plane waves in all channels. In this approximation the T-matrix elements may be factorized into one part depending on the momentum transferred to the final nucleus and another part which is the probability function given by the internal momentum in the projectile.

The extension to distorted waves will be carried out in two steps. First some of the exit channels will be described by distorted waves. This occurs in the quasifree breakup model (QFBM), where the breakup is thought to occur via the nuclear interaction of the target nucleus with only a part of the projectile (participant). The remaining part of the projectile is assumed to continue essentially undisturbed (spectator). The Coulomb distortions of the projectile in the entrance channel and the spectator in the exit channel are taken into account semiclassically. In this model the T-matrix element is still separable, with one part reflecting the momentum distribution of the projectile and another part, depending on the transferred momentum, resembling the T-matrix element as if the participant were a free particle.

In the distorted-wave breakup model (DWBM) distorted waves will be used in all channels.

This model also provides absolute cross sections. At the end of this section a comparison between QFBM and DWBM will be made. Finally, a summary will be given of some models applied to, e.g., deuteron and heavy-ion projectile breakup.

B. A semiempirical model to relate inclusive and coincident cross sections for proton and deuteron spectra

In Sec. V we have seen that many of the observed properties in the inclusive proton and deuteron spectra are related to the properties of the projectile. Furthermore, we have seen that the inclusive cross sections can be well reproduced by the coincidence measurements. These observations suggest that there is a relation between the inclusive yields and the coincidence yields via the properties of the projectile. For the case of ^{3}He, Aarts (1983) and Aarts, Malfliet, de Meijer, and van der Werf (1984) have proposed a scheme based on the simple, but rather realistic assumption that the spectroscopic factors of the partition of ^{3}He into $p+d$, $p+\hat{d}$, and $n+{}^2$He are all equal to unity. Here $\hat{d}$ and ^{2}He represent the virtual states, with $S=0$ and $T=1$ in the $n+p$ and $p+p$ system, respectively. The cross-section scheme, presented in Table V, can be set up by making additional assumptions.

TABLE V. Schematic presentation of spectator and participant cross sections (Aarts, 1983; Aarts, Malfliet, de Meijer, and van der Werf, 1984).

Cross section	Spectator	Participant	Yield Proton spectator	Yield Proton participant	Yield Deuteron spectator
X_0	^{2}He$(p+p)$	n	$2X_0$		
X_0	d	p		X_0	X_0
X_0	$\hat{d}(p+n)$	p	X_0	X_0	
X_1	n	^{2}He$(p+p)$		$2X_1$	
X_1	p	d	X_1	X_1	
X_1	p	$\hat{d}(n+p)$	X_1	X_1	
X_2		$n+{}^2$He$(p+p)$		$2X_2$	
X_2		$p+d$		$2X_2$	
X_2		$p+\hat{d}(n+p)$		$2X_2$	
Total yield			$3X_0+2X_1$	$2X_0+4X_1+6X_2$	X_0

TABLE VI. Total angle-integrated inclusive cross sections for the proton bump (A), the deuteron bump (B), and the proton tail (C), together with the cross sections for the one-participant (X_0), the two-participant (X_1), and the three-participant (X_2) processes (Aarts, 1983; Aarts, Malfliet, de Meijer, and van der Werf, 1984).

Target	A (mb)	B (mb)	C (mb)	X_0 (mb)	X_1 (mb)	X_2 (mb)
^{12}C	140±20	35± 5	400± 80	35±4	18±2	43± 5
^{28}Si	230±25	60± 8	900±100	60±8	25±3	133±15
^{58}Ni	330±35	85±10	1800±100	85±9	38±4	247±25

(i) Absorptive breakup is the only contributing channel;
(ii) all composite particles (d, $\bar{d}$, ^{2}He, and ^{3}He) that are absorbed will be reemitted statistically as protons or neutrons;
(iii) the transition amplitudes add incoherently; and
(iv) the interactions of the individual constituents with the target nucleus are the same ($V_{p_1A}=V_{p_2A}=V_{nA}$).

The first assumption is based on the observation that absorptive processes are found to be dominant processes contributing to the inclusive (^{3}He,p) and (^{3}He,d) bump cross sections at forward angles. The second assumption is justified by the measurements with one telescope at forward angles (10°) and the other at 145°, where almost exclusively protons were found to be in coincidence with charged particles detected at $\theta=10°$ (Aarts, 1983; Aarts, Malfliet, de Meijer, and van der Werf, 1984).

The probability P for observing two particles in coincidence can be deduced from the scheme presented in Table V. The probabilities are labeled with indices denoting the type of particle: s for spectator protons, p for participant protons, and d for spectator deuterons. By defining the quantities $A=3X_0+2X_1$, $B=X_0$, and $C=2X_0+4X_1+6X_2$, one obtains the following generalizations:

(i) If one observes in one detector system a *spectator* proton, then the probability that the particle in the second detector system is a spectator proton or a participant proton is given by $P_{ss}=2X_0/A$ and $P_{sp}=(X_0+2X_1)/A$, respectively.
(ii) If one observes in one detector system a *participant* proton then the probability that the particle in the other system is a spectator proton, a participant proton, or a spectator deuteron is given by $P_{ps}=(X_0+2X_1)/C$, $P_{pp}=(2X_1+6X_2)/C$, and $P_{pd}=X_0/C$, respectively.

From Table V it follows that the quantities A, B, and C correspond to experimental quantities. These quantities are the total angle and energy-integrated inclusive cross sections for the proton continuum bump, deuteron continuum bump, and proton tail, respectively. The cross sections X_0, X_1, and X_2 can be deduced from the quantities A, B, and C and subsequently the probabilities P. Table VI presents the comparison between the calculated and experimental probabilities. The authors estimate the errors to be about 15%. The agreement between the values is surprisingly good and this simple model seems to be a useful tool to describe the global features for the breakup reactions.

This simple model for ^{3}He also allows an estimate of the contributions of the breakup processes ($3X_0+3X_1$) to the total geometrical reaction cross section given by πR_0^2. At 52 MeV it is found that for the targets ^{12}C, ^{28}Si, and ^{58}Ni breakup accounts for about 20% of the total reaction cross section.

C. Formal reaction theory

This section deals with some of the basic expressions used as starting points for the description of the cross section in various models. A reaction in which the projectile a collides with the target nucleus A leading to the production of n particles may be written as

$$a+A\rightarrow 1+2+3+\cdots+n\ . \tag{6.1}$$

The general expression for the differential cross section for this reaction in the laboratory system is given by Terrall (1970):

$$d\sigma=\frac{2\pi}{\hbar^2}\frac{m_a}{k_a}|T_{fi}|^2(2\pi\hbar)^3\delta^{(4)}(P_i-P_f)\prod_{j=1}^{n}\frac{d^3p_j}{(2\pi\hbar)^3}\ . \tag{6.2}$$

In this expression the reduced mass and momentum in the incident channel are approximated by the mass and momentum of the projectile. The conservation of momenta and energy is contained in the 4-δ function $\delta^{(4)}(P_i-P_f)$, where P_i and P_f are given by

$$P_i=(E_a+E_A,\mathbf{p}_a+\mathbf{p}_A)$$
and
$$P_f=\left[\sum_j E_j-Q,\sum_j \mathbf{p}_j\right]\ . \tag{6.3}$$

Here E_j and $\mathbf{p}_j$ are the kinetic energy and momentum of particle j, respectively, and Q denotes the reaction Q value. The quantity T_{fi} is the transition-matrix element. Equation (6.2) essentially contains two parts.

(i) The kinematics of the reaction represented by the phase-space factor:

$$\rho(E_1,\ldots,E_n)\prod_{j=1}^{n}d^3p_j=(2\pi\hbar)^3\delta^{(4)}(P_i-P_f)\prod_{j=1}^{n}\frac{d^3p_j}{(2\pi\hbar)^3}\ . \tag{6.4}$$

This factor determines the available phase space for the reaction products in the exit channel (see Sec. II).

(ii) The dynamics of the reaction represented by the transition-matrix element or transition amplitude T_{fi}. This quantity gives the probability for the transition from the incident channel to a specific final channel.

For the introduction of the distorted waves and the Born approximation we refer to standard textbooks (e.g., Jackson, 1970). The transition amplitudes in the distorted-wave Born approximation (DWBA) then reduce to the familiar expressions (Jackson, 1970):

$$T_{fi}^{\text{post}}=\langle\varphi_f \mid U_f \mid \chi_i^{(+)}\rangle+\langle\chi_f^{(-)} \mid W_f \mid \chi_i^{(+)}\rangle \ , \quad (6.5a)$$

$$T_{fi}^{\text{prior}}=\langle\chi_f^{(-)} \mid U_i \mid \varphi_i\rangle+\langle\chi_f^{(-)} \mid W_i \mid \chi_i^{(+)}\rangle \ . \quad (6.5b)$$

In these expressions χ and φ represent the distorted waves and stationary scattering states, respectively. The potentials U and W are the constituents of the potential V, which is separated into a part that describes the elastic scattering in the particular channel (U) and a part which causes the transition (W). This implies that for any reaction channel the first terms in Eqs. (6.5a) and (6.5b) vanish, since the potentials U do not connect the initial (i) and final (f) states. In the actual calculations of the transition amplitudes further simplifying assumptions are made. The expressions in Eqs. (6.5) indicate the equivalence of the post and prior forms in the DWBA. This equivalence may be destroyed in the actual calculations due to additional assumptions.

For comparison with experimental data the double and triple differential cross sections can be calculated from Eq. (6.2) by integrating over all nonobserved momenta and summing over all possible configurations of outgoing particles. This results in

$$\frac{d^3\sigma}{d\Omega_1 d\Omega_2 dE_1}=\frac{2\pi}{\hbar^2}\frac{m_a}{k_a} \mid T_{fi} \mid^2 \rho(E_1) \ , \quad (6.6)$$

and

$$\frac{d^2\sigma}{d\Omega_1 dE_1}=\frac{8\pi^2}{\hbar^2}\frac{m_a}{k_a} \mid T'_{fi} \mid^2 \rho(E_1) \ . \quad (6.7)$$

In Eqs. (6.6) and (6.7) $\rho(E)$ is the phase-space factor for only one particle being observed, as given by Eqs. (26) and (27) of Ohlsen (1965). The matrix element $\mid T'_{fi} \mid$ in Eq. (6.7) is the matrix element $\mid T_{fi} \mid$ in Eq. (6.6) averaged over the solid angle Ω_2.

D. Serber model

In one of the earlier breakup studies Helmholtz *et al.* (1947) observed, in the bombardment of a target with 190-MeV deuterons, a narrow beam of high-energetic neutrons. The neutrons were produced with an average energy of about half the beam energy. In order to explain these data Serber (1947) proposed that the deuteron strikes the edge of the nucleus. In this process the proton is stripped off, whereas the neutron misses the target and continues with its momentum $\mathbf{p}$ at the moment of breakup. This momentum is thought to be composed out of the momentum of the neutron corresponding to beam velocity, $\mathbf{p}_0$, and its internal momentum in the projectile, $\mathbf{p}_i$, such that

$$\mathbf{p}=\mathbf{p}_0+\mathbf{p}_i \ . \quad (6.8)$$

In the Serber model the probability of observing a particle with momentum $\mathbf{p}$ is given by

$$\mid T_{fi}(E) \mid^2=P(\mathbf{p})\sim \mid \Phi(\mathbf{p}_i) \mid^2 , \quad (6.9)$$

where the relation between $\mathbf{p}$ and $\mathbf{p}_i$ is given by Eq. (6.8) and $\Phi(\mathbf{p}_i)$ is the Fourier transform of the relative wave function of the spectator particle in the projectile. Substituting this result into Eq. (6.7) yields

$$\frac{d^2\sigma}{d\Omega\, dE}\sim \mid \Phi(\mathbf{p}_i) \mid^2 [E(E_{\max}-E)]^{1/2} , \quad (6.10)$$

in which $E_{\max}$ is the kinematically allowed maximum energy. In the Serber model the cross section is target independent.

This model has also been applied to breakup data obtained with ^{3}He and ^{4}He beams. Figure 43 shows inclusive deuteron spectra from the bombardment of ^{90}Zr with 70-MeV ^{3}He at several angles together with curves representing the results of calculations using Eq. (6.10) (Matsuoka *et al.*, 1978). In these calculations the internal wave function was approximated by a Yukawa function and the calculated cross sections are normalized to the peak cross sections at $\theta_{\text{lab}}=13°$. These calculations reproduce the general trend in the peak energies, widths, and angular dependences of the bump spectra. The forward peaking of the angular distributions is also fairly well reproduced by the calculations. Further improvements

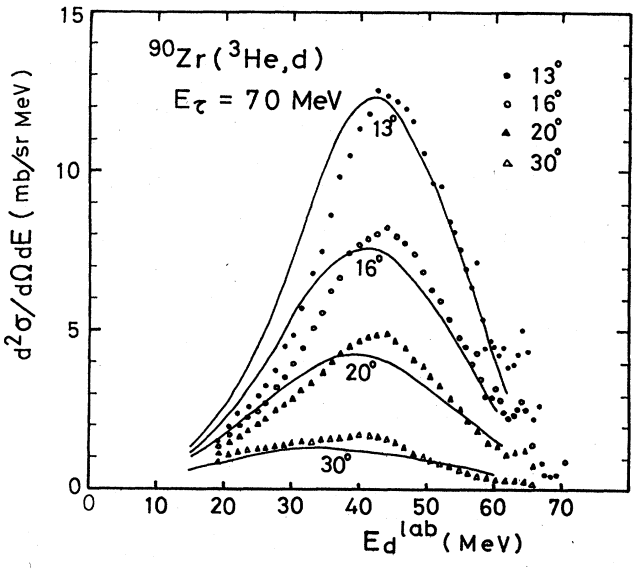

FIG. 43. Spectrum of deuterons from the bombardment of ^{90}Zr with 70-MeV ^{3}He, at several lab angles. The solid curves are calculated from Eq. (6.10) using a Yukawa wave function for the Fermi motion (Matsuoka *et al.*, 1978).

could be obtained by including the effect of the Coulomb force. These corrections involve an adjustment of the magnitude and direction of the momenta for a grazing trajectory and are usually referred to as the local Coulomb corrected momenta (McVoy and Nemes, 1980). Similar results have been obtained by Wu *et al.* (1978) for inclusive ^{3}He energy spectra for 140-MeV α particles on ^{209}Bi. In their calculation a wave function of the Eckart form was used and local momenta were employed.

E. Cross sections in the plane-wave Born approximation

In the plane-wave Born approximation (PWBA) it is assumed that the distortions by nuclear and Coulomb forces are small on the scattering wave functions and hence that the scattering wave functions in the entrance and exit channels can be represented by plane waves. In the spectator-participant approach it is assumed that the projectile a consists of the spectator b and the participant x. If we write for the reaction

$$a\{b+x\}+A\rightarrow b+\{x+A\}\rightarrow b+y+B \tag{6.11}$$

the T-matrix element in the post representation [Eq. (6.5a)] is given by

$$T_{\rm post}^{\rm PW}=\langle\chi_f^{(-)}\,|\,W_f\,|\,\chi_i^{(+)}\rangle\ . \tag{6.12}$$

In this expression

$$W_f=V_{bx}(\mathbf{r}_{bx})\ , \tag{6.13a}$$

$$|\,\chi_i^{(+)}\rangle=|\exp(i\mathbf{k}_a\cdot\mathbf{R}_a)\Psi_a(\mathbf{r}_{bx},\xi_b,\xi_x)\Psi_A(\xi_A)\rangle\ , \tag{6.13b}$$

and

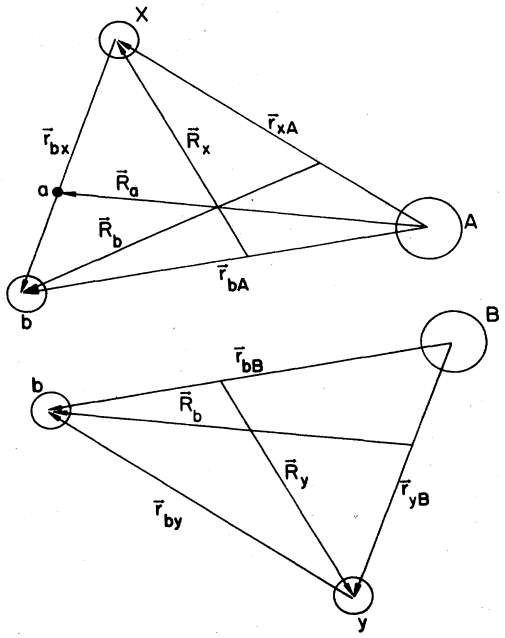

FIG. 44. Coordinate system used in the calculations.

$$\langle\chi_f^{(-)}|=\langle\exp(-i\mathbf{k}_b\cdot\mathbf{R}_b-i\mathbf{k}_x\cdot\mathbf{R}_x)\Psi_b(\xi_b)\times\Psi_y(\xi_y)\Psi_B(\xi_B)|\ . \tag{6.13c}$$

In these equations Ψ_a, Ψ_b, Ψ_y, Ψ_A, and Ψ_B represent the intrinsic wave functions of the particles a, b, y, A, and B, respectively, ξ denotes their internal coordinates, and the other coordinates are displayed in Fig. 44. We should like to point out that the relation between the coordinates of y and x and of B and A has not been indicated explicitly in Eqs. (6.13b) and (6.13c).

For the relative simple case of elastic breakup ($y=x$ and $B=A$) Eq. (6.12) may be written as

$$\mathcal{T}_{\rm post}^{\rm PW}=\int\int d\mathbf{R}_a d\mathbf{r}_{bx}\exp(-i\mathbf{k}_b\cdot\mathbf{R}_b-i\mathbf{k}_x\cdot\mathbf{R}_x)\langle\Psi_b(\xi_b)\Psi_x(\xi_x)\,|\,V_{bx}(\mathbf{r}_{bx})\,|\,\Psi_a(\mathbf{r}_{bx},\xi_b,\xi_x)\rangle\exp(i\mathbf{k}_a\cdot\mathbf{R}_a)\ . \tag{6.14}$$

With the usual expansion of Ψ_a as

$$\Psi_a(\mathbf{r}_{bx},\xi_b,\xi_x)=(c^2s)^{1/2}\varphi_a(\mathbf{r}_{bx})\Psi_b(\xi_b)\Psi_x(\xi_x)+\cdots \tag{6.15}$$

the integration over the internal coordinates can be carried out and the matrix element separates into

$$\mathcal{T}_{\rm post}^{\rm PW}=(c^2s)^{1/2}\int d\mathbf{R}_a\exp(i\mathbf{Q}\cdot\mathbf{R}_a)\int d\mathbf{r}_{bx}V_{bx}(\mathbf{r}_{bx})\psi_a(\mathbf{r}_{bx})e^{-i\mathbf{q}\cdot\mathbf{r}_{bx}}\ . \tag{6.16}$$

In these equations $(c^2s)^{1/2}$ is the spectroscopic amplitude for the decomposition of the projectile into b and x, and $\psi_a(\mathbf{r}_{bx})$ is the normalized radial wave function of b in the projectile a. The vectors $\mathbf{Q}$ and $\mathbf{q}$ represent the momentum transfer to the target and the internal momentum of the projectile, respectively, and are given by

$$\mathbf{Q}=\mathbf{k}_a-\mathbf{k}_b-\mathbf{k}_x \tag{6.17a}$$

and

$$\mathbf{q}=\mathbf{k}_b-\mathbf{k}_x\ . \tag{6.17b}$$

The second integral in Eq. (6.16) can be further reduced,

because V_{bx} is the potential that binds b and x to form a with binding energy ε_a, so that ψ_a obeys the equation

$$\left[-\frac{\hbar^2}{2\mu_{bx}}\nabla^2+V_{bx}\right]\psi_a=\varepsilon_a\psi_a \ . \tag{6.18}$$

From Eq. (6.18) it follows that

$$V_{bx}(\mathbf{r}_{bx})\psi_a(\mathbf{r}_{bx})=\left[\varepsilon_a-\frac{q^2}{2\mu_{bx}}\right]\psi_a(\mathbf{r}_{bx}) \ . \tag{6.19}$$

Substitution in Eq. (6.16) yields

$$\mathcal{T}^{\mathrm{PW}}_{\mathrm{post}}=(c^2s)^{1/2}\left[\varepsilon_a-\frac{q^2}{2\mu_{bx}}\right]\int d\mathbf{R}_a\exp(i\mathbf{Q}\cdot\mathbf{R}_a)\int d\mathbf{r}_{bx}\psi_a(\mathbf{r}_{bx})e^{-i\mathbf{q}\cdot\mathbf{r}_{bx}} \ . \tag{6.20}$$

So the matrix element for elastic breakup in the post form of the PWBA separates into a part depending on the internal momentum $\mathbf{q}$ of the spectator in the projectile and a part depending on the transferred momentum $\mathbf{Q}$. The part depending on $\mathbf{q}$ equals the Fourier transform with respect to $\mathbf{q}$ of the radial wave function of the spectator in the projectile multiplied by the factor $q^2/2\mu_{bx}$. The part depending on the transferred momentum will for integration limits 0 and ∞ be a delta function in $\mathbf{Q}$. This means that in the post form of PWBA the cross section for elastic breakup in practice will be zero.

In the prior representation Eqs. (6.12) and (6.13a) can be written as

$$T^{\mathrm{PW}}_{\mathrm{prior}}=\langle\chi_f^{(-)}\,|\,W_i\,|\,\chi_i^{(+)}\rangle \ , \tag{6.21}$$

with $W_i=V_{xA}(\mathbf{r}_{xA})$ in the spectator approximation. For elastic breakup the T-matrix element in the prior form can be derived to be

$$\begin{aligned}\mathcal{T}^{\mathrm{PW}}_{\mathrm{prior}}&=(c^2s)^{1/2}\int d\mathbf{r}_{xA}\exp(i\mathbf{Q}\cdot\mathbf{r}_{xA})V_{xA}(\mathbf{r}_{xA})\\&\quad\times\int d\mathbf{r}_{bx}\psi_a(\mathbf{r}_{bx})e^{-i\mathbf{q}\cdot\mathbf{r}_{bx}}\\&=T^{\mathrm{PW}}_{xA}(\mathbf{Q})\Phi(\mathbf{q}) \ .\end{aligned} \tag{6.22}$$

So in the prior form the matrix element is a product of the internal momentum distribution and the T matrix for the interaction of the participant x with the target nucleus.

The comparison between Eqs. (6.20) and (6.22) clearly demonstrates that the approximations made in PWBA are so severe that they completely destroy the equivalence between post and prior form descriptions.

Compared to the Serber model, the expression in Eq. (6.22) contains a modification due to the participant-target nucleus interaction, $T^{\mathrm{PW}}_{xA}(\mathbf{Q})$. As shown in Fig. 43, the Serber model overpredicts the widths of the bumps in the inclusive spectra. It has been shown by Shyam *et al.* (1979) that this modification reduces the width of the bump to approximately the experimental value observed in the ^{209}Bi(α,^{3}He) reaction at $E_\alpha=140$ MeV and $\theta_{\mathrm{c.m.}}=14°$.

The elastic-breakup data for the reaction (^{3}He,pd) on ^{12}C, ^{51}V and ^{90}Zr at $E(^3\mathrm{He})=90$ MeV have been analyzed in the framework of the post form DWBA by Matsuoka *et al.* (1980), who introduce a cutoff radius R_c to account for absorption and to avoid the delta function in Q in Eq. (6.20). Moreover, they replace

$$\langle\Psi_b(\xi_b)\Psi_x(\xi_x)\,|\,V_{bx}(\mathbf{r}_{bx})\,|\,\Psi_a(\mathbf{r}_{bx},\xi_b,\xi_x)\rangle$$

in Eq. (6.14) by $(c^2s)^{1/2}D_0f(r_{bx})$, where D_0 is the zero-range constant and $f(r_{bx})$ is a normalized range function of the interaction V_{bx} (Bassel, 1966). This means that Matsuoka *et al.* use a more sophisticated approach than pure PWBA. In their post-form representation the first term in Eq. (6.20) reduces to

$$\int_{R_a\geq R_c}d\mathbf{R}_a\exp(i\mathbf{Q}\cdot\mathbf{R}_a)=-4\pi R_c^2j_1(QR_c)/Q \ . \tag{6.23}$$

With a Yukawa-type range function

$$f(r)=\frac{\beta^2}{4\pi}\frac{e^{-\beta r}}{r}$$

the second integral becomes

$$\int d\mathbf{r}_{bx}\exp(-i\mathbf{q}\cdot\mathbf{r}_{bx})f(r_{bx})=\frac{\beta^2}{\beta^2+q^2} \ . \tag{6.24}$$

Combining these results leads to a T-matrix element:

$$T^{\mathrm{PW}}_{\mathrm{post}}=-(\tfrac{3}{2})^{1/2}D_0 4\pi R_c^2\frac{j_1(QR_c)}{Q}\frac{\beta^2}{\beta^2+q^2} \ . \tag{6.25}$$

The calculations are carried out for two values of the range parameter β, $\beta=0.5$ fm^{-1}, corresponding to an interaction radius of about 2 fm, and $\beta=\infty$, corresponding to the usual zero-range approximation. For D_0 the standard (^{3}He,d) value $D_0=-172.8$ MeV fm$^{3/2}$ was used. The cutoff radius was adjusted to optimize the fit to the coincident spectra of the p-d correlation.

Figure 45 shows the coincident deuterons for the elastic-breakup reactions at $\theta_d=15°$ for various proton angles. The calculated cross sections are multiplied for each angle by the factor shown in the figure. This factor increases rapidly with proton angle, indicating that the magnitude of the calculated cross sections decreases much faster than the experimental ones. This can more clearly be seen in the corresponding angular correlation presented in the upper part of Fig. 46. The calculated projected deuteron spectra, which reproduce the data well as far as peak energies and widths are concerned, reflect the oscillations in the spherical Bessel function $j_1(QR_c)$. The data presented in Fig. 45 correspond to cases where the protons and deuterons were detected at opposite sides of the beam and hence involve small momentum transfers.

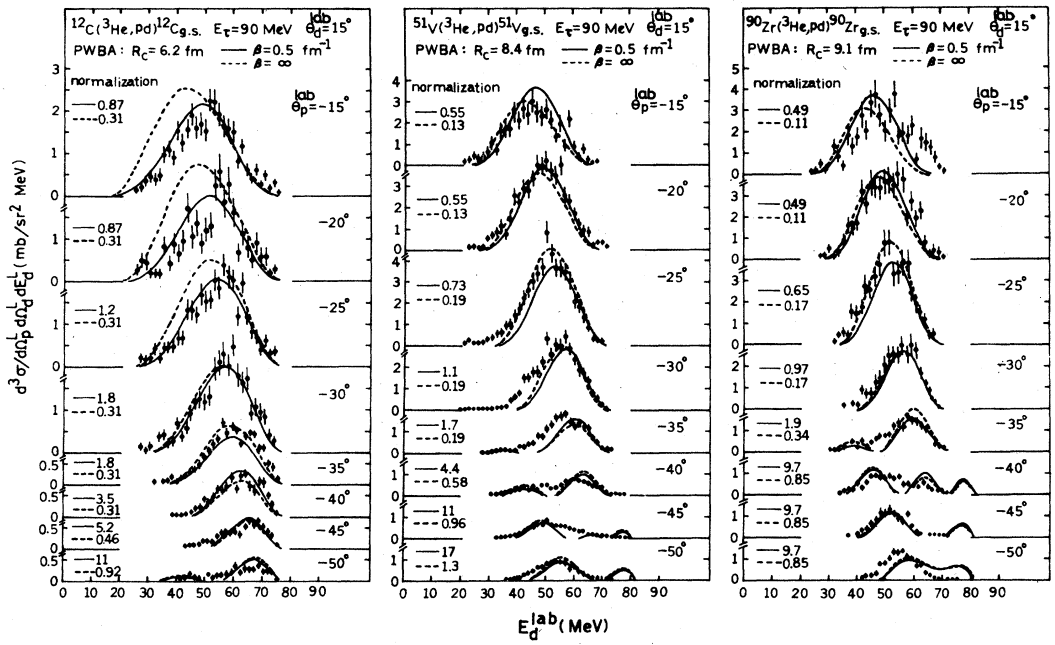

FIG. 45. Spectra of coincident deuterons in the ^{12}C, ^{51}V, $^{90}Zr(^3He,pd)$ elastic-breakup reactions as a function of the proton lab angle with the deuteron lab angle fixed at 15°. The solid and dashed curves are the results of the PWBA calculations. The calculated cross sections are multiplied by the factor shown in the figure for each angle (Matsuoka *et al.*, 1980).

The comparison between the calculated and experimental angular correlations as presented in Fig. 46 show that the calculated correlations drop off too rapidly for all cases. As is to be expected, the PWBA calculations will lose validity with increasing momentum transfer. Such effects are also visible in the projected deuteron spectra for θ_p fixed at $\theta_p = 15°$ and θ_d variable (Fig. 47). In addition to the more rapidly changing normalization factor compared to the results presented in Fig. 46, the peak energies and widths are no longer reproduced.

In conclusion, it can be stated that PWBA indicates that elastic breakup indeed occurs at the nuclear surface. The distortions due to the Coulomb and nuclear fields for these momentum transfers are too large, however, for a PWBA treatment.

F. Cross sections in the quasifree breakup model

1. Outline of the theory

The *quasifree breakup model* (QFBM) has been developed by Aarts *et al.* (1982), Aarts (1983), and Aarts, Malfliet, de Meijer, and van der Werf (1984) to describe the ^{3}He breakup data on ^{12}C, ^{28}Si, and ^{58}Ni at $E_{^3He} = 52$ MeV. It is based on the experimental observation of spectatorlike particles, indicating that the nuclear interaction between projectile and target nucleus might be approximated by the interaction between one of the constituents (the participant) with the target nucleus. Because the prior form of the T matrix contains the interaction potentials between the constituents of the projectile and the target explicitly, QFBM is formulated in the prior form [see Eq. (6.21)]. In the QFBM it is assumed that the breakup process is caused only by the short-range interactions and that the long-range Coulomb interaction V_{aA}^C primarily distorts the incoming wave. The short-range interactions occur only between the participant x and the target nucleus A, and the only interaction considered between the spectator b and A is the Coulomb interaction ($V_{ba} = V_{ba}^C$). It is assumed that the distributions of the Coulomb interaction on the incoming wave of the projectile and the outgoing wave of the spectator can be described by the Coulomb waves $F_a^{(+)}$ and $F_b^{(-)}$, respectively. The T-matrix element for the reaction schematically denoted in Eq. (6.11) under those assumptions can be obtained by substituting in Eq. (6.21):

$$W_i = V_{aA} - V_{aA}^C = V_A + V_{xA} - V_{aA}^C$$
$$= (V_{xA} - V_{xA}^C) + (V_{bA} - V_{bA}^C) = V_{xA} - \frac{Z_x}{Z_A} V_{aA}^C , \tag{6.26a}$$

$$|\chi_i^{(+)}\rangle = |F_a^{(+)}\Psi_a\Psi_A\rangle , \tag{6.26b}$$

and

$$\langle\chi_f^{(-)}| = \langle F_b^{(-)}\chi_y^{(-)}\Psi_b\Psi_y\Psi_B| . \tag{6.26c}$$

In these equations Ψ represents the intrinsic wave functions for the particles involved, depending on their inter-

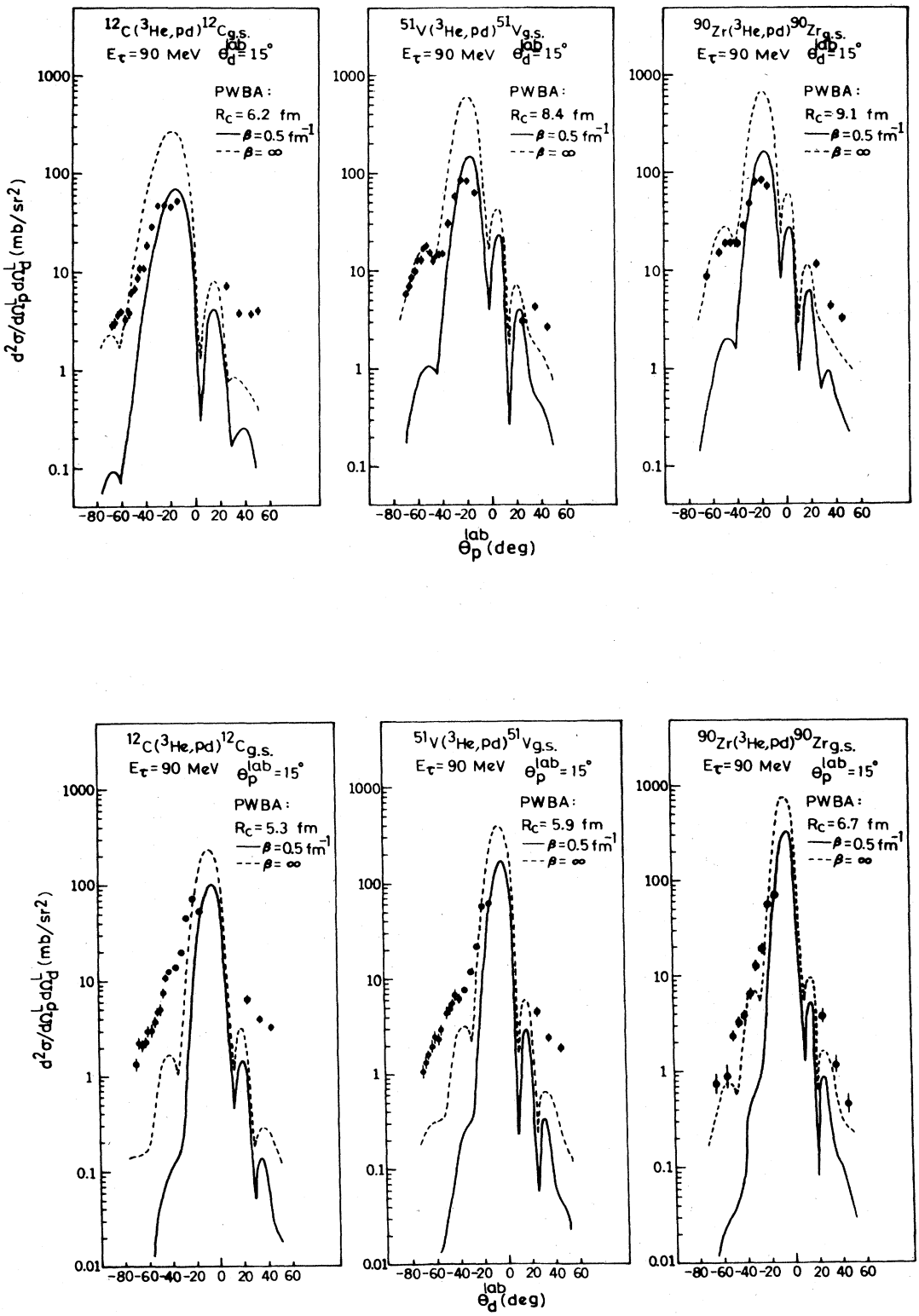

FIG. 46. Angular distribution of p-d correlations in the ^{12}C, ^{51}V, $^{90}Zr(^3He,pd)$ elastic-breakup reactions. The upper part presents the cross sections as a function of proton angle with the deuteron angle fixed at $\theta_d = 15°$, the lower part as a function of deuteron angle with the proton angle fixed at $\theta_p = 15°$. The solid and dashed curves represent PWBA calculations for various range parameters (Matsuoka *et al.*, 1980).

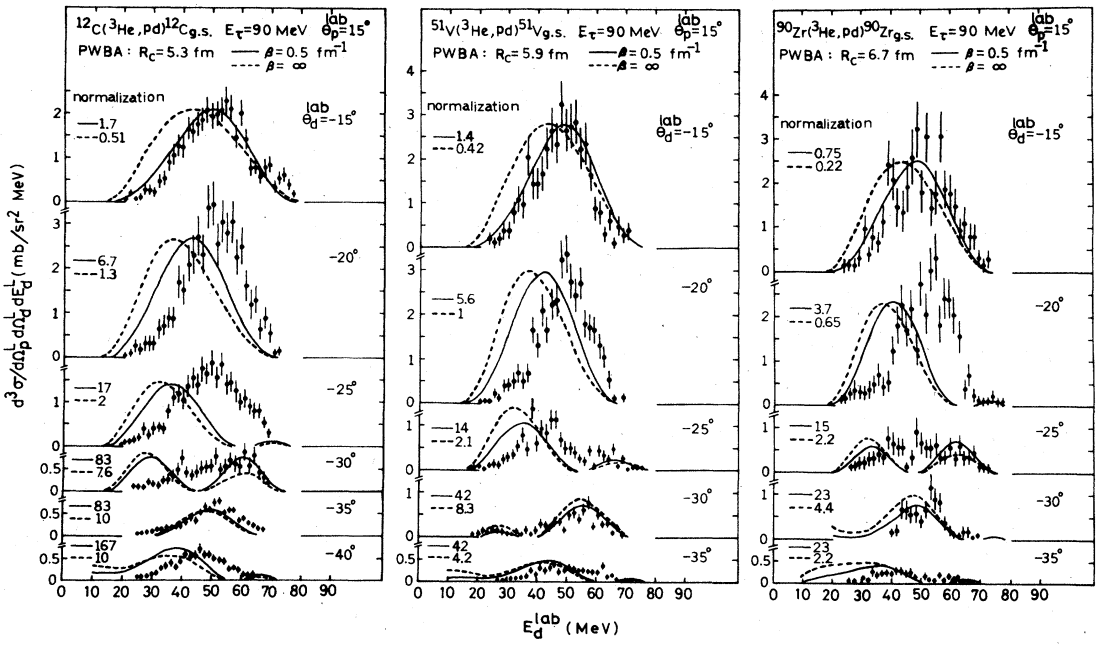

FIG. 47. Spectra of coincident deuterons in the ^{12}C, ^{51}V, $^{90}Zr(^3He,pd)$ elastic-breakup reactions as a function of the deuteron lab angle with the proton lab angle fixed at 15°. The solid and dashed curves are the results of PWBA calculations. The calculated cross sections are multiplied by the factor shown in the figure for each angle (Matsuoka *et al.*, 1980).

nal coordinates [see Eqs. (6.13b) and (6.13c)], and $\chi_y^{(-)}$ denotes the full (nuclear plus Coulomb) elastic optical scattering wave of the outgoing particle y. The charges of the particles are indicated by Z. In this way the long-range Coulomb interaction does not contribute to the interaction causing the breakup, but still has an effect on the wave functions. Expanding the projectile wave function according to Eq. (6.15) and subsequently integrating over the internal coordinates of the spectator b, we find that the matrix element reduces to

$$T_i^{QF}=(c^2s)^{1/2}\left\langle F_b^{(-)}\chi_y^{(-)}\Psi_b\Psi_y\Psi_B\left|V_{xA}-\frac{Z_x}{Z_a}V_{aA}^C\right|F_a^{(+)}\psi_a\Psi_x\Psi_A\right\rangle . \tag{6.27}$$

With local Coulomb-corrected momenta the $F(\mathbf{k},\mathbf{r})$ will be approximated by a plane wave $\varphi(\mathbf{k}',\mathbf{r})$ (McVoy and Nemes, 1980; Aarts *et al.*, 1982; Aarts, 1983). If the masses of A and B are about equal and both larger than the masses of the other particle, one approximates $\mathbf{r}_{bB}\sim\mathbf{r}_{bA}$ and the T-matrix element factorizes as

$$T_{fi}^{QF}=\int d\mathbf{r}_{xA}\chi_y^{(-)*}(\mathbf{k}_{yB},\mathbf{r}_{yB})\left[V_{xA}(\mathbf{r}_{xA})-\frac{Z_x}{Z_a}V_{aA}^C(\mathbf{r}_{xA})\right]\exp[i(\mathbf{k}'_{aA}-\mathbf{k}'_{bA})\cdot\mathbf{r}_{xA}]$$
$$\times\int d\mathbf{r}_{bx}\psi_a(\mathbf{r}_{bx})\exp\left[-i\left[\mathbf{k}'_{bB}-\frac{m_b}{m_a}\mathbf{k}'_{aA}\right]\cdot\mathbf{r}_{bx}\right]=T_{xA}^{QF}(\mathbf{Q})\Phi(\mathbf{q}) . \tag{6.28}$$

In this equation

$$\mathbf{q}=\mathbf{k}'_{bB}-\frac{m_b}{m_a}\mathbf{k}'_{aA} \tag{6.29a}$$

and

$$\mathbf{Q}=\mathbf{k}'_{aA}-\mathbf{k}'_{bB}-\mathbf{k}_{yB} . \tag{6.29b}$$

The result in Eq. (6.28) resembles that of Eq. (6.22). The main differences between T_{xA}^{PW} and T_{xA}^{QF} are the use of local Coulomb corrected momenta in T_{xA}^{QF} and the use of distorted waves for the participant. The use of the distorted waves causes T_{xA}^{QF} to depend not only on $\mathbf{Q}$ but also slightly on E_x.

In the following the T-matrix element T_{xA} will be evaluated for various conditions specified by b, y, and B in Eq. (6.11).

(i) Inclusive reactions: only particle b is observed.

(ii) Elastic breakup: $y=x$ and $B=A$.

(iii) Inelastic breakup: $y=x$ and $B=A^*$, where A^* denotes an excited state in the target nucleus.

(iv) Breakup transfer $y=(x\pm z)$ and $B=(A\mp z)$, where B denotes the residual nucleus in either its ground state or its excited state and z represents the transferred particle.

(v) Absorptive breakup: $y=y_1$; $B=C$, where y_1 denotes a set of particles emitted from the compound system $\{x+A\}$ and C represents the residual compound system.

It should be pointed out that the assumption of a plane wave for the spectator b implies that no absorption of the spectator will take place. This will lead to an overestimate of the calculated cross section.

a. Inclusive reactions

The inclusive reaction may be represented as

$$a+A\rightarrow b+\{x+A\}\rightarrow b+1+2+\cdots+n\ , \tag{6.30}$$

where only particle b will be detected. The differential cross section for this process follows from the substitution of the T-matrix element in the quasifree approach [Eq. (6.28)] into Eq. (6.2):

$$d\sigma=\frac{2\pi}{\hbar^2}\frac{m_a}{k_a}\mid T_{xA}(\mathbf{Q})\mid^2\Phi^2(\mathbf{q})\delta^4(P_i-P_f)d^3p_b \times\prod_{j=1}^{n}\frac{d^3p_j}{(2\pi\hbar)^3}\ . \tag{6.31}$$

The double-differential cross section is obtained by integrating Eq. (6.31) over all nonobserved momenta and summing over all possible configurations of outgoing particles [see Eq. (6.7)]:

$$\frac{d^2\sigma}{d\Omega_b dE_b}=\frac{\hbar c^2 s}{(2\pi\hbar)^3}\frac{k_x k_b m_a m_b}{k_a m_x}\tilde{\sigma}_{xA}(\mathbf{Q})\Phi^2(\mathbf{q})\ . \tag{6.32}$$

Here $\tilde{\sigma}_{xA}$ represents the participant-target cross section that in the partial wave expansion may be written as

$$\tilde{\sigma}_{xA}=\frac{\pi}{k_x^2}\sum_{l_x}(2l_x+1)(1-\mid\tilde{\eta}_{l_x}\mid^2)\ . \tag{6.33}$$

In this expression l_x is the orbital angular momentum of the participant x, and $\tilde{\eta}_{l_x}$ is a modified reflection coefficient for the $\{x+A\}$ system. Both l_x and $\tilde{\eta}_{l_x}$ are determined from the corresponding l_a and η_{l_a} for the projectile a by taking into account the internal motion. For details see Aarts *et al.* (1982), Aarts (1983), and Aarts, Malfliet, de Meijer, and van der Werf (1984). The essential point in this approach is the fact that $\tilde{\sigma}_{xA}$ is calculated from the projectile properties.

Summarizing, one finds that the cross section in Eq. (6.32) factorizes into (i) a spectator momentum distribution $\Phi^2(\mathbf{q})$, which mainly determines the shape of the inclusive spectrum, and (ii) the participant formation cross section $\tilde{\sigma}_{xA}(\mathbf{Q})$, which determines the magnitude of the cross section and depends on the transmission of the incident particle.

b. Absorptive breakup

The basic assumption for this process is that the interaction between participant and target leads to the formation of a compound nucleus, which deexcites by the emission of particles. The formation part will be described in terms of the QFBM, and the deexcitation will be given in terms of a thermodynamic model (Fermi-gas model). The difference with the description of the formation cross section for the inclusive reaction described in Sec. VI.F.1.a is the fact that the momentum distribution of particle 1 has to be taken into account explicitly in the case of absorptive breakup. In the inclusive breakup cross section the integration over the one-particle momentum distributions for all different configurations of nonobserved particles is carried out implicitly. As shown by Aarts (1983) and Aarts, Malfliet, de Meijer, and van der Werf (1984), the cross section of the process may be calculated under the following assumptions.

(i) The dependence on the angular momentum l in the formation may be neglected.

(ii) The deexcitation of the compound system $\{x+A\}$ takes place through the emission of particles in which the probability for a configuration of n particles is, in first order, given by the available phase-space factor for the n particles in the exit channel.

(iii) The compound system $\{x+A\}$ contains only single nucleons in complete thermal equilibrium with Fermi-Dirac one-particle momentum distributions d^3f_i/d^3p_i.

Under these assumptions the quadruple-differential cross section can be written as (Aarts, 1983; Aarts, Malfliet, de Meijer, and van der Werf, 1984)

$$\frac{d^4\sigma}{d\Omega_b d\Omega_1 dE_b dE_1}=(2\pi\hbar)^{-3}2\pi m_a m_b m_1\frac{k_b k_1}{k_a}T_c(\tilde{E}_1)N(E_x)\Phi^2(\mathbf{q})\frac{d^3f_1}{d^3p_1}\ . \tag{6.34}$$

In this equation $N(E_x)$ is the formation cross section for the compound system $\{x+A\}$ given by

$$N(E_x)=\frac{1}{2}\frac{\hbar^2c^2s}{(A_A+A_x)k_x m_x}\sum_{l_x}(2l_x+1)(1-\mid\tilde{\eta}_{l_x}\mid^2)\ , \tag{6.35}$$

where $\tilde{\eta}_{l_x}$ are the modified reflection coefficients.

The Coulomb-barrier transmission coefficient, $T_c(\tilde{E}_1)$, has been introduced to account for the effects of the Coulomb barrier on the emission of the charged particles

from the compound system (see, e.g., Gasiorowitz, 1974). The factor d^3f_1/d^3p_1 in Eq. (6.34) represents the one-particle momentum distribution [see also Aarts (1983) and Aarts, Malfliet, de Meijer, and van der Werf (1984)].

Summarizing, one finds that the cross section in Eq. (6.34) is the product of three contributions.

(i) The spectator momentum distribution $\Phi^2(\mathbf{q})$, describing the spectator particle b and containing the effects of the Coulomb distortion via the local Coulomb-corrected momenta $\mathbf{q}$,

(ii) the one-particle momentum distribution d^3f_1/d^3p_1, which describes the emission of the particle 1 from a compound system that is in complete thermal equilibrium, and

(iii) the function $N(E_x)$, which is directly related to the formation cross section of the compound system [Eq. (6.35)]. The formation cross section is determined by the transmission properties of the projectile in the incident channel.

The various energy spectra may be obtained from Eq. (6.34) by integrating over the energy of one of the outgoing particles b or 1. Their shape will be determined predominantly by the momentum distribution of the observed particle for which the energy has *not* been integrated out; their magnitude is mainly determined by the formation cross section through the function $N(E_x)$.

c. Elastic breakup, inelastic breakup, and breakup transfer

In elastic breakup, inelastic breakup, and breakup transfer the interaction between the participant x and the target nucleus A will be elastic scattering, inelastic scattering, or nucleon transfer, respectively. Except for some modifications the T-matrix elements will be those used to describe the free processes. A distinction will be made between elastic breakup and the two nonelastic breakup reactions due to the role of the Coulomb part in the free elastic scattering. The interaction of Eq. (6.26a) is rewritten as

$$V_{xA}-\frac{Z_x}{Z_a}V_{aA}^C=(V_{xA}-V_{xA}^{(0)})+\left[V_{xA}^{(0)}-\frac{Z_x}{Z_a}V_{aA}^C\right], \quad (6.36)$$

where $V_{xA}^{(0)}$ represents the interaction responsible for the pure elastic (nuclear plus Coulomb) scattering of the participant by the target nucleus. The T-matrix element T_{fi}^{QF} of Eq. (6.27) may be separated into $T_{fi}^{(0)}$, the transition amplitude for elastic breakup, and $T_{fi}^{(1)}$, the amplitude for inelastic breakup or breakup transfer, depending on the final state. Equation (6.27a) then becomes (for elastic breakup, inelastic breakup, and breakup transfer, respectively)

$$T_{fi}^{(0)}=(c^2s)^{1/2}\left\langle F_b^{(-)}\chi_x^{(-)}\left|V_{xA}^{(0)}-\frac{Z_x}{Z_a}V_{aA}^C\right|F_a^{(+)}\psi_a\right\rangle \quad (6.37a)$$

and

$$T_{fi}^{(1)}=\begin{cases}(c^2s)^{1/2}\langle F_b^{(-)}\chi_x^{(-)}\Psi_{A^*}\mid V_{xA}-V_{xA}^{(0)}\mid F_a^{(+)}\psi_a\Psi_A\rangle & (6.37b)\\ (c^2s)^{1/2}\langle F_b^{(-)}\chi_y^{(-)}\Psi_y\Psi_B\mid V_{xA}-V_{xA}^{(0)}\mid F_a^{(+)}\psi_a\Psi_x\Psi_A\rangle\ . & (6.37c)\end{cases}$$

These T-matrix elements can again be factorized as

$$T_{fi}^{(0)}=T_{xA}^{(0)}(\mathbf{Q})\Phi(\mathbf{q}) \quad (6.38a)$$

and

$$T_{fi}^{(1)}=T_{xA}^{(1)}(\mathbf{Q})\Phi(\mathbf{q})\ , \quad (6.38b)$$

where $\mathbf{q}$ and $\mathbf{Q}$ are given by Eq. (6.29).

For the inelastic-breakup and the breakup-transfer channels the transition amplitudes $T_{xA}^{(1)}$ are approximated by the amplitude for the free $x+A$ inelastic scattering or transfer reaction and are calculated from the DWBA reactions cross section according to the expression

$$|T_{xA}^{(1)}(\mathbf{Q})|^2=\frac{(2\pi\hbar^2)^2}{\mu_i\mu_0}\frac{k_i}{k_0}\left[\frac{d\sigma}{d\Omega}\right]^{\mathrm{DWBA}}, \quad (6.39)$$

with μ_i and μ_0 being the reduced masses and $\hbar k_i$ and $\hbar k_0$ the relative momenta in the incoming and outgoing channels, respectively. The center-of-mass differential cross section for the inelastic scattering or the transfer reaction, calculated in DWBA, is denoted by $(d\sigma/d\Omega)^{\mathrm{DWBA}}$.

For elastic breakup the transition amplitudes are the free $x+A$ elastic scattering amplitudes corrected for the contributions of the interaction $(Z_x/Z_A)V_{aA}^C$. This correction is accomplished by a smooth l cutoff in the partial-wave summation of the free $x+A$ elastic scattering amplitudes (Aarts *et al.*, 1982; Aarts, 1983). Finally, one obtains

$$T_{xA}^{(0)}(\mathbf{Q})=\frac{\pi i\hbar^2}{\mu k}(c^2s)^{1/2}\sum_l(2l+1)P_l(\cos\theta)(1-|\tilde{\eta}_l|^2)\times[\exp(2i\delta_l)-1]\ , \quad (6.40)$$

with μ being the reduced mass, $\hbar k$ the relative momentum of the $x+A$ system, and δ_l the full (nuclear plus Coulomb) phase shift.

d. Breakup reactions with two spectator particles

A large portion ($\sim 40\%$) of the bump in the ^{3}He-induced inclusive proton spectrum is due to a process in which two protons with spectator characteristics are emitted. Aarts (1983) and Aarts, Malfliet, de Meijer, and van der Werf (1984) argue that this process is due to a quasi-free interaction of the ^{3}He projectile with the neutron as participant. Schematically such a reaction can be written as

$$a\{b+c+x\}+A \rightarrow b+c+\{x+A\} , \tag{6.41}$$

for which the T matrix separates into

$$T_{fi}(\mathbf{Q},\mathbf{p},\mathbf{q}) = T_{xA}(\mathbf{Q})\Phi(\mathbf{p},\mathbf{q}) . \tag{6.42}$$

Here $\mathbf{Q}$, $\mathbf{q}$, and $\mathbf{p}$ are similar to the corresponding terms defined in Eq. (6.29). Since only the two spectator particles are detected, a summation is made over all possible interactions between the participant x and the target nucleus. The T-matrix element T_{xA} will be the matrix element for an inclusive reaction. For the inclusive reactions the substitution of Eq. (6.42) into Eq. (6.2), integrating over all nonobserved momenta and summing over all possible configurations of outgoing particles yields, comparable to Eq. (6.32),

$$\frac{d^4\sigma}{d\Omega_b d\Omega_c dE_b dE_c} = \frac{\hbar^2 c^2 s}{(2\pi\hbar)^6}\frac{k_x k_b k_c}{k_a}\frac{m_a m_b m_c}{m_x} \times \tilde{\sigma}_{xA}(\mathbf{Q})\Phi^2(\mathbf{p},\mathbf{q}) . \tag{6.43}$$

Again there are two major contributions.

(i) The momentum distribution $\Phi^2(\mathbf{p},\mathbf{q})$ of the two spectators in the projectile. This factor, which reflects the properties of the projectile, mainly determines the shape of the spectra.

(ii) The cross section $\tilde{\sigma}_{xA}(\mathbf{Q})$, defined in Eq. (6.33), depending on the transmission coefficients of the projectile. This factor mainly determines the magnitude of the process.

2. Comparison with the data

a. Inclusive reactions

Figure 48 shows the comparison of the calculations with the experimental data for the ^{28}Si(^{3}He,p) and ^{28}Si(^{3}He,d) reactions. The calculated spectra are obtained with Eq. (6.32). The curves have been adjusted to the data by multiplying them with an overall normalization constant of $\frac{1}{2}$ for protons and $\frac{1}{8}$ for deuterons. The shape of the bump and the change of its position and magnitude are rather well reproduced by these calculations.

The ratio of four between the normalization constants with proton and deuteron spectators turns out to be approximately the same for all processes. The normalization constant originates from the fact that in the QFBM plane waves are used for the spectator in the exit channel and hence no absorption of the spectator particle is taken into account in the calculation. The difference of a factor of 4 in the normalization constant is related to the difference in absorption between protons and deuterons. This is supported by comparing transmission coefficients for both particles at beam velocity energies with standard optical model parameters (Aarts, 1983).

In Figs. 26(a) and 26(b) the dashed curves represent the calculations of the energy-integrated cross section of the bump. The same normalizations as above were used for all three targets. At forward angles the calculations reproduce the data well. At backward angles contributions with a larger momentum transfer become significant. The deviations might indicate that the assumption

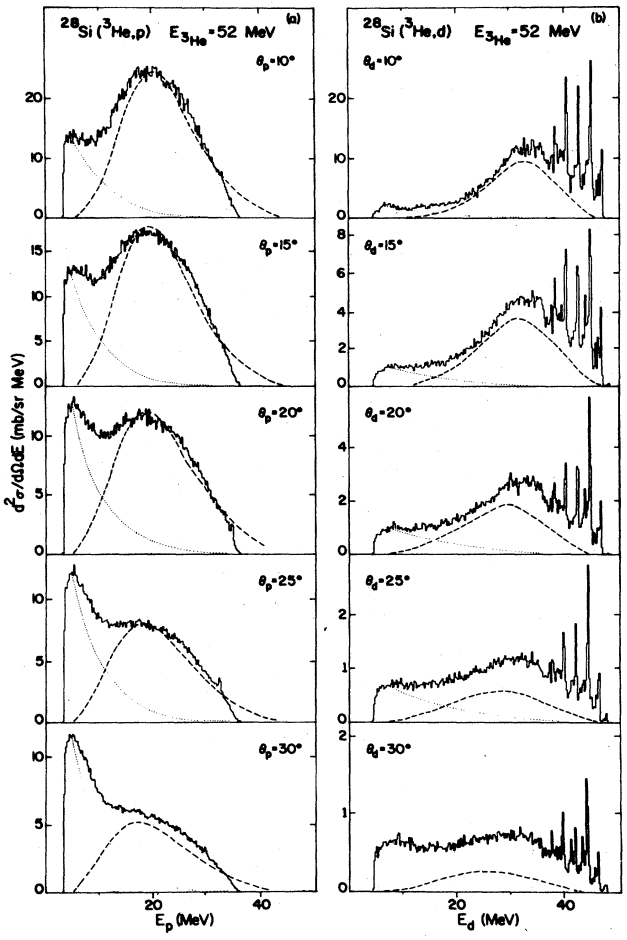

FIG. 48. Inclusive proton and deuteron energy spectra from the (^{3}He,p) and (^{3}He,d) reactions on ^{28}Si. The dashed lines represent the results from the QFBM calculations (see text). The dotted lines indicate the shape of the spectra at $\theta_{lab}=70°$ (Aarts, 1983; Aarts, Malfliet, de Meijer, and van der Werf, 1984).

of low-momentum transfer required for the spectator breakup is no longer fulfilled. These deviations are also visible in the previous example, where in comparison with the (^{3}He,d) spectra, deviations in magnitude are observed for $\theta_d > 20°$ (see Fig. 48).

The dashed lines in Fig. 27 represent the calculated centroid position of the bump. These calculations reproduce the centroids rather well for ^{12}C and ^{28}Si but overestimate the value of ^{58}Ni by about 1 MeV. For deuterons the calculated centroids are about 2 MeV lower than experimentally observed. Although the deuteron spectra might still contain some unobserved states that shift the centroid upwards, it is likely that deviations arise from an overestimate of the effect of the classical Coulomb corrections. In the pure spectator assumption, applied here, the only spectator-target interaction is the repulsive Coulomb interaction. If contributions from the attractive nuclear interaction are present in the spectator-target interaction, the Coulomb deflection will partly be reduced. In Sec. VI.G.4 we will come back to this question.

The calculated widths of the bumps are in good agreement with the data (Aarts, 1983; Aarts, Malfliet, de Meijer, and van der Werf, 1984). The energy dependence of the width has been calculated for the ^{28}Si(^{3}He,d) reaction only and is indicated as a solid line in Fig. 30. The comparison indicates that the calculations reproduce the energy dependence well and shows that in the case of ^{3}He the available phase space changes the energy dependence of the bump width from a function proportional to $\sqrt{E}$ to one being almost linearly dependent on E (see also Sec. V.B.1.b).

b. Absorptive breakup

In Fig. 49 some results of the calculations from the absorptive-breakup model are shown in the case of the ^{12}C,^{28}Si,^{58}Ni(^{3}He,pd) reaction with the deuteron as a spectator. The corresponding angular correlations for the ^{28}Si(^{3}He,pd) reaction which is obtained by integrating the results of Eq. (6.34) over the energies of both particles b and 1 is shown in Fig. 50. The curves have been normalized to the data by multiplying them with a factor of $\frac{1}{4}$. This normalization factor is roughly the same for all three target nuclei. From Figs. 49 and 50 it is clear that both the spectra and the angular correlations are very well reproduced by the model calculations. Calculations for the ^{12}C,^{28}Si,^{58}Ni(^{3}He,pp) absorptive-breakup reactions are

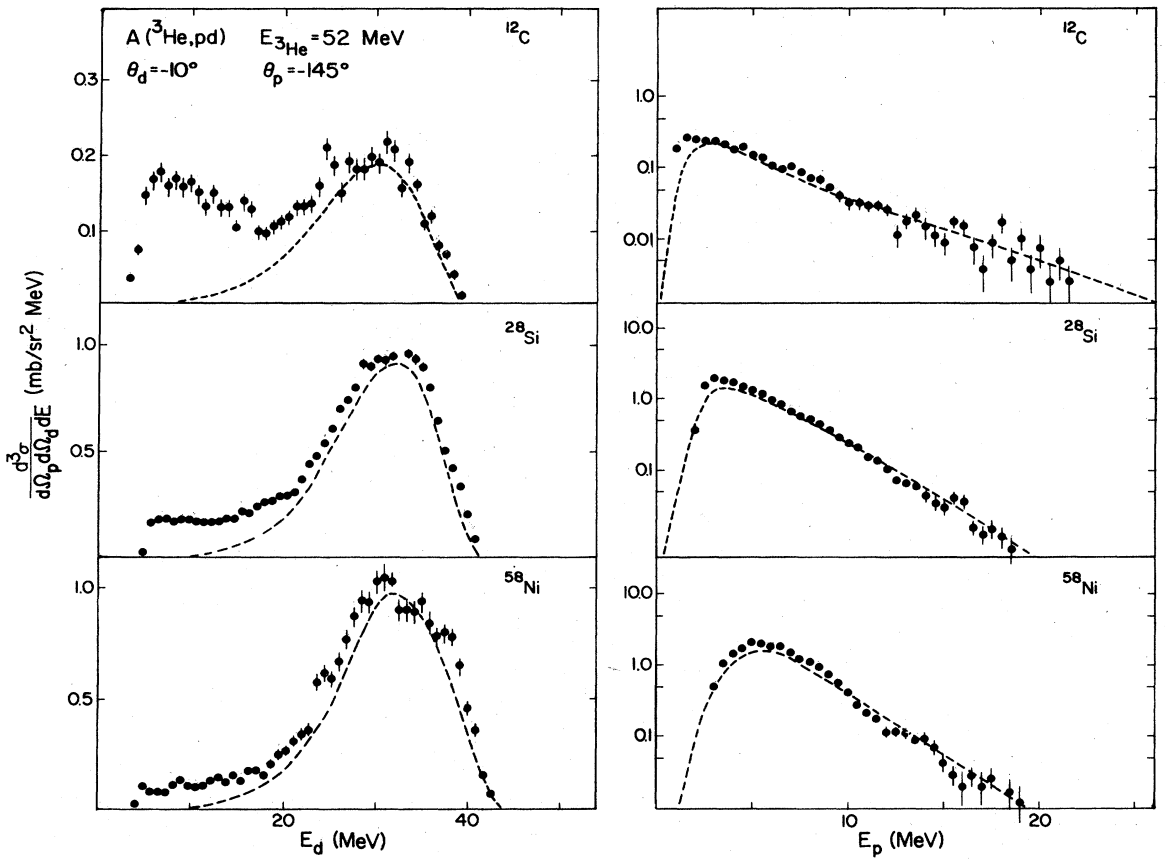

FIG. 49. Projected deuteron (left) and proton energy spectra (right) from the (^{3}He,pd) absorptive-breakup reaction on ^{12}C, ^{28}Si, and ^{58}Ni at $\theta_d = -10°$ and $\theta_p = -145°$. The curves represent the results of QFBM calculations discussed in Sec. VI.F.1.b (Aarts, 1983; Aarts, Malfliet, de Meijer and van der Werf, 1984).

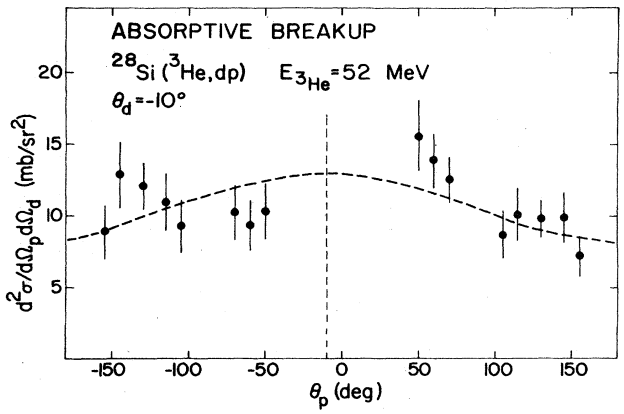

FIG. 50. Proton-deuteron angular correlation for the ^{28}Si(^{3}He,pd) absorptive breakup reaction with θ_d fixed at $\theta_d = -10°$. The dashed line represents the QFBM calculation with the deuteron as a spectator discussed in Sec. VI.F.1.b (Aarts, 1983; Aarts, Malfliet, de Meijer, and van der Werf, 1984).

presented in Fig. 51, where the results are shown for those cases in which the detection angle of the *statistically emitted* proton was fixed at $\theta_p = -10°$ [Fig. 51(b)] as well as for those cases where the detection angle of the *spectator* proton was fixed at $\theta_p = -10°$ [Fig. 51(c)]. In all cases the normalization factor was taken to be unity, and from the comparison it is apparent that the calculated and experimental cross sections are in good agreement.

Again, the ratio of the normalization constant for the proton as spectator over the one for the deuteron as spectator is equal to a factor of 4. This result was also obtained for the calculations of the inclusive breakup cross sections in Sec. VI.F.2.a.

c. Elastic breakup, inelastic breakup, and breakup transfer

An example of the comparison of the calculations with experiment is given in Fig. 52, where the *elastic-breakup* reaction data and calculations are shown for the ^{28}Si(^{3}He,pd)^{28}Si(gs) case with θ_p fixed at $\theta_p = -10°$. Similar results for the QFBM data are also obtained for ^{12}C and ^{58}Ni targets (Aarts, 1983; Aarts, Malfliet, de Meijer, and van der Werf, 1984). Figure 52 shows the results of PWBA as well as QFBM calculations (dashed and solid lines, respectively). The PWBA calculations shows the same behavior as for the 90-MeV data of Matsuoka *et al.* (1980) presented in Figs. 46 and 47. From the comparison it is clear that the QFBM calculations under the assumption of a proton spectator give a rather good fit to

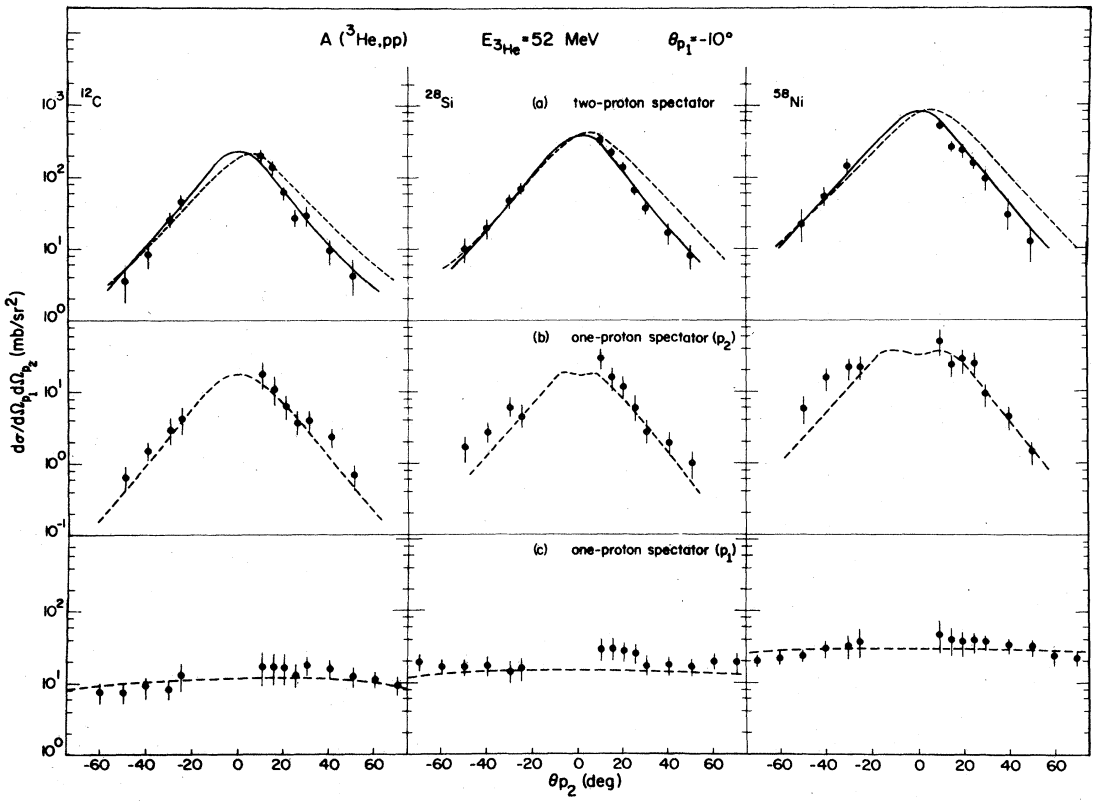

FIG. 51. Proton-proton angular distributions from the (^{3}He,pp) reaction on ^{12}C, ^{28}Si, and ^{58}Ni with the detection angle of one proton (p_1) fixed at $\theta_{p_1} = -10°$. The curves represent the QFBM results for two-proton spectator breakup with a Gaussian (dashed) and a double Hulthén wave function (solid line) (see Sec. VI.F.1.d) (a), and the QFBM absorptive breakup calculations discussed in Sec. VI.F.1.b (b) and (c) (Aarts, 1983; Aarts, Malfliet, de Meijer, and van der Werf, 1984).

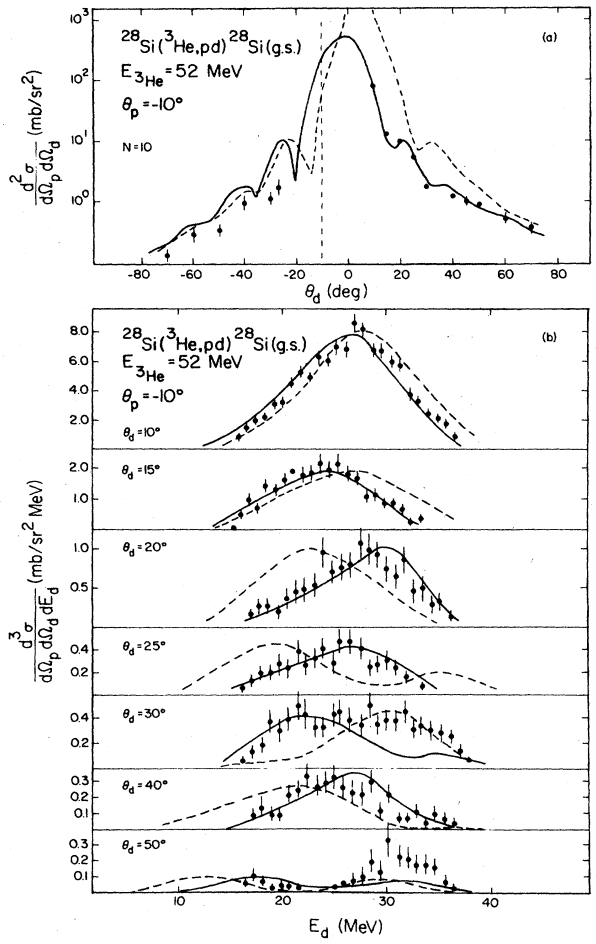

FIG. 52. Angular correlation from the ^{28}Si(^{3}He,pd)^{28}Si(gs) elastic-breakup reaction at $E_{^3\mathrm{He}}=52$ MeV with the proton detection angle fixed at $\theta_p=-10°$. (b) Corresponding projected deuteron energy spectra in the range $10\leq\theta_d\leq 50°$. The solid curves represent the results of the QFBM calculations. The PWBA calculations are indicated by the dashed curves. Both angular correlations are normalized to the data by an overall multiplication with a factor $1/N$, where $N=10$. The QFBM calculations for the projected energy spectra are normalized with the same factor N, while the PWBA are normalized to give the best fit (Aarts *et al.*, 1982).

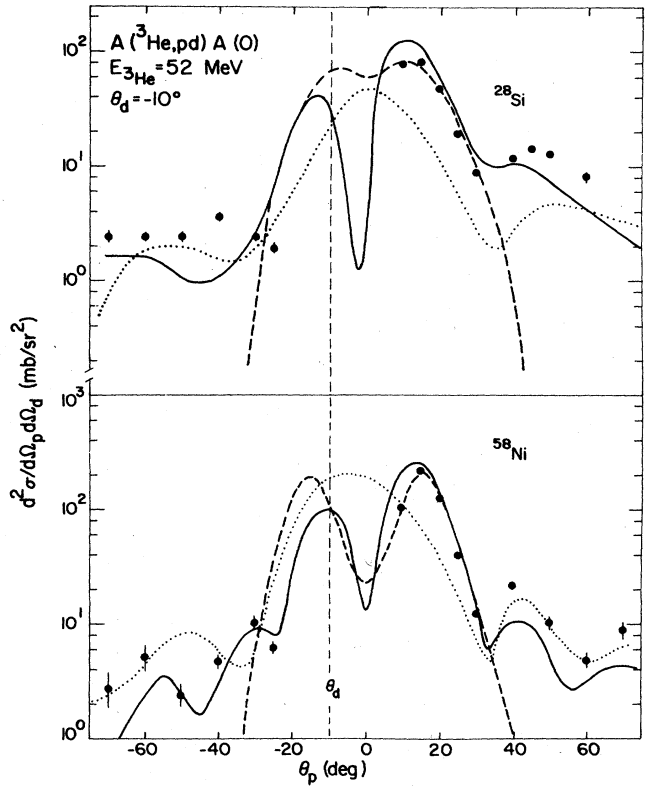

FIG. 53. Proton-deuteron angular correlations from the (^{3}He,dp) elastic-breakup reactions on ^{28}Si and ^{58}Ni with the deuteron angle fixed at $\theta_d=-10°$. The curves represent the results of the QFBM calculations with either proton (dashed) or deuteron (dotted) as spectator (see Sec. VI.F.1.c). The solid lines represent DWBM calculations according to the method of Baur *et al.* (Sec. VI.G) (Aarts, 1983; Aarts, Malfliet, de Meijer, van der Werf, Baur *et al.*, 1984).

both the angular correlation and the projected deuteron energy spectra. The deficiencies of the PWBA calculations have been removed by a more realistic description of the entrance and exit channels. The QFBM calculations overestimate the experimental cross section by a factor of 10, mainly due to the fact that no spectator absorption was taken into account in the calculations.

Figure 53 shows the comparison of several calculations with the elastic breakup data for ^{3}He on ^{28}Si and ^{58}Ni with θ_d fixed at $\theta_d=-10°$. Initially the forward angle data seem to indicate that in this angular region the proton is the spectator; at more backward angles the data indicate that the deuteron becomes the spectator. From Fig. 54, where the corresponding projected deuteron energy spectra are shown, it is clear that the spectra at forward angles are consistent with a proton spectator calculation but that at backward angles the spectra are not reproduced in shape by a proton spectator but by a deuteron spectator QFBM calculation. We will come back to this point in Sec. VI.G. In the *inelastic-breakup* reactions the same normalization constants were needed as in the elastic-breakup cases. It should be pointed out that the calculations with a deuteron spectator needed again a four times smaller normalization constant than the calculation with a proton spectator.

Some examples of results from the QFBM calculations for the *breakup-transfer* reaction on ^{28}Si are presented in Figs. 55 and 36. In the (^{3}He,pt) and (^{3}He,$p\,^3$He) cases the reaction is considered to proceed as a proton spectator and the pickup of a neutron and proton, respectively. In the case of the (^{3}He,dd) reaction one deuteron is spectator and the other one is the result of a neutron pickup by the participant proton. Since the roles can be interchanged, two calculations have been carried out for the angular

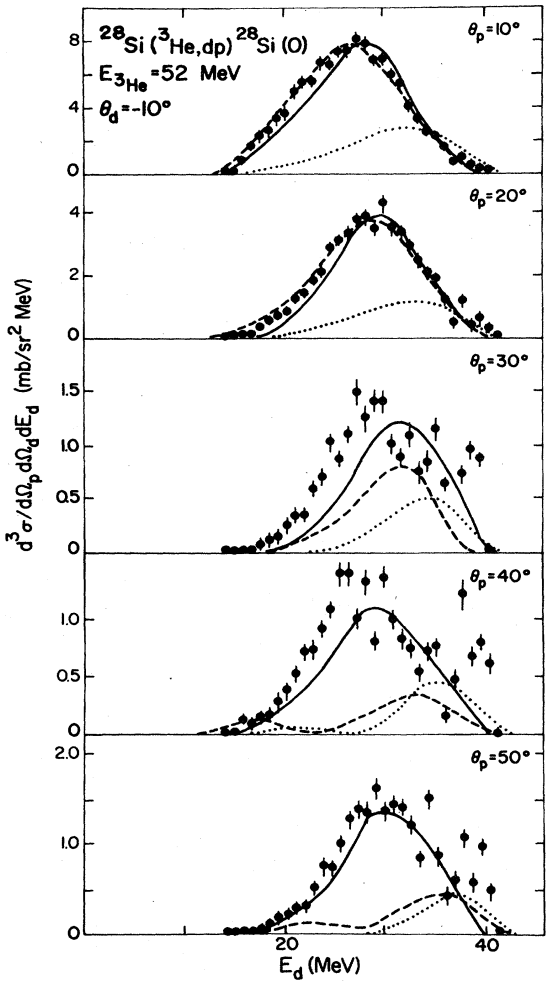

FIG. 54. Projected deuteron energy spectra from the ^{28}Si(^{3}He,pd) elastic-breakup reaction with θ_d fixed at $\theta_d = -10°$. The dashed and dotted curves represent the results of the QFBM calculations (see Sec. VI.F.1.c) with a proton and a deuteron spectator, respectively. The solid line represents the DWBM calculations according to the method of Baur *et al.* (Aarts, 1983; Aarts, Malfliet, de Meijer, van der Werf, Baur *et al.*, 1984).

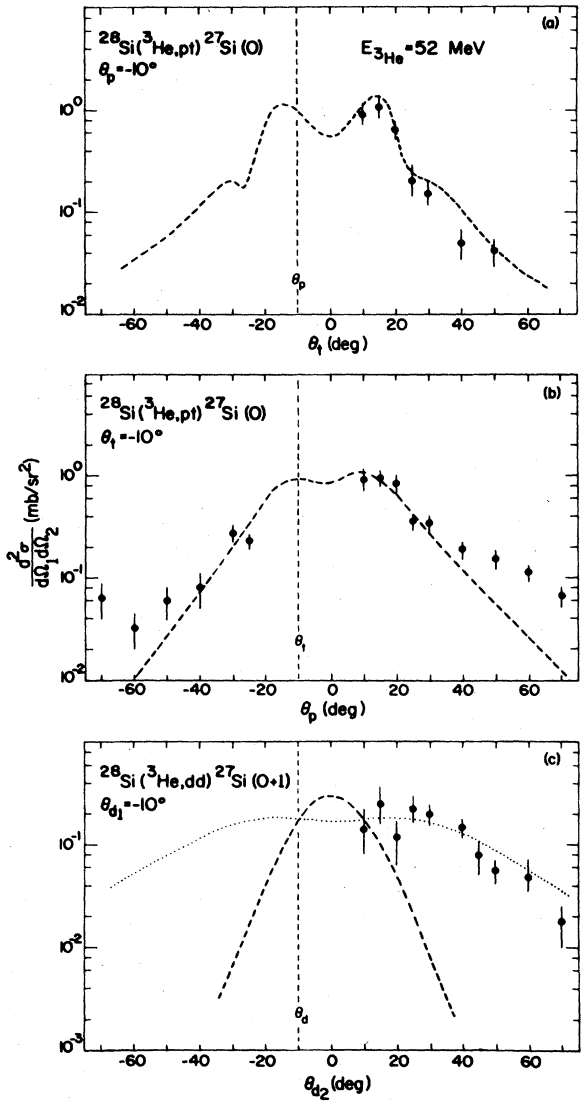

FIG. 55. Angular correlations from the ^{28}Si(^{3}He,pt) ^{28}Si(gs) reaction with the proton angle θ_p fixed at $\theta_p = -10°$ (a), the triton angle fixed at $\theta_t = -10°$ (b), and from the ^{28}Si(^{3}He,dd) ^{27}Si(0+1) reaction with one deuteron angle fixed at $\theta_d = -10°$ (c). The curves represent the QFBM calculations with the proton as spectator in (a) and (b). In part (c) the calculations for the fixed deuteron's being the spectator are indicated by a dotted line. The dashed line represents the calculations in which the "moving" deuteron (participant angle fixed) was spectator (Aarts, 1983).

correlations. The comparison in Fig. 55 indicates that the QFBM results reproduce the p-t coincidences very well, even in the case of large momentum transfer [Fig. 55(a)]. The deviations at large proton angles in Fig. 55(b) (θ_t fixed at $\theta_t = -10°$) are probably due to unresolved contributions from proton-unbound states populated in the (^{3}He,t) reaction. These contributions are significantly smaller in cross sections for θ_p fixed at $\theta_p = -10°$ and large θ_t and therefore do not show up in Fig. 55(a). The data in Fig. 55(c) are well reproduced by calculations assuming the deuteron at $\theta_d = -10°$ to be the spectator. In the cases where the proton [Figs. 55(a) and 55(b)] and the deuteron [Fig. 55(c)] are the spectator the normalization constants amount to $\frac{1}{10}$ and $\frac{1}{40}$, respectively. These constants are the same as those found for the elastic- and inelastic-breakup cases. The results in Fig. 36 indicate that the QFBM also reproduces the shape of the projected energy spectra. A comparison with earlier published PWIA calculations show that the width of PWIA calculations was too great compared to the data but that this deficiency is removed in the QFBM calculation.

d. Breakup with two spectator particles

In their calculations Aarts (1983) and Aarts, Malfliet, de Meijer, and van der Werf (1984) have tried for $\Phi(\mathbf{p},\mathbf{q})$ in Eq. (6.42) a Gaussian wave function and a double Hulthén wave function. The results will be indicated by dashed and solid lines, respectively.

Figure 51(a) shows the results of the calculations of the angular correlations for the (^{3}He,pp) reactions on ^{12}C, ^{28}Si, and ^{58}Ni. The calculations were multiplied by a factor of $\frac{1}{3}$ for the double Hulthén and of $\frac{1}{2}$ for the Gaussian wave function. The calculations with the double Hulthén fit the data very well; those with the Gaussian wave function do not decrease as rapidly. This effect is related to the fact that the Gaussian wave function does not reproduce the tail of the ^{3}He wave function. This effect is also observed in the projected proton energy spectra shown in Fig. 56.

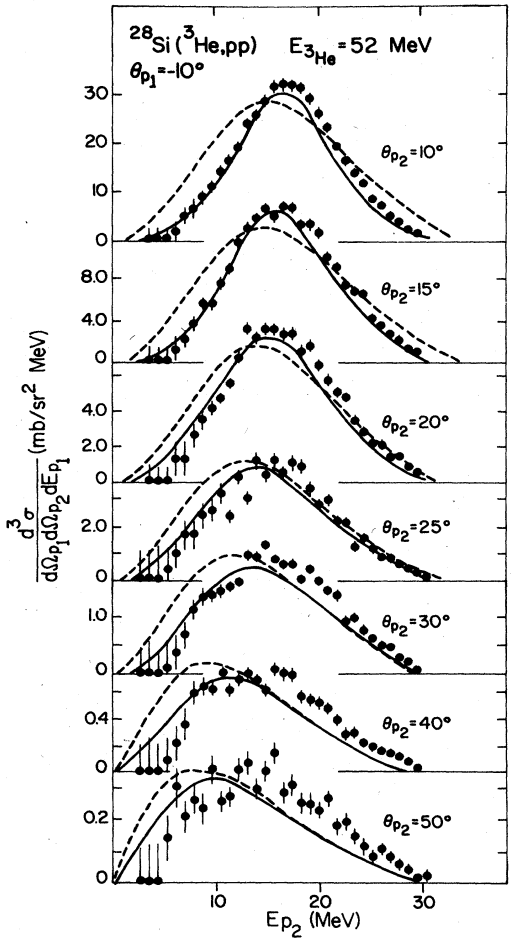

FIG. 56. Projected proton energy spectra for the two-proton spectator part of the ^{28}Si(^{3}He,pp) reaction with θ_{p_1} fixed at $\theta_{p_1} = -10°$. The curves represent the results of the QFBM calculations employing a wave function for the two spectator protons in ^{3}He by a double Hulthén (solid lines) or a Gaussian wave function (dashed lines). For details on the data points see Aarts *et al.* (1983).

3. Conclusions

In conclusion one may state that the general properties of the inclusive data obtained with the 52-MeV ^{3}He beam are well reproduced by the quasifree breakup model. The deviations of the calculations from the data occur for the cases of large momentum transfer and for the case of the classical Coulomb corrections for the peak position of the bump in the inclusive spectra. Both cases indicate that these deviations are due to the pure spectator properties imposed on particle b.

The absorptive-breakup data are well described in the QFBM framework, except for absolute normalization. The ratio between the normalization constants for proton and deuteron spectators, however, is identical to that for other processes.

It can be concluded that the QFBM calculations reproduce the shape of the inelastic-breakup and breakup-transfer data very well. For elastic breakup the proton spectator data are reasonably well reproduced, although the data at larger proton angles in case of the correlation with $\theta_d = -10°$ could not be reproduced. This could partly be due to an interference between proton and deuteron spectator processes which is not yet calculable or to another process in which no pure spectator is present. The fact that the normalization constants for elastic breakup, inelastic breakup, and breakup transfer are the same suggests that the flux going into the spectator is overestimated. In order to calculate more realistic absolute magnitudes it has been suggested (Aarts, 1983; Aarts, Malfliet, de Meijer, and van der Werf, 1984) to introduce reflection coefficients for the elastic scattering of the spectator. In that case the definition of pure spectator is no longer valid.

The QFBM calculations for the two-proton spectators and the neutron as participant are also in good agreement with the data. The QFBM calculations are therefore a good tool for describing the extensive set of breakup data, both inclusive and coincidence, obtained with 52-MeV ^{3}He on ^{12}C, ^{28}Si, and ^{58}Ni. It is unfortunate that this model has not yet been applied to other breakup data.

G. Cross sections in the distorted-wave breakup model

1. Outline of the theory

In the DWBA approach to elastic breakup the wave functions for the entrance and exit channel are given by

$$\langle \chi_f^{(-)} | = \langle \chi_b^{(-)} \chi_y^{(-)} \Psi_y \Psi_B | \tag{6.44a}$$

and

$$| \chi_i^{(+)} \rangle = | \chi_a^{(+)} \Psi_a \Psi_A \rangle \ . \tag{6.44b}$$

In case of breakup reactions the T-matrix element in the post and prior forms is given, according to Eqs. (6.5) and (6.15), by

$$T_{fi}^{\text{post}}=\langle\chi_f^{(-)}\mid V_{bx}\mid\chi_i^{(+)}\rangle=(c^2s)^{1/2}\langle\chi_b^{(-)}\chi_y^{(-)}\Psi_y\Psi_B\mid V_{bx}\mid\chi_a^{(+)}\psi_a\Psi_x\Psi_A\rangle\ , \tag{6.45a}$$

$$T_{fi}^{\text{prior}}=\langle\chi_f^{(-)}\mid V_{bA}+V_{xA}\mid\chi_i^{(+)}\rangle=(c^2s)^{1/2}\langle\chi_b^{(-)}\chi_y^{(-)}\Psi_y\Psi_B\mid V_{bA}+V_{xA}\mid\chi_a^{(+)}\psi_a\Psi_x\Psi_A\rangle\ . \tag{6.45b}$$

If one replaces in Eq. (6.45b) $\chi_b^{(-)}$ and $\chi_a^{(+)}$ by local Coulomb-corrected plane waves, one obtains the matrix element used in the QFBM calculations in Sec. VI.F. This approximation and the assumption that only one-particle interacts with the target nucleus are the differences between the general DWBA approach and QFBM.

In this section we will review the model of Baur and Trautmann (1972,1973,1976), Baur *et al.* (1976,1980a, 1980b), and Pampus *et al.* (1978). The T-matrix is calculated in the DWBA post formalism and the zero-range approximation. We will refer to this model as the *distorted-wave breakup model* (DWBM).

a. Elastic breakup

The zero-range approximation yields

$$V_{bx}(\mathbf{r}_{bx})\psi_a(\mathbf{r}_{bx})=D_0'\delta(\mathbf{r}_{bx})\ , \tag{6.46}$$

where D_0' is the zero-range constant for the vertex $a\rightarrow b+x$. In this approximation the sixfold integral in Eq. (6.45a) reduces to a threefold integral. If one in addition neglects recoil effects, the T-matrix element reduces to

$$T_{fi}^{(0)}=D_0\int d^3r\,\chi_b^{(-)*}(\mathbf{k}_b,\mathbf{r})\chi_x^{(-)*}(\mathbf{k}_x,\mathbf{r})\times\chi^{(+)}(\mathbf{k}_a,\mathbf{r})\Lambda(r)P(r)\ . \tag{6.47}$$

The D_0 used in this and following equations also includes the factor $(c^2s)^{1/2}$. The functions $\Lambda(r)$ and $P(r)$ take the finite-range and nonlocality effects into account (see, e.g., Austern, 1970), and are given in Baur (1976). Here we should like to point out that the zero-range approximation reduces the projectile to a point particle which has an infinitely broad momentum distribution. This would mean that all information in the momentum distribution would be lost in the zero-range approximation. In the approach of Baur *et al.* this is partially restored by the Lorentzian-shaped function $\Lambda(r)$. Although this might be appropriate for light ions, it could have serious implications for projectiles like Li.

The double differential cross section is written as

$$\frac{d^2\sigma^{\text{el}}}{d\Omega_b dE_b}=\frac{m_a m_b m_x}{4(\pi\hbar^2)}\frac{k_b k_x}{k_a}\sum_{l_x m}\mid T_{l_x m}^{(0)}\mid^2\ . \tag{6.48}$$

As will be shown in the next section, the reduced T-matrix element $T_{l_x m}^0$ plays an important role in the evaluation of the inclusive cross section for the nonelastic breakup reactions.

b. Nonelastic breakup

In the DWBM all processes other than elastic breakup, like inelastic breakup, breakup transfer, absorptive breakup, and population of highly excited unbound states, are not calculated individually but called *nonelastic breakup.*[1]

In the DWBM the inclusive cross section for the nonelastic breakup reaction may be calculated from the transition amplitudes for the elastic-breakup process by using the unitarity of the S matrix. The first step in the evaluation of the T-matrix element, $T_{fi}^{(1)}$, is the integration over the internal coordinates ξ_A and ξ_x of the particles A and x. This gives the radial wave function χ_{l_x}, which is called the wave function of the transferred particle x. Neglecting all spin dependence results in the following partial wave expansion:

$$\int d\xi_x\int d\xi_A\Psi_y^*(\xi_y)\Psi_B^*(\xi_B)\chi_y^{(-)*}(\mathbf{k}_y,\mathbf{r})\Psi_x(\xi_x)\Psi_A(\xi_A)\equiv 4\pi\sum_{l_x m}i^{l_x}\chi_{l_x}^{\beta}(r)Y_{l_x m}(\hat{r})Y_{l_x m}^*(\hat{k}_\beta)\ . \tag{6.49}$$

The $\chi_{l_x}^{\beta}(r)$ of Eq. (6.49) presents the radial form factors for the system $\{x+A\}_\beta$ in the reaction channel β. These form factors may be calculated from model wave functions (e.g., by the coupled-channels method). This, however, is rather difficult and impractical if many reaction channels are open.

In the DWBM a surface approximation is used—i.e., the main contribution to the transition amplitude comes from the region at the edge of the nucleus. In this region the radial form factor $\chi_{l_x}^{\beta}$ may be expressed in terms of the scattering matrix element $S_{\alpha\beta}$, which connects the elastic channel α to β:

$$\chi_{l_x}^{\beta}(r)=\delta_{\alpha\beta}j_{l_x}(k_x r)+\left[\frac{m_x k_x}{m_\beta k_\beta}\right]^{1/2}\tfrac{1}{2}(S_{\alpha\beta}-\delta_\alpha)h_{l_x}^{+}(k_x,r)\ , \tag{6.50}$$

where the $j(kr)$ and $h(kr)$ denote the Bessel and Hankel functions, respectively, and m_β and $\hbar k_\beta$ the mass and

[1]As mentioned before, Baur *et al.* in their articles name these processes *inelastic breakup.* Since this leads to confusion with previously identified processes, we have changed the name.

momentum of the system $\{x+A\}$ in the channel β.

By using the relations given in Eq. (6.50), we can express the radial form factor $\chi^{\beta}_{l_x}$ in terms of the radial wave function for elastic scattering ($\chi^{\alpha}_{l_x}=\chi_{l_x}$). This yields

$$\chi^{\beta}_{l_x}=\left[\frac{m_x k_x}{m_\beta k_\beta}\right]^{1/2}\frac{S_{\alpha\beta}}{S_{\alpha\alpha}-1}[\chi_{l_x}(k_x,r)-j_{l_x}(k_x r)]\ . \tag{6.51}$$

It should be noted that in the expression of Eqs. (6.50) and (6.51) the effects from the Coulomb interaction are neglected.

In complete analogy to the situation for the elastic-breakup reaction, the integration over all angles of $\hat{k}_\beta$ may be carried out analytically to obtain again a reduced T-matrix element $T^{(1)\beta}_{l_x m}$, for the nonelastic breakup channel β:

$$T^{(1)\beta}_{l_x m}=\left[\frac{m_x k_x}{m_\beta k_\beta}\right]^{1/2}\frac{S_{\alpha\beta}}{S_{\alpha\alpha}-1}D_0\int d^3r\,\chi^{(-)*}_b(\mathbf{k}_b,\mathbf{r})[\chi_{l_x}(k_x,r)-j_{l_x}(k_x r)]Y_{l_x m}(\hat{r})\chi^{(+)}_a(\mathbf{k}_a,\mathbf{r})\Lambda(r)P(r)\ . \tag{6.52}$$

This expression was derived in the zero-range approximation; standard finite-range and nonlocality corrections have been used. Furthermore, it should be mentioned that the radial form factor $\chi^{\beta}_{l_x}$ has been extended somewhat arbitrarily into the region inside the nuclear interaction. This extrapolation, however, gives the proper boundary condition [$\chi^{\beta}_{l_x}(0)=0$]. Since the interior region is expected to contribute little to the DWBA integral, the results are only slightly influenced by this procedure.

It should be noted that with the approximations introduced above, the entire dependence on the channel β is contained in the factor

$$\left[\frac{m_x k_x}{m_\beta k_\beta}\right]^{1/2}S_{\alpha\beta}\ .$$

The contribution of the nonelastic processes to the inclusive cross section is then obtained by summing over all nonelastic channels:

$$\frac{d^2\sigma^{\text{nonel}}}{d\Omega_b dE_b}=\frac{m_a m_b m_x}{4(\pi\hbar^2)^3}\frac{k_b k_x}{k_a}\sum_{l_x m}\sum_{\beta\neq\alpha}\frac{|S_{\alpha\beta}|^2}{|S_{\alpha\alpha}-1|^2}D_0^2\left|\int d^3r\,\chi^{(-)*}_b(\mathbf{k}_b,\mathbf{r})[\chi_{l_x}(k_x,r)-j_{l_x}(k_x r)]\right.$$
$$\left.\times Y_{l_x m}(\hat{r})\chi^{(+)}_a(\mathbf{k}_a,\mathbf{r})\Lambda(r)P(r)\right|^2\ . \tag{6.53}$$

The unitarity of the S matrix (Jackson, 1970) leads to

$$\sum_{\beta\neq\alpha}|S_{\alpha\beta}|^2=1-|S_{\alpha\alpha}|^2\ . \tag{6.54}$$

Using the definition of the elastic and total reaction cross section in the l_xth partial wave (Jackson, 1970)

$$\sigma^{\text{el}}_{l_x}=\frac{\pi}{k_x^2}(2l+1)|1-S_{\alpha\alpha}|^2 \tag{6.55a}$$

and

$$\sigma^{\text{react}}_{l_x}=\frac{\pi}{k_x^2}(2l+1)(1-|S_{\alpha\alpha}|^2)\ , \tag{6.55b}$$

we find the total inclusive cross section due to nonelastic processes to be given by

$$\frac{d^2\sigma^{\text{nonel}}}{d\Omega_b dE_b}=\frac{m_a m_b m_x}{4(\pi\hbar^2)^3}\frac{k_b k_x}{k_a}\sum_{l_x m}\frac{\sigma^{\text{react}}_{l_x}}{\sigma^{\text{el}}_{l_x}}|T^{(0)}_{l_x m}-\tilde{T}_{l_x m}|^2\ . \tag{6.56}$$

Here the reduced T-matrix elements, $T^{(0)}_{l_x m}$, are the transition amplitudes for the elastic-breakup contribution to the inclusive cross section [Eqs. (6.47) and (6.48)], and the T-matrix elements $\tilde{T}_{l_x m}$ are defined as

$$\tilde{T}_{l_x m}=D_0\int d^3r\,\chi^{(-)*}_b(\mathbf{k}_b,\mathbf{r})j_{l_x}(k_x r)Y_{l_x m}(\hat{r})\times\chi^{(+)}_a(\mathbf{k}_a,\mathbf{r})\Lambda(r)P(r)\ . \tag{6.57}$$

The method of using the surface approximation for the form factor and the unitarity of the S matrix was first proposed by Vincent and Fortune (1973). Recently Austern and Vincent (1981) and Kasano and Ichimura (1982) have derived a closed formula for the inclusive-breakup cross sections. In their approach the cross section is the expectation value of an optical model Green's function for the unobserved system. The optical potential automatically takes into account the transitions to the states of the $\{x+A\}$ system without the need for surface approximation or explicit analyses of form factors as carried out above. For the nonelastic contribution to the inclusive cross section Kasano and Ichimura (1982) find in our present notation

$$\frac{d^2\sigma^{\text{nonel}}}{d\Omega_b dE_b}=\frac{2^6\mu_a\mu_b\mu_x^2}{\hbar^8 k_a^3 k_b k_x^2}\frac{D_0^2}{c^2}\sum_{l_x m}\int_0^\infty dr\, W_x(r)\left|\sum_{l_b l_a} R_{l_x}^{l_b l_a}(r)\mathscr{Y}_{l_x m}^{l_b l_a *}(\hat{k}_b,\hat{k}_a)\right|^2 . \tag{6.58}$$

In this expression $W_x(r)=-\operatorname{Im}U_x(r)$ is the imaginary part of the optical potential for the participant and the function $\mathscr{Y}$ is given by

$$\mathscr{Y}_{l_x m}^{l_b l_a}(\hat{k}_b,\hat{k}_a)=\sum(l_b m'' l_a m' \mid l_x m)Y_{l_x m}(\hat{k}_p)Y_{l_a m'}(\hat{k}_a) . \tag{6.59}$$

The function $R_{l_x}^{l_b l_a}(r)$ is given by

$$R_{l_x}^{l_b l_a}(r)=\int_0^\infty r' f_{l_x}(r_<)h_{l_x}(r_>)\times\langle\chi_{k_b}^{(-)}\mid V_{bx}\mid\chi_{k_a}^{(+)}\rangle dr' , \tag{6.60}$$

with f_l and h_l being the regular and outgoing radial wave functions for the potential U_x, respectively.

The surface approximation used in the DWBM was found to give similar results as the methods based on the Green's function (Austern and Vincent, 1981; Kasano and Ichimara, 1982).

In conclusion, the essential assumptions used in the DWBM are the following.

(i) The model is based on a formalism in which both constituents of the projectile have a full (nuclear plus Coulomb) elastic scattering interaction with the target nucleus.

(ii) The wave functions of all particles are given by optical model scattering waves and hence include absorption. This allows the calculation of absolute cross sections.

(iii) The transition amplitudes are evaluated in the DWBA post representation by using the zero-range approximation with standard nonlocality and finite-range corrections.

For the calculation of the contributions of the nonelastic breakup to the inclusive cross section it is furthermore assumed that

(iv) the surface approximation is valid, and

(v) effects from the Coulomb interaction can be neglected in the radial form factor given in Eqs. (6.50) and (6.51).

2. Comparison with experimental data

The DWBM has been used for a variety of inclusive and coincidence measurements. Calculations for the breakup of the deuteron were found to be in good agreement with data at low incident energies $7.5<E_d<25$ MeV (Baur *et al.*, 1976; Pampus *et al.*, 1978; Kleinfeller *et al.*, 1981) and at higher energies $E_d=56$ and 80 MeV (Shyam, 1983; Bechstedt *et al.*, 1980). Quite recently the inclusive t-, ^{3}He-, and α-particle spectra from ^{6}Li-induced breakup reactions at $E_{^6\text{Li}}=156$ MeV were analyzed with the DWBM (Neumann *et al.*, 1982). It was shown that the shape of the inclusive spectra is well reproduced but that the calculations fail to predict the angular distributions correctly. As possible explanations the authors suggest that the deficiency is likely due to the zero-range approximation which constrains the internal momentum distribution of the outgoing particles. They also point to a possible cause related to the use of the optical-model potentials derived from elastic scattering, which are strongly influenced by the breakup process itself.

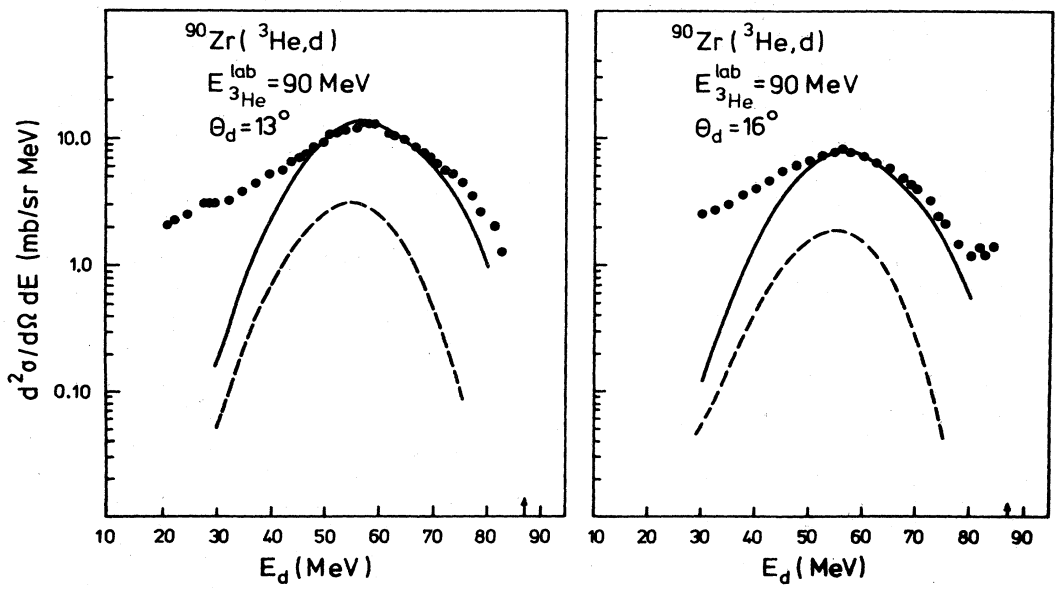

FIG. 57. Comparison of experimental ^{90}Zr(^{3}He,d) inclusive spectra (Matsuoka *et al.*, 1978) with the DWBM calculations (solid line) for inclusive breakup. The calculated contribution due to elastic breakup is shown separately as the dashed line (Shyam *et al.*, 1980).

For ^{3}He-induced breakup reactions inclusive and coincident (elastic breakup) data have been analyzed in the DWBM framework. Shyam *et al.* (1980) have analyzed the inclusive and elastic breakup data of Matsuoka *et al.* (1978,1980), as discussed before in Sec. VI.A. Figure 57 shows the inclusive deuteron spectra at $\theta_d = 13°$ and 16° together with the DWBM calculations and indicates that the bump in the spectrum is reasonably well reproduced. The calculations seem to underpredict the widths of the spectra (see also Fig. 43). The *p-d* angular correlations for elastic breakup on ^{51}V and ^{90}Zr have been analyzed with the DWBM. The comparison is presented in Fig. 58. A reasonable agreement is obtained for the data with $\theta_p < 0°$, but the calculations fail to reproduce the data at $\theta_p > 0°$. The calculations show a pronounced diffractive structure that is not present in the data. In our opinion, this fit to the data is comparable to the fit shown in Fig. 46. No explanation is given by Shyam *et al.* for the discrepancies.

The DWBM calculations of the projected deuteron energy spectra for $\theta_p < 0°$ (where the angular correlations are best fitted) are compared to the data in Fig. 59. The peak shape and positions are well reproduced. We should like to point out that a comparable agreement in shape was obtained in the PWBA analysis presented in Fig. 45. Except for the absolute normalization, not much improvement was achieved by these elaborate calculations. It is unfortunate that Shyam *et al.* have not presented calculations for the cases with θ_p fixed, where the PWBA calculations do not reproduce the experimental data.

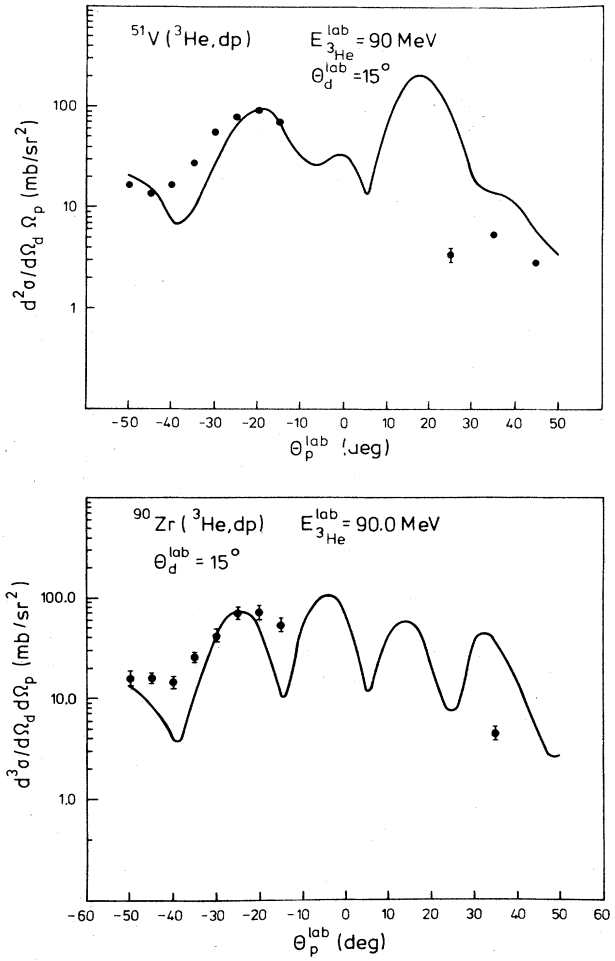

FIG. 58. Proton angular distributions for the ^{51}V(^{3}He,*dp*)^{51}V and ^{90}Zr(^{3}He,*dp*)^{90}Zr ground-state reactions with $\theta_d = 15°$, integrated over the deuteron energies. The DWBM calculations (solid line) are compared to the experimental results of Matsuoka *et al.* (1980) (Shyam *et al.*, 1980).

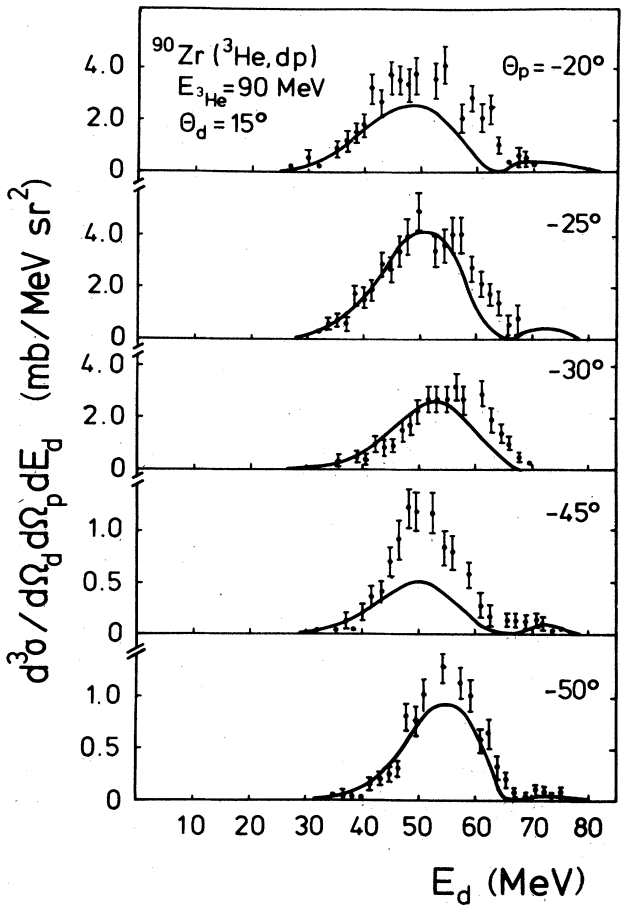

FIG. 59. Deuteron energy spectrum for the ^{90}Zr(^{3}He,*dp*)^{90}Zr ground state coincidence cross section. Experimental results (Matsuoka *et al.*, 1980) are shown for various proton angles θ_p. The deuteron angle $\theta_d = 15°$ is kept fixed. The DWBM calculations are given by lines (Shyam *et al.*, 1980).

A DWBM analysis has also been carried out for the inclusive (^{3}He,*d*) and (^{3}He,*pd*) elastic-breakup data at $E_{^3He} = 52$ MeV with θ_d fixed at $\theta_d = -10°$ of Aarts (1983) and Aarts, Malfliet, de Meijer, and van der Werf (1984). Figure 60 shows the inclusive deuteron spectra for the ^{3}He-induced reactions on ^{28}Si and ^{58}Ni. The dashed line represents the total contribution to the inclusive bump spectrum from elastic plus nonelastic breakup processes. The contribution from elastic breakup only is indicated by the dotted line. The elastic breakup accounts for only a minor part of the inclusive cross section. Similar observations have been made in other breakup studies.

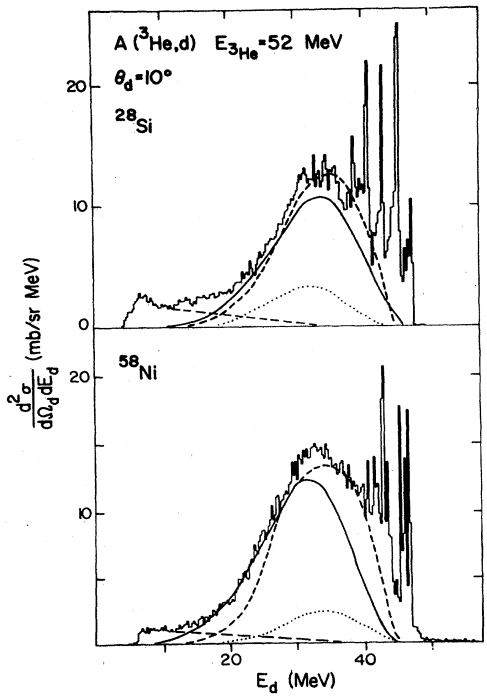

FIG. 60. Inclusive deuteron-energy spectra from the (^{3}He,d) reaction on ^{28}Si and ^{58}Ni at $\theta_d = 10°$. The curves represent the results from the QFBM calculations (solid lines) and from the DWBM calculations for the elastic-breakup reaction (dotted lines) and the total (elastic plus nonelastic) breakup reaction (dashed line). The lower dashed lines represent the experimental shape of the continuum spectra at $\theta_d = 70°$ (Aarts, 1983; Aarts, Malfliet, de Meijer, van der Werf, Baur *et al.*, 1984).

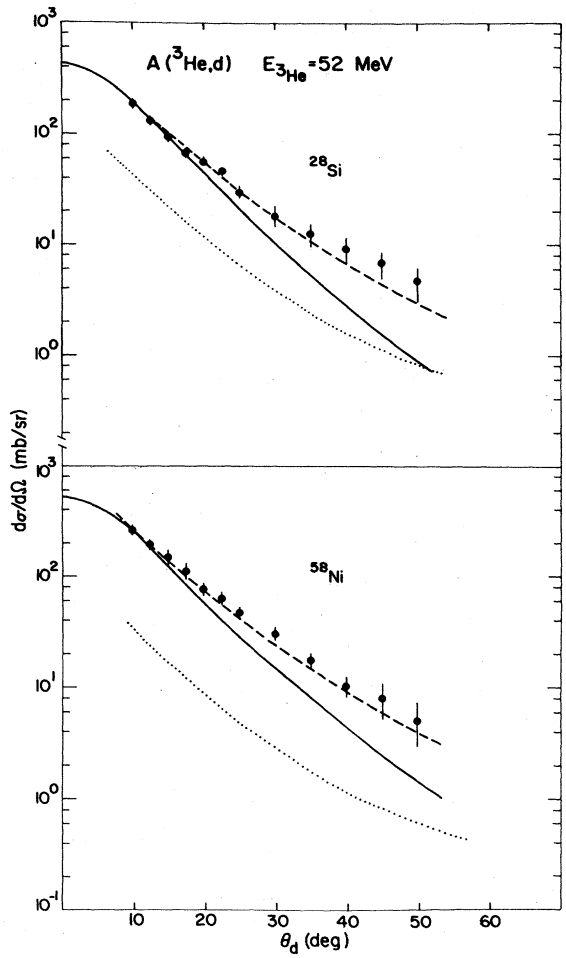

FIG. 61. Angular distributions for the energy integrated cross sections of the continuum bump in the inclusive deuteron spectra from the (^{3}He,d) reaction on ^{28}Si and ^{58}Ni. The curves represent the results of the calculations with the QFBM (solid lines), and with the DWBM for the elastic breakup reaction (dotted lines) and the total (elastic plus nonelastic) breakup reaction (Aarts, 1983; Aarts, Malfliet, de Meijer, van der Werf, Baur *et al.*, 1984).

The calculations for the angular distributions of the energy-integrated cross sections with the DWBM are compared to the data in Fig. 61. The calculations for the elastic-breakup reaction, indicated with the dotted line, again are only a minor part of the total inclusive cross section (dashed line). Both curves have approximately the same slope, and the ratio of elastic to total cross section is 0.24 and 0.14 for ^{28}Si and ^{58}Ni, respectively. Experimentally (see Table III), the values are 0.29 ± 0.07 and 0.28 ± 0.07, respectively. For ^{28}Si the calculations reproduce the elastic-breakup cross section; for ^{58}Ni they underestimate it by a factor of 2.

Figure 53 shows the comparison of the DWBM calculations for elastic breakup (solid lines). As with the ^{3}He data at 90 MeV (see Fig. 58), the calculations at 52 MeV show a strong diffractive pattern which is in good agreement with the data. (Note that in Fig. 58 the deuteron angle is fixed at a positive deuteron angle, whereas in Fig. 53 the fixed angle is at a negative deuteron angle. The negative angles θ_p in one figure therefore correspond to the positive θ_p in the other figure.)

Some of the projected deuteron energy spectra for the elastic breakup on ^{28}Si with θ_d fixed at $\theta_d = -10°$ are calculated with the DWBM and presented as solid lines in Fig. 54, after multiplying the calculations by a normalization constant of 0.6, 0.8, 0.8, 1.0, or 1.7 for the angles $\theta_p = 10°$, 20°, 30°, 40°, and 50°, respectively. It is clear that the experimental data are again well reproduced.

At higher velocities inclusive data and elastic-breakup reaction data obtained with 172.5-MeV α beams on ^{58}Ni have also been analyzed in the framework of the DWBM (Budzanowski *et al.*, 1979). Figure 62 presents the inclusive triton spectrum at $\theta_t = 9.5°$. The solid line represents the results of the DWBM calculation for the total inclusive cross section. Although the shape is well reproduced, the magnitude is about $\frac{2}{3}$ of the experimental value. This discrepancy is attributed by Budzanowski *et al.* (1978) to the presence of preequilibrium processes. The dashed line represents the contribution of elastic

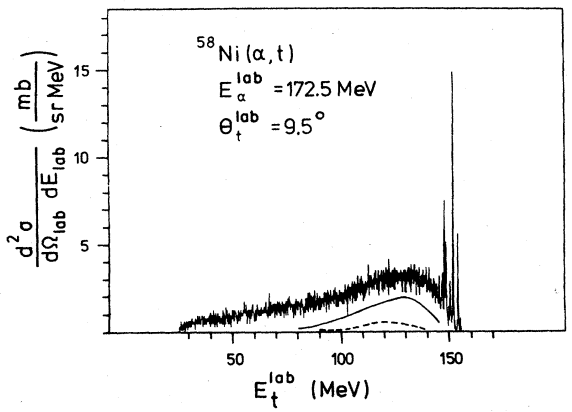

FIG. 62. Inclusive spectra of tritons from the ^{58}Ni(α,t) reaction at $E_\alpha = 172.5$ MeV. The solid line represents the results of the DWBM calculation which is a sum of the elastic and nonelastic breakup. The dashed line represents only the elastic breakup (Budzanowski *et al.*, 1979).

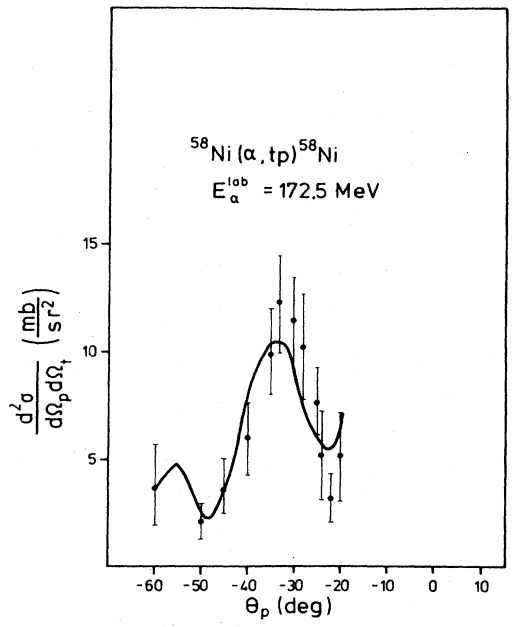

FIG. 63. Angular distribution of the proton-triton correlation in the reaction ^{58}Ni(α,tp)^{58}Ni at $E_\alpha = 172.5$ MeV as a function of proton angle with triton angle fixed at $\theta_t = 10°$. The solid curve represents the results of the DWBM calculation (Budzanowski *et al.*, 1979).

breakup only. Its contribution to the calculated total inclusive cross section is about $\frac{1}{4}$. From Fig. 62 it can be seen that the peak of the elastic contribution is shifted downwards in energy by about 15 MeV, indicating that the proton probably is the spectator. Calculations have been made for the inclusive ^{3}He spectra from the reaction ^{62}Ni($\alpha,^3$He) at 172.5 MeV (Budzanowski *et al.*, 1978). At forward angles the calculations reproduce the spectra well even in magnitude. This seems to contradict the explanation of the discrepancy in the (α,t) spectrum in terms of preequilibrium emission, since this cross section should be about the same for the (α,t) and ($\alpha,^3$He) reactions.

The calculations for the proton-triton angular correlations for the elastic breakup of α particles on ^{58}Ni are compared to the data (see Sec. V.C.2) in Fig. 63. The strongly oscillatory pattern in the data is very well reproduced by the DWBM calculations.

3. Conclusions

The DWBM has so far been applied only to inclusive data and elastic-breakup data. For these cases the DWBM gives an excellent account of the data. It reproduces both the energy-integrated cross sections and the projected energy spectra in shape as well as in magnitude. This agreement is obtained for a range of energies and target nuclei for ^{3}He as well as ^{4}He projectiles. It should be pointed out that in the case where both PWBA and DWBM calculations are available, comparable agreements with the data are obtained. However, absolute cross sections are reproduced only with DWBM calculations. Unfortunately, no DWBM calculations have been published for those cases where the PWBA calculations failed, as, e.g., in the (^{3}He,pd) elastic breakup data with θ_p fixed. Such calculations would be a crucial test for the DWBM to show that, in addition to the absolute normalization, essential improvements can be obtained over the PWBA calculations.

4. Comparison between the QFBM and DWBM calculations

The discussion on the differences between the two models reviews the work by Aarts (1983) and Aarts, Malfliet, de Meijer, van der Werf, Baur *et al.* (1984). In their work calculations have been compared for 52-MeV ^{3}He data on ^{28}Si and ^{58}Ni.

In Fig. 60 the results of the calculations with the two models are compared for the shape of the inclusive deuteron spectra at $\theta_d = 10°$. The main difference between the two calculations is the slightly lower centroid for the QFBM calculations. A similar result was also observed in Fig. 27, where it was concluded that this shift might be due to an overestimate of the Coulomb corrections in the QFBM. In the QFBM calculations these corrections are made semiclassically. Whether this conclusion is realistic remains to be seen, since the particle-particle coincidences discussed in Sec. V.A indicate that part of the deuteron bump at the high-energy side is due to unresolved states populated in the (^{3}He,d) reaction. Such transitions are *not* included in the QFBM calculations but are present in the DWBM calculations. This also explains why in Fig. 60 the DWBM calculations extend to higher energies than

the QFBM. The difference between the dashed and solid curves indicates the amount of stripping to unbound particle states.

From the comparison of the angular distributions of the inclusive deuteron bumps shown in Fig. 61 one observes that the DWBM calculations reproduce the data very well, whereas the QFBM calculations decrease too rapidly. This indicates that the plane-wave approximations for the spectator are no longer valid for the larger-momentum transfers and that these discrepancies are removed when full elastic scattering waves are applied. It is unfortunate that no comparison was made for the angular distribution of the inclusive proton bump, where the QFBM results give a better account of the data (see Fig. 26).

The comparison between the model calculations becomes more difficult for the case of the p-d elastic-breakup angular correlations with the deuteron fixed at $\theta_d = -10°$, as shown in Fig. 53. Two QFBM calculations are presented, one with the proton as a spectator (dashed line) and one for a deuteron spectator (dotted line). At forward angles the curves of the DWBM follow the proton-spectator calculations of the QFBM. For angles of $|\theta_p| \geq 30°$ the proton-spectator contribution decreases rapidly and the deuteron spectator seems to become dominant. Initially an analysis in terms of DWBM seems to suggest that the angular correlation is a sum of the contributions of the two spectator processes. The fit to the projected deuteron energies as presented in Fig. 54, however, does not support this suggestion. At $|\theta_p| \leq 30°$ the DWBM calculations support the proton spectator QFBM calculations. At larger angles neither the proton nor deuteron spectator QFBM calculations reproduce the shape, and the DWBM calculations suggest that both the proton and the deuteron interact strongly with the target. Whether this failure of the QFBM is again related to the plane-wave approximation for the spectator deuteron or whether the spectator approach is not valid anymore is not yet clear.

It has been shown by Aarts (1983) and Aarts, Malfliet, de Meijer, van der Werf, Baur *et al.* (1984) that the transition-matrix elements for elastic breakup in the QFBM and DWBM become equal if one replaces the distorted waves of the projectile and the spectator in the DWBM by Coulomb-modified plane waves. Therefore, the only missing part in the QFBM is the absorption of the spectator (the distortions in the projectile have already been taken into account via the modified $\tilde{\eta}_l$ [see Eq. (6.40)]). It is remarkable that at forward angles the main effect of the absorption is on the magnitude of the absolute cross sections and that, e.g., the shape of the projected spectra is almost identical in the two models.

From this section and Sec. VI.F it can be concluded that (i) the results of the calculations from the breakup model presented by Baur *et al.* are in good agreement with the experimental data qualitatively as well as quantitatively, and (ii) the results of the calculations from the distorted-wave breakup model and the quasifree breakup model are qualitatively in good agreement with each other at forward angles (i.e., small momentum transfer). Thus it is obvious that in the (qualitative) analysis of breakup reactions the spectator-participant approach, presented in the QFBM, is a useful tool, since it provides a transparent description of all observed processes within the same framework. This enables us to identify and compare the different breakup-related reaction channels. If the absolute magnitude of the cross sections becomes an important quantity in the analysis, the QFBM in its present form cannot be used. In these cases the more elaborate calculations from the DWBM are needed—at the moment restricting the analysis to the elastic-breakup and the inclusive nonelastic-breakup channels. The DWBM calculations, however, do not distinguish between direct-breakup contributions and transitions to unbound states at high excitation energies. This might lead to confusion in cases where the cross sections for these processes become comparable as is, e.g., the case for the $(\alpha,{}^3\mathrm{He})$ and (α,t) spectra discussed in Sec. V.A.

5. Other DWBA approaches

In addition to the DWBA approach of Baur *et al.* as discussed in the preceding section, there have been the approaches of Udagawa and Tamura (1980) and Goto *et al.* (1980). These approaches are based on the formalism of Rybicki and Austern (1972) and are formulated in a prior form of the DWBA.

The model of Udagawa and Tamura was first developed for the breakup of heavy-ion–induced reactions and hence written in exact-finite range DWBA. In the formulation of the T-matrix element, the transition amplitude in the prior form deviates from the ones in Eq. (6.45) in the description of the wave function of the outgoing channel:

$$T_{fi} = \langle \chi_b^{(-)}(\mathbf{k}'_b,\mathbf{r}_b)\chi_x^{(-)}(k'_x,r_x) \mid U_{bA} + U_{xA} \mid \varphi_x(r_x)\chi_a^{(+)}(\mathbf{k}_a,\mathbf{r}_a)\rangle \ , \tag{6.61}$$

where $\chi_x^{(-)}$ now denotes the *continuum* wave functions of the relative motion between b and x in the reaction

$$a + A \rightarrow a^* + A \rightarrow b + x + A \ . \tag{6.62}$$

This implies that the reaction is described as a sequential breakup process. Since the model is applied to direct-projectile breakup data, we will discuss the results in this section. The approach of Goto *et al.* (1980) is analogous to that of Udagawa and Tamura. Instead of calculating the T-matrix element directly, as was done by Rybicki and Austern (1972), they introduce several approximations, which are mainly based on the relatively high incident energy and the assumed strongly peripheral charac-

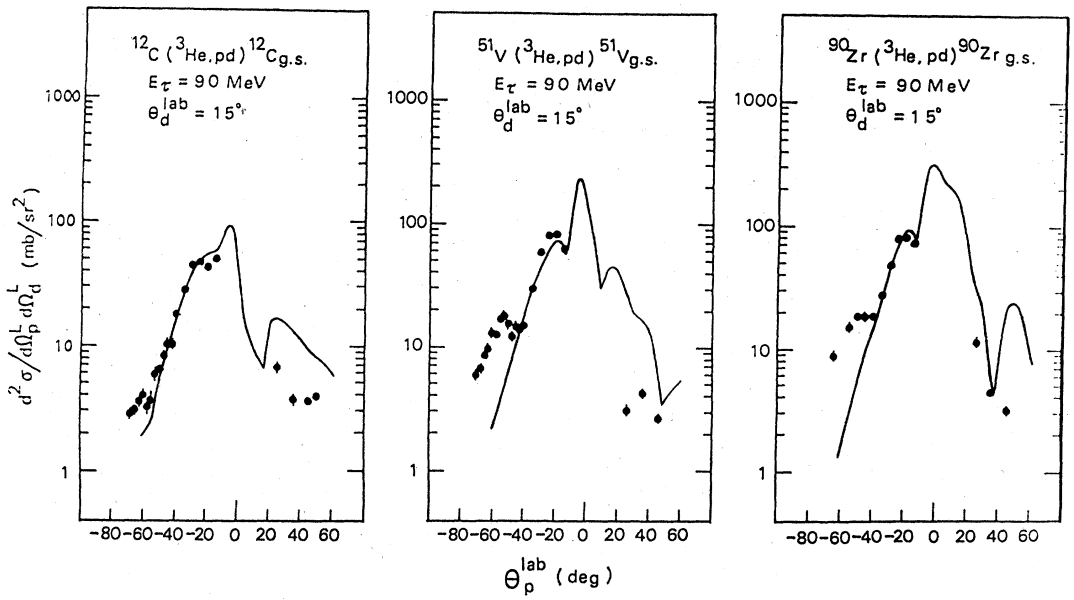

FIG. 64. Comparison of the calculations for p-d angular correlations with the experiments (Goto *et al.*, 1980).

ter of these reactions.

Both calculations have been compared with some of the data from Matsuoka *et al.* (1980). Figure 64 shows the comparison of the calculations by Goto *et al.* (1980) for the elastic-breakup reactions on ^{12}C, ^{51}V, and ^{90}Zr with θ_d fixed at $\theta_d = 15°$. The calculations by Udagawa and Tamura (1980) are compared with the ^{51}V data in Fig. 65. In both cases the calculations of the double-differential cross section fit the data only for θ_p between $-15°$ and $-40°$, where the momentum transfer is small. The results are comparable to the PWBA and DWBM calculations shown in Figs. 46 and 58, respectively. The corresponding results for the triple-differential cross section (the projected deuteron spectra) are compared to the data in Fig. 66. The calculated peak position shifts towards higher energies with increasing proton angle. The peak position is about 5 MeV too low at $\theta_p = -15°$ and 20 MeV too high at $\theta_p = -50°$. In comparison, both the PWBA calculations shown in Fig. 45 and the DWBM calculations given in Fig. 59 describe these triple-differential cross sections better.

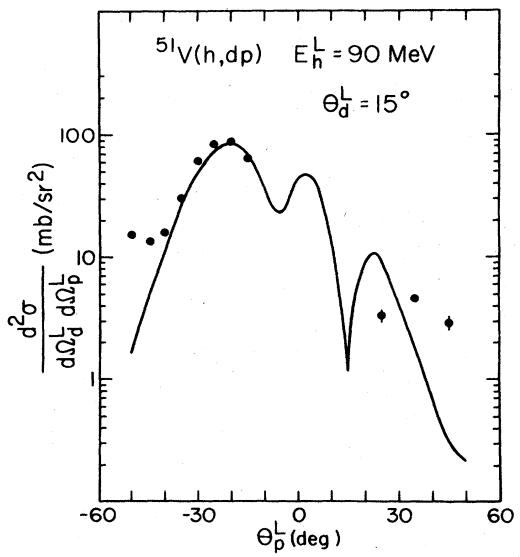

FIG. 65. Double-differential cross section of the $^{51}V(^3He,dp)^{51}V$ reaction at $E_{^3He} = 90$ MeV. The data are taken from Matsuoka *et al.* (1980), while the solid line represents the calculation (Udagawa and Tamura, 1980).

We should like to point out that we view the application of this model to ^3He with caution. Such a model might be physically justified in the case of heavy-ion—induced breakup reactions, where sequential breakup has been observed experimentally. However, for the deuteron (Rybicki and Austern, 1972) it was found that such a model was inadequate for describing the breakup. Recently Matsuoka *et al.* (1982,1983) applied the method of Rybicki and Austern to the analysis of their elastic deuteron breakup data obtained at $E_d = 56$ MeV. Again only for small momentum transfer could they describe the angular correlations. They also have serious troubles in fitting their projected proton energy spectrum. On the contrary, good fits to both the angular correlation and the projected energy spectra of Matsuoka *et al.* (1982) were obtained by Baur *et al.* (1983) with the DWBM. Calculations by Kamimura *et al.* (1983) with the coupled-discretized continuum channels method (CDCC) also give a good description of the angular correlation. In this model the continuum states are discretized, and the cou-

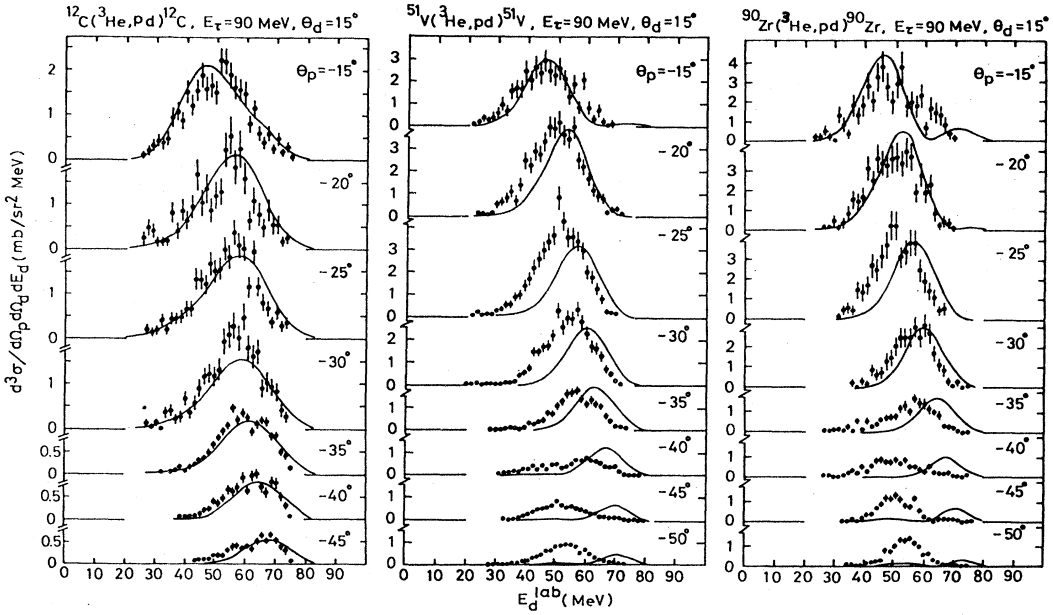

FIG. 66. Comparison of the calculations for coincident deuteron spectra with the experimental data of Matsuoka *et al.* (1980) (Goto *et al.*, 1980).

pling between them is taken into account. The reaction is thought to proceed via the excitation of the projectile to its continuum.

Considering the evidence of spectator breakup for ^{3}He and its successful description in the DWBM and QFBM, we propose the following possible explanation of the failure of the calculations of Goto *et al.*, Udagawa and Tamura, and Matsuoka *et al.* and the success of the calculations of Kamimura *et al.* We start from the T matrix in the DWBM in the prior form, Eq. (6.44b), which should be equivalent to the post form description used by Baur *et al.* Next we expand the wave function of the exit channel into a complete set of orthogonal functions. Such a complete set of functions might, e.g., contain the $\chi^{(-)}_{^3\mathrm{He}}\varphi_{^3\mathrm{He}}$ as used by Udagawa and Tamura, Goto *et al.*, Matsuoka *et al.*, and Kamimura *et al.* The difference is that the first three groups restrict themselves to only one term in the expansion, whereas Kamimura *et al.* use a more complete set. Apparently, the single term in the expansion works reasonably well for small momentum transfer, but a more complete set is necessary to describe the data at larger momentum transfer. The application of these models to direct-breakup data should be regarded with caution.

VII. CONCLUSIONS AND PERSPECTIVES

A. Summary and conclusions

In the study of nuclear reaction mechanisms a classification has often been made in terms of the impact parameter which results in a separation between central and peripheral processes. There is growing evidence, especially at higher incident energies, that for peripheral processes an important part of the reaction cross section is due to breakup reactions. Since this seems to be a general phenomenon for all energetic complex projectiles, He-induced breakup reactions are of special interest. They are, on the one hand, simpler and therefore one hopes more understandable than heavy ions, but on the other hand, they are complicated enough to be considered a doorway to a better insight in the mechanism of heavy-ion reactions.

In this paper the experimental data on breakup phenomena obtained with ^{3}He and ^{4}He projectiles and their interpretation within different theoretical models have been reviewed. Because inclusive experiments usually can give only global information about the breakup processes, exclusive experiments are essential for the detailed understanding of the reaction mechanisms. This requires a knowledge of three-body kinematics, since a certain detector geometry strongly selects the observable processes, even to the extent that processes with a small total cross section might give the impression of being dominant. This might lead to a misinterpretation of the data. Examples of such a selection are coincidence measurements at small relative angles which preferentially give information on the sequential-breakup process. It was shown that in order to unravel the broad structures observed in inclusive experiments, the highly energetic light particles have to be detected in coincidence over a wide dynamic energy range and, although it may sound paradoxical, with a good energy resolution. This last requirement is necessary in order to separate the breakup contributions

from all other reaction processes, such as transitions to closely spaced discrete states.

He-induced sequential breakup processes have been investigated with $\vec{d}$, ^{2}He, α^*, and Li* isotopes in the outgoing channel. From these studies information on the reaction mechanism and on the nuclear structure could be deduced. New nuclear structure data are almost exclusively obtained with the $(\alpha,^2\text{He})$ reaction. This reaction shows a similar selectivity in populating high-spin states, such as the (α,d) reaction, and angular distributions of the $(\alpha,^2\text{He})$ reactions can be well described with DWBA calculations using a deuteron optical model potential for the outgoing ^{2}He. This reaction provides additional structure information to the (t,p) reaction, which mainly populates low-spin states. It is our feeling that the possibilities of obtaining unique structure information (high angular-momentum transfer and isospin selection rules) have not been fully exploited yet. Although it is beyond the direct scope of this paper, we should like to point out the potential power of the $(d,^2\text{He})$ reaction. In view of the present interest in, e.g., Gamow-Teller resonances, this reaction provides a tool for studying the inverse reactions of (p,n) and $(^3\text{He},t)$, since monoenergetic neutron and high-energy triton beams are hardly available at present.

Descriptions of the reaction mechanism of sequential breakup processes reviewed in this article are mainly restricted to the $(^3\text{He},\vec{d})$, $(^3\text{He},^2\text{He})$, and (α,α^*) reactions. The factorization of the cross sections into a formation and a decay part was found to work well. The formation process can be described by standard DWBA, indicating the peripheral nature of the reaction. For mutual excitation observed in the (α,α^*) reaction, coupled-channel effects were found to be important. The decay part in the sequential breakup is governed by the final-state interaction. Calculations with realistic interactions satisfactorily describe the data, especially the normalization constant of the one-nucleon transfer reactions.

Strong sequential breakup processes have also been observed in light heavy-ion reactions (e.g., van Driel, Gonggrijp *et al.*, 1981; Rae *et al.*, 1981). However, this process is more complicated due to the possible mutual excitation of both constituents. Although coherent and noncoherent breakup processes have been introduced, no satisfactory description for these breakup processes is available as yet.

In inclusive experiments of ^{3}He-induced direct breakup a bump was found to be centered roughly on the beam-velocity energy. The cross sections were found to be strongly forwardly peaked and to be proportional to $A^{1/3}$, indicating that breakup is a peripheral process. Detailed angular correlation measurements revealed that the following processes contribute to the breakup bump: (i) elastic breakup, (ii) inelastic breakup, and (iii) absorptive breakup. *Elastic* and *inelastic breakup* are the processes in which the ^{3}He projectile dissociates into a proton and a deuteron, while leaving the target nucleus in its ground state and an excited state, respectively. Elastic breakup was found to be about an order of magnitude stronger than inelastic breakup, but the two processes together account for only a minor part of the bump cross section. The major part arises from *absorptive breakup,* in which the deuteron does not interact with the target nucleus and the proton is captured. This absorptive breakup process is reminiscent of the incomplete fusion observed in heavy-ion collisions (e.g., Wilczyński *et al.*, 1982). Both processes account for a major part of the corresponding reaction cross section for the larger partial waves.

The results of ^{4}He-induced direct breakup are less extensive but indicate again a peripheral breakup process and the presence of spectator breakup. The intensity ratio between protons, deuterons, tritons, and ^{3}He bumps was estimated and found to be independent of the target nucleus and to be the same for $E_\alpha = 80$ and 160 MeV. Coincidence experiments between charged particles confirm that absorptive breakup is the dominant process for the α particle, as well. However, the angular correlations show an additional component which is strongly forwardly peaked.

Descriptions of the direct-breakup processes are presented within the Serber model, the plane-wave Born approximation, and the distorted-wave Born approximation. The Serber model allows for the calculation of the shape only in inclusive spectra. The plane-wave breakup model also allows the calculation of the elastic-breakup angular correlations and projected energy spectra. The attractive feature of the plane-wave approximation is that the transition amplitude for the breakup process becomes separable into a part depending on a two-body interaction and a part depending on the momentum distribution in the projectile. In the distorted-wave Born approximation such a factorization is in general not possible.

Two more sophisticated models exist; one of them, the quasifree breakup model, is explicitly based on the observations of a spectator and a participant. By assuming plane waves for the outgoing spectator, one can maintain the factorization of the transition amplitude. Elastic breakup, inelastic breakup, breakup transfer, and absorptive breakup are described as similar to elastic scattering, inelastic scattering, nucleon transfer, and capture reactions. Due to the use of plane waves in the model (no absorption of the spectator) the cross sections are overestimated. However, the relative intensities between elastic breakup, inelastic breakup, and breakup transfer are reproduced in the model calculations (Aarts *et al.*, 1982; Aarts, 1983; Aarts, Malfliet, de Meijer, and van der Werf, 1984). In the second DWBA breakup model, the distorted-wave breakup model of Baur *et al.* (1980a), absolute cross sections can also be calculated—however, only for elastic breakup and the contribution of the nonelastic processes together. This model also has been successfully applied to a large variety of mainly inclusive measurements.

As mentioned earlier, breakup reactions account for a considerable part of the total reaction cross section. Therefore, one might expect a relation between the breakup cross sections and the parameters of the optical model. For deuterons such a relation was first established by Johnson and Soper (1970). From standard optical model

parameters total reaction cross sections were calculated to be 1320 and 1080 mb for ^{3}He- and ^{4}He-induced reactions on ^{28}Si at 52 and 65 MeV, respectively (Aarts, 1983; Aarts, Malfliet, de Meijer and van der Werf, 1984). At 65 MeV the contribution of breakup processes is small (de Meijer *et al.*, 1983), whereas at 52 MeV (about the same beam velocity) the total breakup cross section for ^{3}He projectiles was found to be 255 mb. Thus the difference in total reaction cross section for ^{3}He- and ^{4}He-induced reactions on ^{28}Si can be accounted for by the difference in breakup cross section, and this effect is embedded in the optical model parameters. In relation to this we point out that in the study of the optical potentials for α particles it was found that at about 80—90 MeV a drastic change in the parameters was required (Put and Paans, 1977). At about the same energy a significant increase of the breakup cross section for the α particle has been observed, indicating that there might be a connection between these two effects.

B. Perspectives

In view of this paper one may conclude that systematic data in this field are scarce. To further understand the physics hidden in the continuum part of particle spectra there is a need for kinematically complete experiments. Depending on the energy and mass of the projectile this means coincidences between one detector placed near the grazing angle and one or more detectors placed such that they cover a wide angular range. With such a setup measurements should be carried out as a function of bombarding energy. Such data as well as coincidence measurements with detectors out of the reaction plane are virtually absent at this moment. As we have seen, the choice of target does not play an essential role, but could facilitate the investigation of certain aspects. For example, with a light target ($A \leq 50$) the particle thresholds are often such that proton emission is favored over neutron emission, or with heavy targets ($A > 200$) fission might be used as a signature for, e.g., absorptive breakup.

One of the differences between ^{3}He and α breakup is the presence of an anisotropic component in, e.g., (α,tp) coincidence measurements; such a process has not been observed in the corresponding $(^3\text{He},dp)$ reaction. The question arises as to which situation is exceptional. For this purpose one would like to investigate the $(^3\text{He},dp)$ reaction at higher energies and study reactions with heavier projectiles with the same detail. In this way the study of He-induced reactions can be considered an intermediate step for the understanding of heavy-ion reactions. It will be interesting to see how breakup processes will show up at higher incident energies, and with heavier projectiles, both experimentally and theoretically. At higher energies the quasifree approach should become more valid, since the difference between the reaction time and the relaxation time of the constituents in the projectile will increase. Such experiments might provide more insight into the role that absorption plays in these reactions. At energies of 100—400 MeV/amu the central part of the optical model potential decreases relative to, e.g., the $\sigma\cdot\tau$ and $\mathbf{L}\cdot\mathbf{S}$ components, and gradually relativistic effects become more important. Thus one could question how well a model description such as QFBM works at those energies and find out if the normalization constant is a good measure of the role of absorption. At these energies a Glauber-type estimate of the distorted wave functions, as recently proposed by Hussein and McVoy (1984), could be useful.

At this moment there are a large number of theoretical models which are claimed to provide a good description of the data. As we have seen, those claims are predominantly based on the description of inclusive spectra and/or the elastic-breakup process. Some of these models and their basic concepts have been discussed in Sec. VI. As noted, the physical concepts of these models are different and often contradictory, so the fact that they all provide a good description of the inclusive data and/or of the elastic-breakup angular correlations indicates that these data are not too sensitive to model descriptions. It would be a great step forward to apply the models to as complete a set of data as possible to find out the physics in these processes.

In all DWBA approaches the calculations for He projectiles have already become very elaborate. This necessarily leads to analytical parametrizations and assumptions of which the limitations are not well defined. This is, for example, the case in the DWBM, where the introduction of the zero-range approximation removes all dependence on the momentum distribution of the projectile. This deficiency is then restored by the finite-range function Λ, which introduces a Lorentzian-shaped distribution. Such an approximation could already lead to difficulties for Li projectiles. Moreover, the fact that the DWBM is formulated in the post form DWBA implies that the potential responsible for the breakup process is the potential that binds the constituents in the projectile. This example demonstrates that apart from the calculational problems the insight in the physics of these models disappears.

Another question that needs attention is the relation between breakup reactions and so-called preequilibrium emission. In Sec. V the $(^3\text{He},pp)$ coincidence data have clearly demonstrated that the inclusive proton spectrum contains contributions from at least two sources of light particles (protons): a targetlike source leading to an exponential-type component in the inclusive spectra and a projectilelike source contributing to a bump near beam-velocity energies. The analysis has shown that these processes are present over a wide angular range and that both components are due to breakup. Furthermore, integration over angle results in a cross section equal to that of the inclusive proton spectrum. In heavy-ion reactions at about 100 MeV/amu (Auble *et al.*, 1983) inclusive spectra show the same features as the spectra of light-ion reactions discussed in the present review: a tail and a bump at beam-velocity energies. At lower bombarding energies (< 30 MeV/amu) the separation is less obvious: two com-

ponents merge smoothly to an exponential tail-like spectrum with a slope that becomes steeper with increasing angle (Awes *et al.*, 1982). These data have commonly been analyzed in terms of a single moving source with a velocity intermediate between beam velocity and that of the compound nucleus (see, e.g., Awes *et al.*, 1982). Although these oversimplifications may serve a purpose for parametrization of data, they could lead to an incorrect picture of the processes taking place in these reactions. In this way, a lot of effort is given to the adjustment of a conceptionally wrong model, instead of investigating these reaction mechanisms in more detail both experimentally and theoretically.

This criticism extends also to the application of descriptions based on the exciton model. This model was originally developed to describe the statistical emission of particles from a single source in reactions induced by very-low—energy projectiles (protons). The description restricts itself to angle-integrated spectra, so all reaction mechanism effects are averaged. We see no justification for such a model for reactions induced by more energetic and heavier projectiles. In our opinion, the need to use a large number of excitons should be taken as a clear warning.

The results from coincidence measurements indicate that the continuum in the particle spectra is due to the contribution of many processes. If these processes are known and common features are observed, a simplified model based on those features can be a useful tool. Based on the present experiences, the light-ion induced reactions seem to be the obvious starting point.

So far we have not yet discussed what can be expected for heavy-ion reactions at >20 MeV/amu, based on the processes observed in light-ion reactions. In the light-ion reactions we mainly focused on the partition of the projectile into two constituents in the ground state ($^3\text{He}\rightarrow p+d$, $\alpha\rightarrow t+p$, $\alpha\rightarrow d+d$), but even for ^{3}He we have seen that the partition also occurred with one unstable constituent ($^3\text{He}\rightarrow p+\bar{d}$, $^3\text{He}\rightarrow n+{}^2\text{He}$). For heavy-ion projectiles the partition will be very likely into one or two constituents which are not in their ground state and may even be particle unstable. This implies that even the spectator will show up as a jet of geometrically correlated (light) particles. In addition, the participant can pick up particles from, or transfer particles to the target nucleus and reach a particle-unstable state. Such a situation can also occur after inelastic scattering by the participant. In twofold coincidences all these spectators and participants will show up as sequential decay, although they arise from a direct breakup process. In order to distinguish between these pseudosequential decay and the real sequential processes, in which the projectile reaches a particle-unstable state via excitation, stripping, or pickup with respect to the projectile as an entity, kinematically complete experiments have to be made. Such experiments will probably require a multidetector setup with a good mass and charge separation and most likely a reasonably good energy resolution.

If these data become available, they need a more fundamental description in the DWBA approach. Finite-range calculations will have to be made, and the calculations will probably be even more evolved. For such calculations one has to find out how strongly absorptive heavy ions are at these energies and how peripheral the actual processes are. Taken altogether, this may lead to the conclusion that a description outside DWBA like the one by Hussein and McVoy (1984) is a better approach.

Finally, we should like to point out that breakup processes can also be used to investigate other phenomena in nuclear physics. Since breakup reactions are strongly localized in l space, the energy and the detection angle of the spectator provide information on the incident energy, linear momentum, and angular momentum of the participant. So a coincidence measurement between the spectator and the fission fragments (absorptive breakup) should reveal the fission probability as function of the excitation energy and angular momentum of the fissioning nucleus. Another application will be in the investigation of neutron-nucleus interactions, by means of reactions in which the neutron is a participant.

ACKNOWLEDGMENTS

The authors wish to thank Dr. E. H. L. Aarts, Dr. G. Baur, Dr. M. Ichimura, Dr. M. Kamimura, Dr. R. A. R. L. Malfliet, Dr. N. Matsuoka, and Dr. S. Y. van der Werf for their helpful discussions, and Dr. P. D. Bond, Dr. R. H. Siemssen, Dr. G. Wenes, and Dr. A. van der Woude for the critical reading of the manuscript.

The technical assistance of Monique Fokke, Geerhard Grave, and Frank den Hollander is gratefully acknowledged.

This work is part of the research program of the "Stichting voor Fundamenteel Onderzoek der Materie" (FOM) with financial support of the "Nederlandse Organisatie voor Zuiver-Wetenschappelijk Onderzoek" (ZWO). One of us (R.d.M.) would like to thank the Japan Society for Promotion of Science (JSPS) and ZWO for financial support that enabled the discussions with the colleagues in Japan.

REFERENCES

Aarts, E. H. L., 1983, Ph.D. thesis, Groningen.

Aarts, E. H. L., A. M. van den Berg, and R. J. de Meijer, 1980, Nucl. Instrum. Methods **176**, 605.

Aarts, E. H. L., R. K. Bhowmik, R. J. de Meijer, and S. Y. van der Werf, 1981, Phys. Lett. **102B**, 307.

Aarts, E. H. L., P. Grasdijk, R. J. de Meijer, and S. Y. van der Werf, 1981, Phys. Lett. **105B**, 130.

Aarts, E. H. L., R. A. R. L. Malfliet, S. Y. van der Werf, and R. J. de Meijer, 1982, Nucl. Phys. A **380**, 465.

Aarts, E. H. L., R. A. R. L. Malfliet, R. J. de Meijer, and S. Y. van der Werf, 1983, in *Proceedings of the 1983 RCNP International Symposium on Light Ion Reaction Mechanism,* edited by

H. Ogata, T. Kamamuri, and I. Katayama (Research Center for Nuclear Physics, Osaka, Japan), p. 581.
Aarts, E. H. L., R. A. R. L. Malfliet, R. J. de Meijer, and S. Y. van der Werf, 1984, Nucl. Phys. A **425**, 23.
Aarts, E. H. L., R. A. R. L. Malfliet, R. J. de Meijer, S. Y. van der Werf, G. Baur, R. Shyam, F. Rösel, and D. Trautmann, 1984, Nucl. Phys. A (to be published).
Arenhövel, H., M. Danos and H. T. Williams, 1971, Nucl. Phys. A **162**, 12.
Auble, R. L., J. B. Ball, F. E. Bertrand, C. B. Fulmer, D. C. Hensley, I. Y. Lee, R. L. Robinson, P. H. Stelson, C. Y. Wong, D. L. Hendrie, H. D. Holmgren, and J. D. Silk, 1983, Phys. Rev. C **28**, 1552.
Austern, N., 1970, *Direct Nuclear Reaction Theories* (Wiley, New York).
Austern, N., and C. M. Vincent, 1981, Phys. Rev. C **23**, 1847.
Awes, T. C., S. Saini, G. Poggi, C. K. Gelbke, D. Cha, R. Legrain, and G. D. Westfall, 1982, Phys. Rev. C **25**, 2361.
Bansal, R. K., and J. B. French, 1964, Phys. Lett. **11**, 145.
Bassel, R. H., 1966, Phys. Rev. **149**, 791.
Baur, G., 1976, Z. Phys. A **277**, 147.
Baur, G., F. Rösel, and D. Trautmann, 1976, Nucl. Phys. A **265**, 101.
Baur, G., R. Shyam, F. Rösel, and D. Trautmann, 1980a, Helv. Phys. Acta **53**, 506.
Baur, G., R. Shyam, F. Rösel, and D. Trautmann, 1980b, Phys. Rev. C **21**, 2668.
Baur, G., R. Shyam, F. Rösel, and D. Trautmann, 1983, Phys. Rev. C **28**, 946.
Baur, G., and D. Trautmann, 1972, Nucl. Phys. A **191**, 321.
Baur, G., and D. Trautmann, 1973, Nucl. Phys. A **199**, 218.
Baur, G., and D. Trautmann, 1976, Phys. Rep. **25C**, 293.
Bechstedt, U., H. Machner, G. Baur, R. Shyam, C. Alderliesten, A. Djaloeis, P. Jahn, C. Mayer-Böricke, F. Rösel, and D. Trautmann, 1980, Nucl. Phys. A **343**, 221.
Block, M. M., 1956, Phys. Rev. **101**, 796.
Bohne, W., M. Hagen, H. Homeyer, H. Lettau, K. H. Maier, H. Morgenstern, and J. Scheer, 1970, Phys. Rev. Lett. **24**, 1028.
Bojowald, J., A. Djaloeis, S. Gopal, C. Mayer-Böricke, W. Oelert, N. G. Puttaswamy, and P. Turek, 1981, KFA-Jülich Annual Report, p. 13.
Bond, P. D., O. Hansen, C. E. Thorn, M. J. LeVine, P. R. Christensen, J. Pontoppidan, F. Videback, Jiang Cheng-Lie, and M. J. Rhoades-Brown, 1982, Phys. Lett. **114B**, 423.
Bousshid, O., H. Machner, C. Alderliesten, U. Bechstedt, A. Djaloeis, P. Jahn, and C. Mayer-Böricke, 1980, Phys. Rev. Lett. **45**, 980.
Brandenburg, R. A., Y. E. Kim, and A. Tubis, 1975, Phys. Rev. C **12**, 1368.
Brown, R. E., J. S. Blair, D. Bodansky, N. Cue, and C. Kavaloski, 1965, Phys. Rev. **138**, 1394.
Budzanowski, A., G. Baur, C. Alderliesten, J. Bojowald, C. Mayer-Böricke, W. Oelert, P. Turek, F. Rösel, and D. Trautmann, 1978, Phys. Rev. Lett. **41**, 635.
Budzanowski, A., G. Baur, R. Shyam, J. Bojowald, W. Oelert, G. Rupi, M. Rogge, P. Turek, F. Rösel, and D. Trautmann, 1979, Z. Phys. A **293**, 293.
Cohen, B. L., E. C. May, and T. M. O'Keefe, 1967, Phys. Rev. Lett. **18**, 962.
Congedo, T. V., I. S. Lee-Fan, and B. L. Cohen, 1980, Phys. Rev. C **22**, 985.
de Meijer, R. J., R. Kamermans, J. van Driel, and H. P. Morsch, 1977, Phys. Rev. C **16**, 2442.
de Meijer, R. J., 1982, in *Proceedings XX Winter School on Nuclear Physics, Bormio,* edited by I. Iori (Ricerca Scientifica ed Educatione Permanente, Milano, Italy), p. 289.
de Meijer, R. J., E. H. L. Aarts, M. B. Greenfield, and W. A. Sterrenburg, 1983, Nucl. Phys. A **402**, 15.
Djaloeis, A., J. Bojowald, S. Gopal, W. Oelert, N. G. Puttaswamy, P. Turek, and C. Mayer-Böricke, 1983, Phys. Rev. C **27**, 2389.
Drumm, P. V., J. B. A. England, O. Karban, J. M. Nelson, J. M. Barnwell, and N. E. Sanderson, 1983, Phys. Lett. **126B**, 155.
Fuchs, H., 1982, Nucl. Instrum. Methods **200**, 361.
Gasiorowic, S., 1974, *Quantum Mechanics* (Wiley, New York).
Glendenning, N. K., 1965, Phys. Rev. **137**, 102.
Goto, A., H. Kamitsubo, H. Sakaguchi, F. Ohtani, N. Matsuoka, A. Shimizu, K. Hosono, T. Saito, M. Kondo, and S. I. Hayakawa, 1980, in *International Symposium on Highly Excited States in Nuclear Reactions,* edited by H. Ikegami and N. Muraoka (Research Center for Nuclear Physics, Osaka, Japan), p. 65.
Helmholtz, A. C., E. M. McMillan, and D. C. Sewell, 1947, Phys. Rev. **72**, 1003.
Henley, E. M., and C. E. Lacy, 1967, Phys. Rev. **160**, 835.
Ho, H., P. Gonthier, M. N. Namboodiri, J. B. Natowitz, L. Alder, S. Simon, K. Hagel, R. Terry, and A. Kohdai, 1980, Phys. Lett. **96B**, 51.
Ho, H., and P. Gonthier, 1981, Nucl. Instrum. Methods **190**, 75.
Ho, H., P. L. Gonthier, G. Y. Fan, W. Kühn, A. Pfoh, L. Schad, R. Wolski, J. P. Wurm, J. C. Adloff, D. Disdier, A. Kamili, V. Rauch, G. Rudolf, F. Schiebling, and A. Strazzeri, 1983, Phys. Rev. C **27**, 584.
Hussein, M. S., and K. W. McVoy, 1984, Nucl. Phys. A (in press).
Inamura, T., M. Ishihara, T. Fukuda, T. Shimoda, and H. Hiruta, 1977, Phys. Lett. **68B**, 51.
Jackson, D. F., 1970, *Nuclear Reactions* (Methuen, London).
Jahn, R., G. J. Wozniak, D. P. Stahel, and J. Cerny, 1976, Phys. Rev. Lett. **37**, 812.
Jahn, R., D. P. Stahel, G. J. Wozniak, J. Cerny, and H. P. Morsch, 1976, Phys. Lett. **65B**, 33.
Jahn, R., D. P. Stahel, G. J. Wozniak, R. J. de Meijer, and J. Cerny, 1978, Phys. Rev. C **18**, 9.
Janetzki, U., Q. K. K. Liu, D. Hahn, H. Homeyer, and J. Scheer, 1976, Nucl. Phys. A **267**, 285.
Jarczyk, L., J. Lang, R. Müller, D. Balzer, P. Viatte, and P. Marmier, 1973, Phys. Rev. C **8**, 68.
Johnson, R. C., and P. J. R. Soper, 1970, Phys. Rev. C **1**, 976.
Johnson, R. C., and P. J. R. Soper, 1972, Nucl. Phys. A **182**, 619.
Kamermans, R., H. P. Morsch, R. J. de Meijer, and J. van Driel, 1979, Nucl. Phys. A **314**, 37.
Kamimura, M., M. Yahiro, Y. Iseri, Y. Sakuragi, M. Nakano, and Y. Fukushima, 1983, in *Proceedings of the 1983 RCNP International Symposium on Light Ion Reaction Mechanism,* edited by H. Ogata, T. Kamamuri, and I. Katayama (Research Center for Nuclear Physics, Osaka, Japan), p. 558.
Kanestrøm, I., and H. Koren, 1969, Nucl. Phys. A **130**, 527.
Kasano, A., and M. Ichimura, 1982, Phys. Lett. **115B**, 81.
Kleinfeller, J., J. Bisplinghoff, J. Ernst, T. Mayer-Kuckuk, G. Baur, B. Hoffmann, R. Shyam, F. Rösel, and D. Trautmann, 1981, Nucl. Phys. A **370**, 205.
Koeslag, H. J., I. Brouwer, P. B. Goldhoorn, M. B. Greenfield, R. J. de Meijer, L. Sterck, G. Vourvopoulos, and W. J. Uytenboogaardt, 1983, KVI Annual Report, 40, and private com-

munication.
Koeslag, H. J., P. B. Goldhoorn, R. J. de Meijer, L. Sterck, and A. van der Woude, 1984, Phys. Lett. **148B**, 275.
Kok, L. P., and A. S. Rinat, 1973, Nucl. Phys. A **156**, 593.
Koontz, R. W., C. C. Chang, H. D. Holmgren, and J. R. Wu, 1979, Phys. Rev. Lett. **43**, 1862.
Koontz, R. W., 1980, Ph.D. thesis, University of Maryland.
Kunz, P. D., 1974, Program DWUCK4, University of Colorado, Boulder, Colorado, U.S.A.
Kunz, P. D., A. Saha, and H. T. Fortune, 1979, Phys. Rev. Lett. **43**, 341.
Lim, T. K., 1972, Nucl. Phys. A **180**, 668.
Matsuoka, N., K. Hatanaka, T. Saito, T. Itahashi, K. Hosono, A. Shimizu, and M. Kondo, 1982, Nucl. Phys. A **391**, 357.
Matsuoka, N., K. Hatanaka, T. Saito, T. Itahashi, K. Hosono, Shimizu, and M. Kondo, 1982, Nucl. Phys. A **391**, 357.
Matsuoka, N., K. Hatanaka, T. Saito, T. Itahashi, K. Hosono, A. Shimizu, M. Kondo, F. Ohtani, and O. Cynshi, 1983, in *Proceedings of the 1983 RCNP International Symposium on Light Ion Reaction Mechanism,* edited by H. Ogata, T. Kamamuri, and I. Katayama (Research Center for Nuclear Physics, Osaka, Japan), p. 527.
Matsuoka, N., A. Shimizu, K. Hosono, T. Saito, M. Kondo, H. Sakaguchi, A. Goto, and F. Ohtani, 1980, Nucl. Phys. A **337**, 269.
Matsuoka, N., A. Shimizu, K. Hosono, T. Saito, M. Kondo, H. Sakaguchi, Y. Toba, A. Goto, F. Ohtani, and N. Nakamishi, 1978, Nucl. Phys. A **311**, 173.
McVoy, K., and M. C. Nemes, 1980, Z. Phys. A **295**, 177.
Migdal, A. B., 1955, Zh. Eksp. Teor. Fiz. **28**, 3.
Motobayashi, T., H. Ejiri, T. Shibata, K. Okado, M. Sasao, K. Maeda, H. Suzuki, A. Shimizu, and H. Sakai, 1984, Nucl. Phys. A **413**, 290.
Motobayashi, T., A. Shimizu, H. Ejiri, K. Okada, H. Sakai, T. Shibita, M. Sasao, H. Suzuki, and K. Maeda, 1981, RCNP Osaka Annual Report, 82.
Nagamiya, S., and M. Gyulassi, 1982, *Advances in Nuclear Physics* (Plenum, New York).
Nemets, O. F., V. M. Pusach, M. V. Sokolov, and B. G. Struzhko, 1968, Proceedings of the International Symposium on Nuclear Structure, Dubna, U.S.S.R.
Neumann, B., H. Rebel, H. J. Gils, R. Planeta, J. Buschmann, H. Klewe-Nebenius, S. Zagromsky, R. Shyam, and H. Machner, 1982, Nucl. Phys. A **382**, 296.
Nomura, M., 1978, in *INS International Symposium on Nuclear Direct Reaction Mechanisms,* Fukuoka, Japan, Contr. Papers, p. 709.
Ohlsen, G. G., 1965, Nucl. Instrum. Methods **37**, 240.
Oppenheimer, J. R., 1935, Phys. Rev. **47**, 845.
Oppenheimer, J. R., and M. Phillips, 1935, Phys. Rev. **48**, 500.
Pampus, J., J. Bisplinghof, J. Ernst, T. Mayer-Kuckuk, J. Rama Rao, G. Baur, F. Rösel, and D. Trautmann, 1978, Nucl. Phys. A **311**, 141.
Perey, G. M., and F. G. Perey, 1976, At. Data Nucl. Data Tables **17**, 1.
Phillips, R. J. N., 1964, Nucl. Phys. **53**, 650.
Put, L. W., and A. M. J. Paans, 1977, Nucl. Phys. A **291**, 93.
Rae, W. D., A. J. Cole, A. Dacal, R. Legrain, B. G. Harvey, I. Mahoney, M. J. Murphy, R. G. Stokstad, and I. Tserruya, 1981, Phys. Lett. **105B**, 417.
Reid, R. V., 1968, Ann. Phys. (N.Y.) **50**, 411.
Rybicki, F., and D. Austern, 1972, Phys. Rev. C **6**, 1525.
Saha, A., R. Kamermans, J. van Driel, and H. P. Morsch, 1978, Phys. Lett. **79B**, 363.
Satchler, G. R., 1972, Part. Nucl. **5**, 105.
Serber, R., 1947, Phys. Rev. **72**, 1008.
Shyam, R., 1983, in *Proceedings of the 1983 RCNP International Symposium on Light Ion Reaction Mechanism,* edited by H. Ogata, T. Kamamuri, and I. Katayama (Research Center for Nuclear Physics, Osaka, Japan), p. 541.
Shyam, R., G. Baur, F. Rösel, and D. Trautmann, 1979, Phys. Rev. **19**, 1246.
Shyam, R., G. Baur, F. Rösel, and D. Trautmann, 1980, Phys. Rev. C **22**, 1401.
Shyam, R., G. Baur, A. Budzanowski, J. Bojowald, H. Dabrowski, C. Mayer-Böricke, W. Oelert, G. Riepe, M. Rogge, P. Turek, F. Rösel, and D. Trautmann, 1983, Phys. Rev. C **27**, 2393.
Stahel, D. P., 1979, Ph.D. thesis, Berkeley, LBL 9706.
Terrall, J. R., 1970, Am. J. Phys. **38**, 1460.
Thompson, W. J., and W. R. Hering, 1970, Phys. Rev. Lett. **24**, 272.
Udagawa, T., and T. Tamura, 1980, Phys. Rev. C **21**, 1271.
van Driel, J., 1980, Ph.D. thesis, Groningen.
van Driel, J., R. Kamermans, R. J. de Meijer, and A. E. L. Dieperink, 1980, Nucl. Phys. **A342**, 1.
van Driel, J., R. Kamermans, and R. J. de Meijer, 1980, Nucl. Phys. A **350**, 109.
van Driel, J., M. N. Harakeh, R. Kamermans, and R. J. de Meijer, 1981, Phys. Rev. Lett. **46**, 525.
van Driel, J., S. Gonggrijp, R. V. F. Janssens, R. H. Siemssen, K. Siwek-Wilczyńska and J. Wilczyński, 1981, Phys. Lett. **98B**, 351.
Vincent, C. M., and H. T. Fortune, 1970, Phys. Rev. C **2**, 782.
Vincent, C. M., and H. T. Fortune, 1973, Phys. Rev. C **8**, 1084.
Watanabe, S., 1958, Nucl. Phys. **8**, 484.
Watson, K. M., 1952, Phys. Rev. **88**, 1163.
Wilczyński, J., K. Siwek-Wilczyńska, J. van Driel, S. Gonggrijp, D. C. J. M. Hageman, R. V. F. Janssens, J. Łukasiak, R. H. Siemssen, and S. Y. van der Werf, 1982, Nucl. Phys. A **373**, 109.
Wozniak, G. J., 1974, Lawrence Berkeley Report LBL 2999.
Wozniak, G. J., D. P. Stahel, J. Cerny, and N. A. Jelly, 1976, Phys. Rev. C **14**, 815.
Wu, J. R., C. C. Chang, and H. D. Holmgren, 1978, Phys. Rev. Lett. **40**, 1013.
Wu, J. R., C. C. Chang, H. D. Holmgren, and R. W. Koontz, 1979, Phys. Rev. C **20**, 1284.
Young, G. R., R. L. Ferguson, A. Gavron, D. C. Hensley, F. E. Obenshain, F. Plasil, A. H. Snell, M. P. Webbe, C. F. Maguire, and G. A. Petitt, 1980, Phys. Rev. Lett. **45**, 1389.